Stimuli-Responsive Self-Assembling Materials Comprising Amphiphilic Copolymers for Localized Remotely Triggered Therapeutic Delivery

By

Samantha Caitlin Collins

B.S.E. Materials Science & Engineering,
Concentration in Nanoscale Materials Science and Engineering
University of Pennsylvania, 2011

SUBMITTED TO THE DEPARTMENT OF CHEMICAL ENGINEERING IN PARTIAL FULFILLMENT OF THE REQUIREMENTS FOR THE DEGREE OF

DOCTOR OF PHILOSOPHY

AT THE
MASSACHUSETTS INSTITUTE OF TECHNOLOGY

FEBRUARY 2017

Signature of Author_ Signature redacted
Department of Chemical Engineering,
Program in Polymers and Soft Matter
December 8th, 2016

Certified by_ Signature redacted
Paula T. Hammond
Head of the Department of Chemical Engineering,
David H. Koch Chair Professor in Engineering
Thesis Supervisor

Certified by_ Signature redacted
Angela M. Belcher
James Mason Crafts Professor,
Professor of Biological Engineering and Materials Science
Thesis Supervisor

Accepted by_ Signature redacted
Daniel Blankschtein
Herman P. Meissner (1929) Professor of Chemical Engineering,
Graduate Officer

Stimuli-Responsive Self-Assembling Materials
Comprising Amphiphilic Copolymers
for Localized Remotely Triggered Therapeutic Delivery

By

Samantha Caitlin Collins

Submitted to the Department of Chemical Engineering on December 9th, 2016
in Partial Fulfillment of the Requirements for the Degree of
Doctor of Philosophy in Chemical Engineering

ABSTRACT

The ability to introduce therapeutic at a specified location and time to a healing traumatic wound deep within the body by external non-invasive stimulus could provide great long-term benefit to patients. In this work, we have examined systems consisting of or including amphiphilic copolymers towards deep-tissue externally triggered localized therapeutic delivery applications.

First, we probed a polyelectrolyte multilayer incorporating poly(L-glutamic acid-triethylene glycol-diclofenac) copolymer micellar aggregates for near-infrared responsive enhanced therapeutic delivery. It was discovered that the films released small-molecule non-steroidal anti-inflammatory drug diclofenac up to five-fold faster during remote irradiation with near-infrared. The near-infrared source was effective at generating more-rapid release from films with tissue mimic penetration depths of at least twelve centimeters. Irradiations in immediate succession produced diminishing rates of release. The highly near-infrared responsive behavior was attributed to a delayed-elution mechanism. In this mechanism, the diclofenac was first hydrolytically cleaved from unimers in the film and then resided within the hydrophobic cores of micellar aggregates until freed by energy imparted by the near-infrared irradiation. Gold nanorods were incorporated into the films to enhance the response of the films to near infrared above controls. Due to non-covalent suspension of the nanorods, aggregation led to a kinetically dependent enhancement of performance.

Next, we improved the synthesis of a copolymer of 2-(dimethylamino)ethyl methacrylate with a spiropyran methacrylate by atom transfer radical polymerization for increased kinetic control. From there, we optimized the composition of this multi-responsive copolymer such that isomerization of the spiropyran moiety brought about a solubility transition surrounding 37°C. This property of the copolymer was designed such that the solubility shift by remote photo-trigger would bring about therapeutic release in a polymer multilayer system analogous to the diclofenac system.

Overall, this work demonstrates the utility of engineering amphiphilic copolymers as a powerful approach to impart remotely triggerable therapeutic release properties for use with implants deeply located within the body.

Thesis Supervisor: Paula T. Hammond
Title: Head of the Department of Chemical Engineering,
David H. Koch Chair Professor in Engineering

Thesis Supervisor: Angela M. Belcher
Title: James Mason Crafts Professor,
Professor of Biological Engineering and Materials Science

THESIS SUPERVISORS

Paula T. Hammond

Head of the Department of Chemical Engineering,
David H. Koch Chair Professor in Engineering
Department of Chemical Engineering
The David H. Koch Institute for Integrative Cancer Research
Massachusetts Institute of Technology

Angela M. Belcher

James Mason Crafts Professor,
Professor of Biological Engineering and Materials Science
Department of Materials Science and Engineering
Department of Biological Engineering
The David H. Koch Institute for Integrative Cancer Research
Massachusetts Institute of Technology

THESIS COMMITTEE

Bradley D. Olsen

Paul M. Cook Career Development Professor
Department of Chemical Engineering
Massachusetts Institute of Technology

Leona D. Samson

Professor of Biological Engineering, Professor of Biology,
Uncas (1924) and Helen Whitaker Professor,
American Cancer Society Research Professor
Department of Biological Engineering
Department of Biology
Massachusetts Institute of Technology

For Mom, Dad, Scott, Grandma, and Nana.

Happy 100th Birthday, Minnie!

Ella and Margo, this is for you.

ACKNOWLEDGMENTS

First, to my thesis advisors Paula and Angie, thank you from the bottom of my heart for your support and mentorship during my time at MIT. You both inspire me every day. From you I have learned both how to approach solving real-world engineering problems and how to be a mentor. I hope our work together continues into the future.

To Brad and Leona, my thesis committee members, thank you for our productive discussions at committee meetings. I would like to thank Prof. Brad Olsen for not only providing his insights into polymer research techniques, but also for opening up his lab to me. Thank you to the whole Olsen Lab for making me feel welcome, and a special thanks to Chris Lam for instrument training.

To Prof. Daniel Blankschtein, I cannot thank you enough for your mentorship throughout my Ph.D. and especially during my Teaching Assistantship with you in Colloid and Surfactant Science.

This work would not have been possible without the collaborative environment fostered in the Hammond and Belcher Labs. Thank you to all of my colleagues in these two research groups.

Many thanks in particular to Wade Wang, Mohi Quadir, and Hongkun He for our chemistry collaborations. Mike McDonald, thank you for our work together on materials characterization in the Institute for Soldier Nanotechnologies and on building apparati. I am also grateful for research discussions with Bryan Hsu, Steven Castleberry, and the layer-by-layer delivery subgroup.

To my early mentors in biological research, thank you Gaelen Hess, Nimrod Heldman, F. John Burpo, and Rana Ghosh.

To Claire Zhang, my undergraduate mentee, thank you for bringing your excitement to learn new things into lab every day. We spent a great three years making things together. I would also like to thank undergraduates Alex Lim and Lisa Savagian for their research efforts.

I would like to thank Peter Jansen and Liz Galoyan, Angie and Paula's administrative assistants, for all of your help with scheduling meetings, ordering chemicals, and finding what's missing. Working with you on these tasks made them enjoyable.

Research specialists in shared experimental facilities have been instrumental in moving this research forward. In the Laboratory for Engineering Materials, Mike Tarkanian lent his expertise in polymer processing and we accomplished our goal beyond expectations. Shiahn Chen, thank you for your generosity with your time and skill in scanning electron microscopy and for our discussions.

I would like to express my gratitude for the Program in Polymers and Soft Matter: to Charles Sing and Matthew Mannarino for taking us under your wing; to Michelle Sing and Lionel Moh, my PPSM classmates; and to all of the PPSM students and professors in our polymer family.

Katie, Anasuya, Helen, Rosanna, Mark, Steven, Eric, Xiao, Sean, David, Julia, Ray, Brian, Tom, Su, and all of the ChemE buds, thanks for the good times.

Noémie and Sofia, I feel so fortunate to have you both as my friends. Thank you, Paula, for bringing us together.

Dear Eleonore, thank you for cheering me on and always knowing exactly what to say.

To Mom and Dad, Scott and Grandma, you believed in me every step of the way. Thank you for being my home, my heart.

This is for my whole family, from our centenarian to our littlest ones.

Samantha Caitlin Collins
December 2016

BIOGRAPHICAL NOTE

EDUCATION

Ph.D.	Massachusetts Institute of Technology – Chemical Engineering	2011-2017
B.S.E.	University of Pennsylvania – Materials Science & Engineering	2007-2011

HONORS AND AWARDS DURING PH.D.

National Science Foundation Graduate Research Fellowship, 2011-2016
Walsh (1937) Memorial Presidential Fellowship, 2011-2012
David H. Koch (1962) Fellowship, 2011-2012

PUBLICATIONS FROM PH.D. RESEARCH

Papers

Samantha C. Collins, Claire B. Zhang, Wade Wang, Erik C. Dreaden, Lisa R. Savagian, Paula T. Hammond, Angela M. Belcher. Near-Infrared Stimulated Enhanced Release of Small Molecule Anti-Inflammatory from Self-Assembled Layer-by-Layer Films for Localized Anti-Fibrotic Application. *In preparation.*

Samantha C. Collins, Hongkun He, Wade Wang, Claire B. Zhang, Paula T. Hammond, Angela M. Belcher. Improved Synthesis and Optimized Composition of a Multi-Responsive Spiropyran Methacrylate Copolymer for Externally Triggered Therapeutic Release Applications. *In preparation.*

Conference Presentation

Collins, S.C.; Zhang, C.B.; Savagian, L.R.; Dreaden, E.C.; Hammond, P.T.; Belcher, A.M. Biocompatible Self-Assembled Layer-by-Layer Films with Nanomaterials for Near-Infrared Actuated Delivery of Non-Steroidal Anti-Inflammatory Drugs. Poster. Materials Research Society (MRS) Meeting, December 2015, Boston, MA, USA.

TABLE OF CONTENTS

Chapter 1:

Introduction and Motivation

Chapter 1. Introduction and Motivation

1.1 Self-Assembly of Polymers Layer-by-Layer on Implants for Localized Therapeutic Delivery

The Layer-by-Layer (LbL) assembly technique[1, 2] involves the modular building of materials one on top of the other on the molecular scale, using materials of complementary functionality to bind the materials together. These complementary functionalities include for example opposing electric charges,[3] hydrogen bond-donor hydrogen bond acceptor pairs,[4] and covalently bonding entities.[5] Polymeric materials can be deposited onto substrates of a variety of three-dimensional architectures using mild assembly conditions, from aqueous solutions and at room temperature, such that biological materials sensitive to harsh conditions can be incorporated. Therapeutics can be incorporated at high loading using this technique.

Layer-by-Layer assembly can be effectively utilized to develop conformal coatings on implants for time-resolved localized delivery of therapeutics (Figure 1.1) at efficacies that cannot be achieved with other delivery methods. Layer-by-Layer coatings on microneedles have been used to successfully administer vaccines transdermally and initiate immune responses many-fold higher vs. intradermal injection.[6, 7] Polymer multilayers containing small interfering ribonucleic acids (siRNA) coating a surgical nylon woven mesh enacted sustained localized knockdown of the target in cells, whereas siRNA delivery is elusive by other methods due to its facile degradation *in vivo*.[8] Biodegradable polymer multilayers assembled Layer-by-Layer onto implants as conformal coatings have been demonstrated to enable the time-resolved delivery of therapeutic materials like antibiotics and growth factors to result in superior tissue regeneration as opposed to short-term burst release.[9, 10]

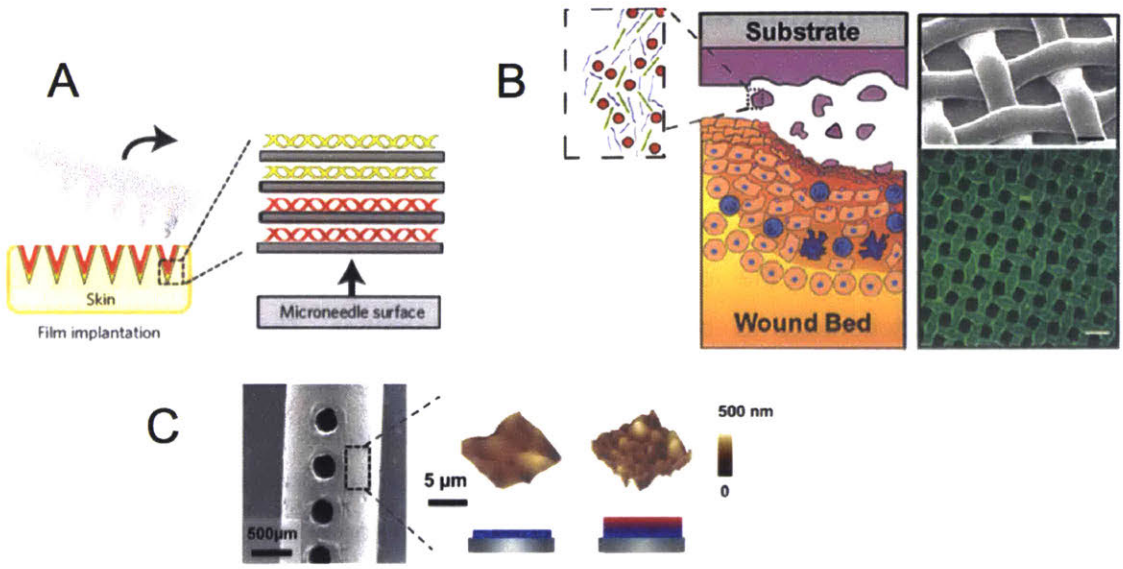

Figure 1.1. Layer-by-Layer assembled polymer multilayer implant coatings for localized delivery of therapeutics. A. Microneedles coated with polymer multilayers encapsulating vaccines instigated favorable immune responses.[7] Adapted with permission from reference.[7] Copyright © 2013, Rights Managed by Nature Publishing Group. B. Surgical suture meshes coated with multilayers preserved the efficacy of small interfering ribonucleic acids for localized knockdown.[8] Adapted with permission from reference.[8] Copyright © 2013 American Chemical Society. C. Bone regeneration scaffolds coated with antibiotics and growth factors achieved bone regeneration.[9] Adapted with permission from reference.[9] Copyright © 2016 American Chemical Society.

1.2 Amphiphilic Polymers for Delayed Hydrophobic Therapeutic Delivery From Self-Assembled Films

The localized release of hydrophobic small molecule therapeutics has been delayed by incorporating the materials into self-assembled films containing amphiphilic polymers. The hydrophilic portions of the polymer associated multivalently with another hydrophilic polymeric material of complementary functionality to grow the Layer-by-Layer architecture and increase the stability and lifetime of the therapeutic depot, while the hydrophobic portion associated with the hydrophobic therapeutic. A variety of polymer architectures have resulted in this amphiphilic functionality, including linear-dendritic block copolymer micelles[11] and polymers with hydrophobic regions along the backbone.[12]

Tethering small molecule drugs[13] or peptides[14, 15] covalently to polyelectrolytes capable of self-assembly into films bound together by multivalent electrostatic interactions further delayed their release from the film over time while preserving their biological activity. One factor contributing to delayed release was the covalent attachment into the film, since hydrolysis of e.g. ester linkages tying the therapeutic into the film slowed the escape of the drug considerably.[13] In addition, polymer-drug conjugates of hydrophobic therapeutics to hydrophilic polymers are by nature amphiphilic. It is therefore plausible that polymer-drug conjugates introduce dual delayed-release functionality derived from hydrophobic association of hydrolyzed therapeutic with covalently bound therapeutic remaining in the film.

1.3 Photoresponsive Nanomaterials for Externally Triggered Delivery in Deeply Located Tissue

1.3.1 The Effect of Irradiation Wavelength on Tissue Penetration Depth

The viable wavelengths for high tissue penetration depth biological imaging using nanoprobes informed the choice of wavelength at which to irradiate through tissue for localized therapeutic applications. The first window of near infrared (NIRI, 700-950 nm)[16] presents more biological transparency than light at shorter wavelengths (Figure 1.2),[17] but in practice has tissue penetration depth limited to 1-2 cm.[18]

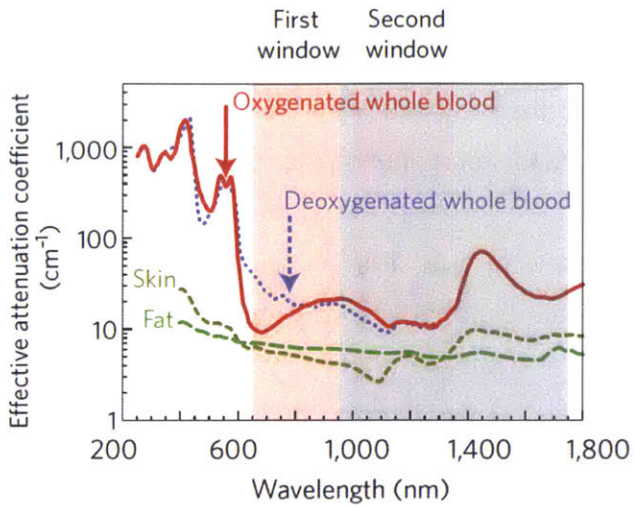

Figure 1.2. Of the two optical windows for biological imaging, the first window (650-950 nm) does not have a deep tissue penetration depth.[18] Greater depths in tissue can be accessed in the second window (NIRII, 950-1700 nm). Irradiating down-conversion nanoparticles *in vivo* at 980 nm and collecting their emission at 1575 nm resulted in superior image acquisition relative to other NIRII probes, two of which were excited at 808 nm.[19] Adapted with permission from reference.[17] Copyright © 2009, Rights Managed by Nature Publishing Group.

The second window of near infrared (NIRII, 950-1700 nm) has dual advantages of high tissue penetration depth and low absorption and scattering by biological materials.[17, 20, 19] For example, images of murine vasculature with high spatiotemporal resolution were obtained using single-walled carbon nanotubes from collecting images in the second near infrared window (1.1-1.4 μm), while images collected from the first near infrared window (800 nm) were indistinct due to substantial scattering and absorbance of the photons by tissue.[21] Therefore, the second window near infrared (950-1700 nm) is of particular interest for high tissue penetration depth applications.

1.3.2 Gold Nanorods as Near Infrared Photothermal Conversion Centers For Therapeutic Applications

Gold nanorods, in comparison to silica-gold nanoshells and gold nanospheres, have been calculated to have superior near infrared absorption and scattering at much smaller particle sizes.[22] Their optical properties have been tuned during synthesis through altering various parameters (Figure 1.3).[23-26] Gold nanorods have been demonstrated for many biomedical applications, including use as imaging and

photothermal chemotherapeutic materials responding to irradiation at 800 nm in the first near infrared window.[27]

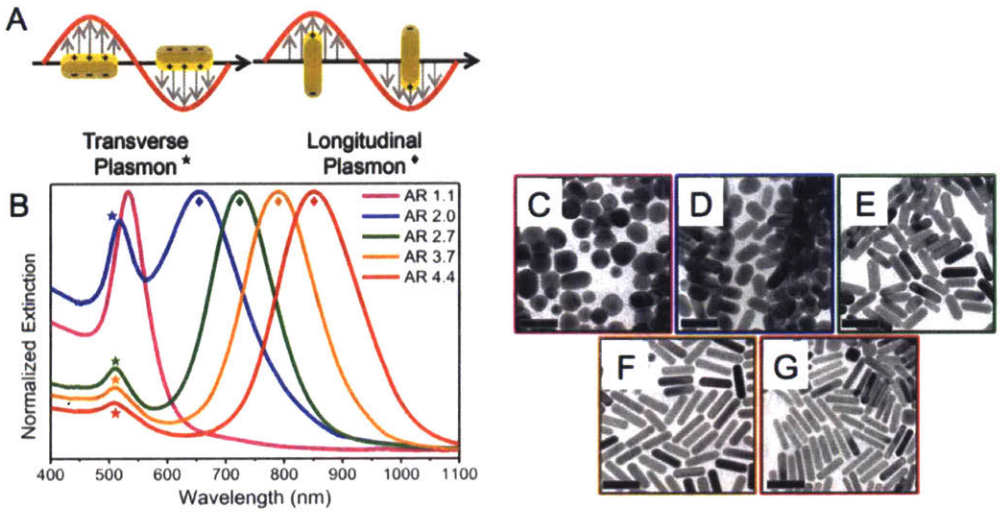

Figure 1.3. The effect of gold nanorod aspect ratio (AR) on optical properties is reflected primarily in the peak position of the longitudinal surface plasmon resonance. A. The conduction band electron oscillation (gray arrows) in resonance with impinging electromagnetic irradiation along the transverse and longitudinal dimensions of a nanorod, i.e. the localized surface plasmon resonances. B. Extinction spectra of gold nanorods with different longitudinal (◆) and transverse (★) extinction peaks corresponding to solutions of gold nanorods with identities shown in transmission electron microscopy images with aspect ratios (C) 1.1, (D) 2.0, (E) 2.7, (F) 3.7, (G) 4.4. Adapted with permission from references.[28, 29] Copyright © 2014, 2016 American Chemical Society.

Incorporation of gold nanorods into Layer-by-Layer films by self-assembly has resulted in red shifting and broadening of the absorption spectrum due to coupling of the gold nanorod longitudinal and/or transverse plasmons with one another.[30] The photothermal conversion efficiency of gold nanomaterials absorbing at a wavelength less than the irradiation wavelength was found to increase by assembling the nanomaterials at close proximity.[31] Therefore, Layer-by-Layer assemblies incorporating gold nanorods can potentially be irradiated in the second window near infrared to attain higher tissue penetration depth.

1.3.3 Attaining Therapeutic Release by Spiropyran Photoisomerization Using Near Infrared

Spiropyran is a photochromic material that undergoes dramatic changes in properties in response to a variety of stimuli.[32] Spiropyran can transform reversibly between two isomers, each with a protonated and de-protonated form, in response to pH and light among other stimuli like solvent polarity and temperature changes. The absorption spectrum and polarity of spiropyran varies considerably with its isomeric state. In order to render this material more robust for localized release applications, the spiropyran must be covalently attached to a support immobilize it and increase photo-stability among other advantages.[33]

Due to the hydrophilic-hydrophobic transformation associated with the merocyanine-spiropyran isomerization, the properties of a polymer can be modulated in response to an external photo-stimulus to produce therapeutic release. For example, the solubility transition of thermoresponsive polymer poly(N-isopropylacrylamide) (PolyNIPAM) has been successfully shifted by incorporating spiropyran side groups and stimulating isomerization.[35]

In order to achieve isomerization by external photo-stimulus with high tissue penetration depth, use can be made of upconversion nanoparticles that absorb light at 980 nm and irradiate in the visible and ultraviolet[36] where spiropyrans absorb. Spiropyran can be combined with upconversion nanoparticles by covalent[37] or non-covalent[38] attachment to trigger delivery of large hydrophilic polyelectrolyte macromolecules[37] or small hydrophobic molecules.[38]

1.4 Thesis Overview and Objectives

This thesis focuses on stimuli-responsive properties of amphiphilic copolymers with the ability to self-assemble. The objective was to develop systems that undergo significant change in response to an externally administered photo-stimulus for the purpose of remotely triggering therapeutic release from implant coatings incorporating the copolymers. The systems were investigated towards high tissue penetration depth applications, where a 980 nm wavelength laser stimulus would be directly or indirectly viable to produce a response in the copolymers.

In Chapter 2, an electrostatic polymer multilayer assembly involving an amphiphilic polymer-drug conjugate was investigated for near-infrared responsive therapeutic release rate properties. The effect of incorporating gold nanorods as photothermal conversion centers into the multilayers in a nano-blend was investigated.

In Appendix A, the gold nanorod-containing polymer multilayer films were studied in more detail. In Appendix B, the effect of introducing clay barrier layers at the surface of the films on the therapeutic release rates was explored.

In Chapter 3, an amphiphilic copolymer containing a photo-isomerizable spiropyran moiety was synthesized by an improved method and its aqueous solubility transitions investigated as a function of the isomeric state of the spiropyran groups.

Chapter 4 presents the main conclusions from the work and recommendations for future directions of scientific study based on this thesis.

1.5 References

1. Decher, G.; Hong, J. D., BUILDUP OF ULTRATHIN MULTILAYER FILMS BY A SELF-ASSEMBLY PROCESS .2. CONSECUTIVE ADSORPTION OF ANIONIC AND CATIONIC BIPOLAR AMPHIPHILES AND POLYELECTROLYTES ON CHARGED SURFACES. *Berichte Der Bunsen-Gesellschaft-Physical Chemistry Chemical Physics* **1991,** *95* (11), 1430-1434.
2. Decher, G., Fuzzy nanoassemblies: Toward layered polymeric multicomposites. *Science* **1997,** *277* (5330), 1232-1237.
3. Lvov, Y.; Decher, G.; Mohwald, H., ASSEMBLY, STRUCTURAL CHARACTERIZATION, AND THERMAL-BEHAVIOR OF LAYER-BY-LAYER DEPOSITED ULTRATHIN FILMS OF POLY(VINYL SULFATE) AND POLY(ALLYLAMINE). *Langmuir* **1993,** *9* (2), 481-486.
4. Stockton, W. B.; Rubner, M. F., Molecular-level processing of conjugated polymers .4. Layer-by-layer manipulation of polyaniline via hydrogen-bonding interactions. *Macromolecules* **1997,** *30* (9), 2717-2725.
5. Kohli, P.; Blanchard, G. J., Applying polymer chemistry to interfaces: Layer-by-layer and spontaneous growth of covalently bound multilayers. *Langmuir* **2000,** *16* (10), 4655-4661.
6. DeMuth, P. C.; Moon, J. J.; Suh, H.; Hammond, P. T.; Irvine, D. J., Releasable Layer-by-Layer Assembly of Stabilized Lipid Nanocapsules on Microneedles for Enhanced Transcutaneous Vaccine Delivery. *Acs Nano* **2012,** *6* (9), 8041-8051.
7. DeMuth, P. C.; Min, Y. J.; Huang, B.; Kramer, J. A.; Miller, A. D.; Barouch, D. H.; Hammond, P. T.; Irvine, D. J., Polymer multilayer tattooing for enhanced DNA vaccination. *Nature Materials* **2013,** *12* (4), 367-376.
8. Castleberry, S.; Wang, M.; Hammond, P. T., Nanolayered siRNA Dressing for Sustained Localized Knockdown. *Acs Nano* **2013,** *7* (6), 5251-5261.
9. Min, J. H.; Choi, K. Y.; Dreaden, E. C.; Padera, R. F.; Braatz, R. D.; Spector, M.; Hammond, P. T., Designer Dual Therapy Nanolayered Implant Coatings Eradicate Biofilms and Accelerate Bone Tissue Repair. *Acs Nano* **2016,** *10* (4), 4441-4450.
10. Shah, N. J.; Hyder, M. N.; Moskowitz, J. S.; Quadir, M. A.; Morton, S. W.; Seeherman, H. J.; Padera, R. F.; Spector, M.; Hammond, P. T., Surface-Mediated Bone Tissue Morphogenesis from Tunable Nanolayered Implant Coatings. *Science Translational Medicine* **2013,** *5* (191), 10.
11. Nguyen, P. M.; Zacharia, N. S.; Verploegen, E.; Hammond, P. T., Extended release antibacterial layer-by-layer films incorporating linear-dendritic block copolymer micelles. *Chemistry of Materials* **2007,** *19* (23), 5524-5530.

12. Smith, R. C.; Riollano, M.; Leung, A.; Hammond, P. T., Layer-by-Layer Platform Technology for Small-Molecule Delivery. *Angewandte Chemie-International Edition* **2009,** *48* (47), 8974-8977.
13. Hsu, B. B.; Park, M. H.; Hagerman, S. R.; Hammond, P. T., Multimonth controlled small molecule release from biodegradable thin films. *Proceedings of the National Academy of Sciences of the United States of America* **2014,** *111* (33), 12175-12180.
14. Hsu, B. B.; Hagerman, S. R.; Jamieson, K.; Castleberry, S. A.; Wang, W.; Holler, E.; Ljubimova, J. Y.; Hammond, P. T., Multifunctional Self-Assembled Films for Rapid Hemostat and Sustained Anti-infective Delivery. *Acs Biomaterials Science & Engineering* **2015,** *1* (3), 148-156.
15. Chluba, J.; Voegel, J. C.; Decher, G.; Erbacher, P.; Schaaf, P.; Ogier, J., Peptide hormone covalently bound to polyelectrolytes and embedded into multilayer architectures conserving full biological activity. *Biomacromolecules* **2001,** *2* (3), 800-805.
16. Weissleder, R., A clearer vision for in vivo imaging. *Nature Biotechnology* **2001,** *19* (4), 316-317.
17. Smith, A. M.; Mancini, M. C.; Nie, S. M., BIOIMAGING Second window for in vivo imaging. *Nature Nanotechnology* **2009,** *4* (11), 710-711.
18. Gao, X. H.; Cui, Y. Y.; Levenson, R. M.; Chung, L. W. K.; Nie, S. M., In vivo cancer targeting and imaging with semiconductor quantum dots. *Nature Biotechnology* **2004,** *22* (8), 969-976.
19. Dang, X. N.; Gu, L.; Qi, J. F.; Correa, S.; Zhang, G.; Belcher, A. M.; Hammond, P. T., Layer-by-layer assembled fluorescent probes in the second near-infrared window for systemic delivery and detection of ovarian cancer. *Proceedings of the National Academy of Sciences of the United States of America* **2016,** *113* (19), 5179-5184.
20. Ghosh, D.; Bagley, A. F.; Na, Y. J.; Birrer, M. J.; Bhatia, S. N.; Belcher, A. M., Deep, noninvasive imaging and surgical guidance of submillimeter tumors using targeted M13-stabilized single-walled carbon nanotubes. *Proceedings of the National Academy of Sciences of the United States of America* **2014,** *111* (38), 13948-13953.
21. Hong, G. S.; Lee, J. C.; Robinson, J. T.; Raaz, U.; Xie, L. M.; Huang, N. F.; Cooke, J. P.; Dai, H. J., Multifunctional in vivo vascular imaging using near-infrared II fluorescence. *Nature Medicine* **2012,** *18* (12), 1841-+.
22. Jain, P. K.; Lee, K. S.; El-Sayed, I. H.; El-Sayed, M. A., Calculated absorption and scattering properties of gold nanoparticles of different size, shape, and composition: Applications in biological imaging and biomedicine. *Journal of Physical Chemistry B* **2006,** *110* (14), 7238-7248.
23. Kozek, K. A.; Kozek, K. M.; Wu, W. C.; Mishra, S. R.; Tracy, J. B., Large-Scale Synthesis of Gold Nanorods through Continuous Secondary Growth. *Chemistry of Materials* **2013,** *25* (22), 4537-4544.
24. Perez-Juste, J.; Liz-Marzan, L. M.; Carnie, S.; Chan, D. Y. C.; Mulvaney, P., Electric-field-directed growth of gold nanorods in aqueous surfactant solutions. *Advanced Functional Materials* **2004,** *14* (6), 571-579.
25. Feng, L. L.; Xuan, Z. W.; Ma, J. B.; Chen, J.; Cui, D. X.; Su, C. W.; Guo, J. M.; Zhang, Y. J., Preparation of gold nanorods with different aspect ratio and the optical response to solution refractive index. *Journal of Experimental Nanoscience* **2015,** *10* (4), 258-267.
26. Ni, W.; Kou, X.; Yang, Z.; Wang, J. F., Tailoring longitudinal surface plasmon wavelengths, scattering and absorption cross sections of gold nanorods. *Acs Nano* **2008,** *2* (4), 677-686.
27. Huang, X. H.; El-Sayed, I. H.; Qian, W.; El-Sayed, M. A., Cancer cell imaging and photothermal therapy in the near-infrared region by using gold nanorods. *Journal of the American Chemical Society* **2006,** *128* (6), 2115-2120.
28. Abadeer, N. S.; Brennan, M. R.; Wilson, W. L.; Murphy, C. J., Distance and Plasmon Wavelength Dependent Fluorescence of Molecules Bound to Silica-Coated Gold Nanorods. *Acs Nano* **2014,** *8* (8), 8392-8406.
29. Burrows, N. D.; Lin, W.; Hinman, J. G.; Dennison, J. M.; Vartanian, A. M.; Abadeer, N. S.; Grzincic, E. M.; Jacob, L. M.; Li, J.; Murphy, C. J., Surface Chemistry of Gold Nanorods. *Langmuir* **2016,** *32* (39), 9905-9921.

30. Vial, S.; Pastoriza-Santos, I.; Perez-Juste, J.; Liz-Marzan, L. M., Plasmon coupling in layer-by-layer assembled gold nanorod films. *Langmuir* **2007,** *23* (8), 4606-4611.
31. Chen, H. J.; Shao, L.; Ming, T. A.; Sun, Z. H.; Zhao, C. M.; Yang, B. C.; Wang, J. F., Understanding the Photothermal Conversion Efficiency of Gold Nanocrystals. *Small* **2010,** *6* (20), 2272-2280.
32. Minkin, V. I., Photo-, thermo-, solvato-, and electrochromic spiroheterocyclic compounds. *Chemical Reviews* **2004,** *104* (5), 2751-2776.
33. Klajn, R., Immobilized azobenzenes for the construction of photoresponsive materials. *Pure and Applied Chemistry* **2010,** *82* (12), 2247-2279.
34. Klajn, R., Spiropyran-based dynamic materials. *Chemical Society Reviews* **2014,** *43* (1), 148-184.
35. Sumaru, K.; Kameda, M.; Kanamori, T.; Shinbo, T., Characteristic phase transition of aqueous solution of poly(N-isopropylacrylamide) functionalized with spirobenzopyran. *Macromolecules* **2004,** *37* (13), 4949-4955.
36. Bagheri, A.; Arandiyan, H.; Boyer, C.; Lim, M., Lanthanide-Doped Upconversion Nanoparticles: Emerging Intelligent Light-Activated Drug Delivery Systems. *Advanced Science* **2016,** *3* (7), 25.
37. Zhou, L.; Chen, Z. W.; Dong, K.; Yin, M. L.; Ren, J. S.; Qu, X. G., DNA-mediated Construction of Hollow Upconversion Nanoparticles for Protein Harvesting and Near- Infrared Light Triggered Release. *Advanced Materials* **2014,** *26* (15), 2424-2430.
38. Chen, S.; Gao, Y. J.; Cao, Z. Q.; Wu, B.; Wang, L.; Wang, H.; Dang, Z. M.; Wang, G. J., Nanocomposites of Spiropyran-Functionalized Polymers and Upconversion Nanoparticles for Controlled Release Stimulated by Near-Infrared Light and pH. *Macromolecules* **2016,** *49* (19), 7490-7496.

Chapter 2:

Near-Infrared Stimulated Enhanced Release of Small Molecule Anti-Inflammatory from Self-Assembled Layer-by-Layer Films for Localized Anti-Fibrotic Application

Chapter 2. Near-Infrared Stimulated Enhanced Release of Small Molecule Anti-Inflammatory from Self-Assembled Layer-by-Layer Films for Localized Anti-Fibrotic Application

Dysregulation of the healing process in traumatic wounds can lead to the progression of a fibrotic disease state. Modulating the healing process in wounds deep within the body post-surgical closure locally and by non-invasive means would provide great long-term benefit to the patient. The objective of this work was to accomplish localized delivery of the non-steroidal anti-inflammatory drug diclofenac by exogenous stimulus with tissue penetration depth on the multi-centimeter scale using a biologically transparent near-infrared 980 nm laser. Films of biocompatible poly(L-lysine) and polymer-drug conjugate poly(L-glutamic acid-triethylene glycol-diclofenac) were self-assembled Layer-by-Layer and combined with near-infrared-absorbing gold nanorods to assess the relative rates of therapeutic release with and without laser stimulation. It was determined that the polymer films were near infrared responsive on their own, and that this response was enhanced by the presence of gold nanorods on a transient basis. The primary mechanism of enhanced release was postulated as the emptying of untethered diclofenac from the hydrophobic domains within the film. With modifications to the fabrication process, these near infrared responsive films might be combined in modular fashion with other anti-fibrotic factors to prevent progression to a disease state in deeply located tissue.

2.1 Introduction

A traumatic wound can lead to dysregulation of the wound healing process and fibrosis. Two of the major pro-fibrotic cytokines are transforming growth factor β (TGF-β) and tumor necrosis factor α (TNF-α), both of which cause fibroblast transformation, proliferation and accumulation, deposition of the extracellular matrix and ultimately tissue destruction and loss of function.[1-3] Fibrogenic cytokines most notably TGFβ were overexpressed in macrophages proximal to developing fibrotic tissue and it has been deduced in the medical community that fibrogenic factors are activated during inflammatory processes.[4] Therefore, releasing anti-inflammatory at knock-down levels at time points during the 72-hr acute inflammatory timeframe could help restore tissue to full health and prevent progression into the fibrosis disease state. The ability to accomplish these doses locally and non-invasively deep within the body presents a challenge.

Among exogenous stimuli-responsive drug delivery mechanisms, a photo-responsive system utilizing excitation with second-window near-infrared (NIR) (950-1700nm) is desirable due to minimal harm to tissue, high tissue penetration depth, and low scattering.[5] Gold nanorods have been successfully utilized as active therapeutic materials that behave as photothermal conversion devices with responsiveness in the near infrared.[6] Gold nanorods have utility in both imaging and photothermal therapeutic applications for cancer.[7, 8] Gold nanorods have also been used to melt peptide hydrogels and release dextran upon exposure to 808 nm light.[9] In most cases, gold nanorod stimulation has been at 808 nm, with the limitation of lower tissue penetration and higher scattering than for a 980 nm stimulus.

The Layer-by-Layer (LbL) assembly technique[10, 11] allows for the modular building of nanoscale blends to yield conformal coatings on implants for sustained and/or sequential localized delivery of therapeutics such as growth factors,[12-15] non-steroidal anti-inflammatory drugs (NSAIDs),[16, 17] antibiotics,[18-21] proteins,[22, 23] and small interfering ribonucleic acids (siRNA).[24] Beyond control of the passive elution of therapeutic from films, responsive Layer-by-Layer assemblies that can be triggered with applied voltage[25, 26] and direct[27] or electrochemically-induced[28] pH changes[29] have been reported.

The current work is preceded by non-degradable Layer-by-Layer assembled gold nanoparticle-containing hollow microcapsules for the release of high molecular weight cargo, by a nanosecond pulsed laser in the near infrared, causing the capsules to burst and the cargo to be completely released.[30-32] The gold nanoparticles' high area fraction in a layer and therefore close proximity led to a red-shifting of their resonance peak.[30] The same microcapsules were used for delivery of macromolecules into the cytosol of cells.[33, 34] The Layer-by-Layer approach for constructing these microcapsules can be applied to fabricate films for localized delivery of therapeutic to tissues.

It was recently demonstrated that by introducing gold nanorods periodically into a Layer-by-Layer system, mechanically robust films with uniformly distributed layers of gold nanorods resulted.[35] Gold nanorods synthesized with cationic surfactant cetyltrimethylammonium bromide (CTAB) have been layered with other materials like polyelectrolytes using electrostatic attraction.[36] The coating polymer chosen for proof-of-concept in the current work was poly(4-styrenesulfonic acid) sodium salt, which is a highly charged polyanion at physiological pH 7.4.

The percent coverage of gold nanorods in each layer of the film can be controlled, by varying the concentration or dip time of the film, to red-shift the absorption maximum.[37] Plasmon

coupling caused a red shift in the longitudinal surface plasmon resonance (LSPR) peak absorption wavelength for the gold nanorods by nearly 100nm.[35] This shifted absorption was hypothesized to allow photothermal-activated drug release by irradiation with a 980 nm laser with efficacy to high tissue penetration depths due to the biologically transparent nature of the 980 nm laser stimulus. If these films were applied locally to a traumatic wound during surgery, subsequent non-invasive laser irradiation might be employed to locally deliver therapeutic deep within the body.

Long-term release of non-steroidal anti-inflammatory drug diclofenac from polypeptide Layer-by-Layer films has been previously demonstrated.[17] The polymer-drug conjugate designed for this purpose, poly(glutamic acid-triethylene glycol-diclofenac) (PGA-Diclof), was layered with poly(L-lysine) (PLL) in polyelectrolyte multilayer films. Films were evaluated for passive release performance.

In the current work, this slow-release system was combined with gold nanorods as photothermal conversion centers with the intention of building a remotely triggered system for enhanced release of diclofenac. Behavior of control films without gold nanorods was also investigated to determine the relative benefit conferred by the nanorods and to analyze the mechanism of therapeutic release from the films. It was determined that the films were near infrared-responsive both with and without gold nanorods. Gold nanorod-containing films were responsive with high tissue mimic penetration depth *in vitro.* A mechanism for enhanced release was proposed and should be studied further. The fabrication method for these films can potentially be optimized to allow further control over the release profile by adding barrier layers to slow passive release.

2.2 Results and Discussion

2.2.1 Effect of Near-Infrared Irradiation on Films With vs. Without Gold Nanorods in a Self-Assembled Nano-Blend

The objective was to achieve nanoscale proximity of the gold nanorods, the near-infrared photothermal conversion centers, with the polymer-drug conjugate to achieve enhanced release by external stimulus. The approach taken to achieve a nano-blend of photothermal converters and prodrug pendant groups was to layer this material in a hexalayer architecture, i.e. gold nanorods every six layers, with the polycation poly(L-lysine) (PLL) and the polyanionic polymer-drug conjugate, poly(L-glutamic acid-triethylene glycol-diclofenac) (PGA-Diclof) (Figure 2.1, Scheme 2.1, Scheme 2.2).

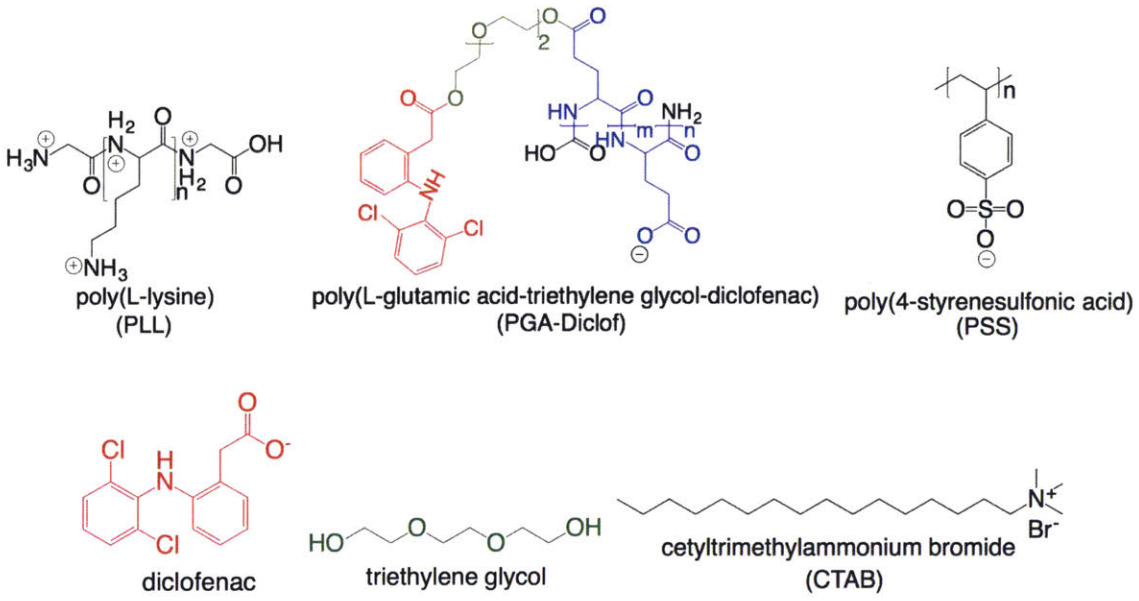

Figure 2.1. Depicted are chemical structures of the non-nanorod components present in the hexalayer films and/or eluting from the films. Poly(L-lysine) is the biocompatible polycation under conditions of film formation (10 mM sodium phosphate buffer, pH 7.4). Poly(L-glutamic acid-triethylene glycol-diclofenac) (PGA-Diclof) is the amphiphilic polymer-drug conjugate that was polyanionic under conditions of film formation (10 mM sodium phosphate buffer, pH 7.4).[17] Cetyltrimethylammonium bromide (CTAB) is the cationic surfactant that suspended the gold nanorods by enclosing them in a bilayer vesicle with the tertiary amine head groups in contact with the gold nanorods and the surrounding medium. Poly(4-styrenesulfonic acid) (PSS) is the polyanion layered onto the CTAB-coated gold nanorods.[36] Diclofenac is the therapeutic cleaved from the polymer-drug conjugate by hydrolysis, which was primarily anionic under conditions of therapeutic release (1x PBS, pH 7.4). Triethylene glycol is the linker that was cleaved from diclofenac and poly(L-glutamic acid) during therapeutic release.

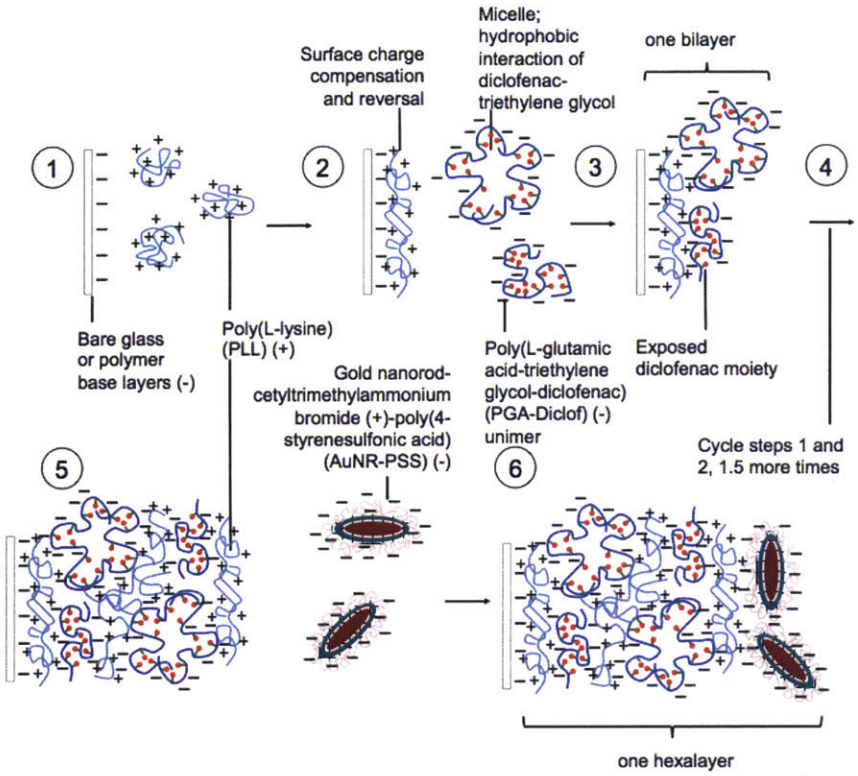

Scheme 2.1. The dip Layer-by-Layer process was used to introduce materials into the film in a modular fashion. Electrostatic attraction between opposing ionic charges held the film together. In all cases, water rinses removed all physisorbed molecules. (1) Poly(L-lysine) (PLL), in 1 mg/mL aqueous sodium phosphate buffer solution as a random coil, was first deposited onto the substrate by electrostatic binding. (2) PLL-terminated films were exposed to aqueous sodium phosphate buffer solution of poly(L-glutamic acid-triethylene glycol-diclofenac) (PGA-Diclof). PGA-Diclof was present in 1 mg/mL aqueous solution with micelle agglomerates 28.8 ± 4.7 nm in size (critical micelle concentration 9.9 μg/mL).[17] Hydrophobic (triethylene glycol)-diclofenac moieties were sequestered from the majority aqueous phase into the micelle cores. Equilibrium between unimers and micelles was established. (3) This constituted one bilayer. Proximity of the protonated amine groups to the ester linkages in PGA-Diclof due to film assembly with PLL sped hydrolysis of ester-bound diclofenac side groups in the film relative to that in aqueous solution.[17, 38] It can be assumed that the diclofenac pendant groups along the unimer chains were much more quickly attacked than those in polymer chains involved in the intact micelles. (4) To create one hexalayer, steps 1 and 2 were cycled accordingly. (5) Polycation-terminated films were exposed to an aqueous solution of gold nanorods encapsulated in a bilayer vesicle of cetyltrimethylammonium bromide (CTAB) and coated with anionic poly(4-styrenesulfonic acid) (PSS). (6) This resulted in hexalayer formation, with nanorods deposited at random orientations.

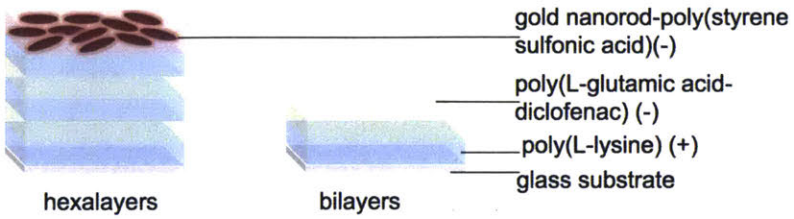

Scheme 2.2. The primary repeating units in the Layer-by-Layer architectures of interest for this study were hexalayers (left) with gold nanorods introduced every sixth layer, and bilayers (right), i.e. two-layer repeating units without gold nanorods.

The film architectures built for study are laid out in Table 2.1. In each case, there was at least one control architecture that contained the polymeric prodrug but not gold nanorods.

Table 2.1. Film Architectures Explored in Near-Infrared Irradiation Studies

Sample	Architecture	Note
$40BL_0$	$(PLL/PGA\text{-}Diclof)_{40}$	No base layers, no nanorods
$20HL_0$	$[(PLL/PGA\text{-}Diclof)_{2.5}/AuNR\text{-}PSS]_{20}$	No base layers, contain nanorods
40BL	$(LPEI/SPS)_{10}/(PLL/PGA\text{-}Diclof)_{40}$	Do not contain nanorods
20HL	$(LPEI/SPS)_{10}/[(PLL/PGA\text{-}Diclof)_{2.5}/AuNR\text{-}PSS]_{20}$	Contain nanorods every sixth layer
40BL-LAP	$(LPEI/SPS)_{10}/(PLL/PGA\text{-}Diclof)_{40}/(PLL/LAP)_{15}$	Capped by clay barrier layer
20HL-LAP	$(LPEI/SPS)_{10}/[(PLL/PGA\text{-}Diclof)_{2.5}/AuNR\text{-}PSS]_{20}/(PLL/LAP)_{15}$	Capped by clay barrier layer
80BL	$(LPEI/SPS)_{10}/(PLL/PGA\text{-}Diclof)_{80}$	Double total drug loading
40HL	$(LPEI/SPS)_{10}/[(PLL/PGA\text{-}Diclof)_{2.5}/AuNR\text{-}PSS]_{40}$	Double total drug loading

KEY

BL: bilayers

HL: hexalayers

LPEI: linear polyethyleneimine

SPS: poly(sodium 4-styrenesulfonate)

PLL: poly(L-lysine)

PGA-Diclof: poly(L-glutamic acid-triethylene glycol-diclofenac)

AuNR-PSS: gold nanorods-poly(4-styrenesulfonic acid)

LAP: Laponite clay platelets

There existed a slow passive release rate of diclofenac from the film under bio-mimicking conditions at 37°C in 10 mM phosphate buffered saline (1x PBS) without stimulation by near infrared. Mean passive release rates from the films were compared with those observed for the same system at different film thicknesses. The release rates were in good agreement with those from previous study on passive release from the bilayer system (Figure 2.2).[17]

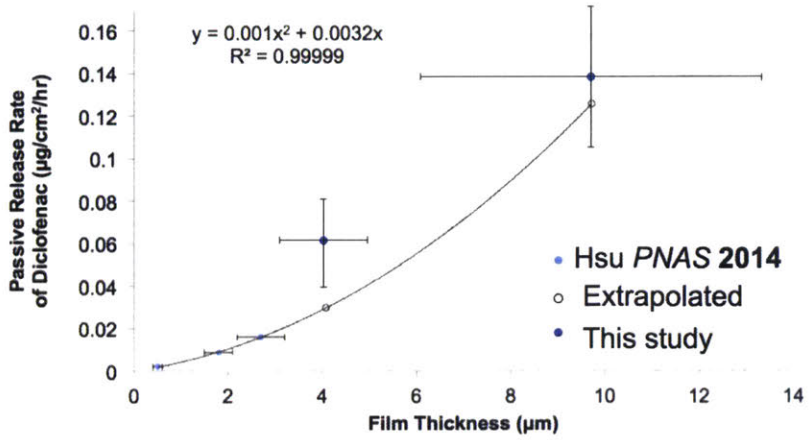

Figure 2.2. Mean passive release rates of diclofenac from forty- and eighty-bilayer (40BL and 80BL) films were in good agreement with previous study of the bilayer system.[17] A polynomial relation was determined between film thickness and the passive release rate of diclofenac from bilayer films. This relation was extrapolated to the film thicknesses examined in the current study.

Bilayer and hexalayer films with and without base layers underwent cycles of release under passive and near-infrared irradiation conditions. First the films were exposed to conditions of passive release *in vitro* (37°C, 1 mL 1x PBS), and then to release under near-infrared irradiation (37°C, 1 mL 1x PBS, 980 nm, 0.697 W/cm^2, 60 min) (Scheme 2.3, Scheme 2.4).

The laser irradiation condition fell well within the Maximum Permissible Exposure (MPE) limits set by the British Standards Institute. By calculations for the MPE of skin to laser irradiation 700-1400 nm from the British Standards Institute, for exposure time from 10 to 30,000 seconds, the maximum power density is $2000C_4$ W/m^2, where $C_4 = 10^{0.002(\lambda-700)}$ for λ = 700-1050 nm. By these calculations, the maximum power density of a 980 nm laser on skin is 0.7262 W/cm^2, greater than the time-averaged 0.697 W/cm^2 incorporated into this study for samples without tissue barriers. The maximum fluence permitted at this 980 nm laser wavelength is 21,785 J/cm^2 (continuous wave laser maximum duration 30,000 seconds), and the fluence used in this study was only 2,509 J/cm^2, almost an order of magnitude lower.

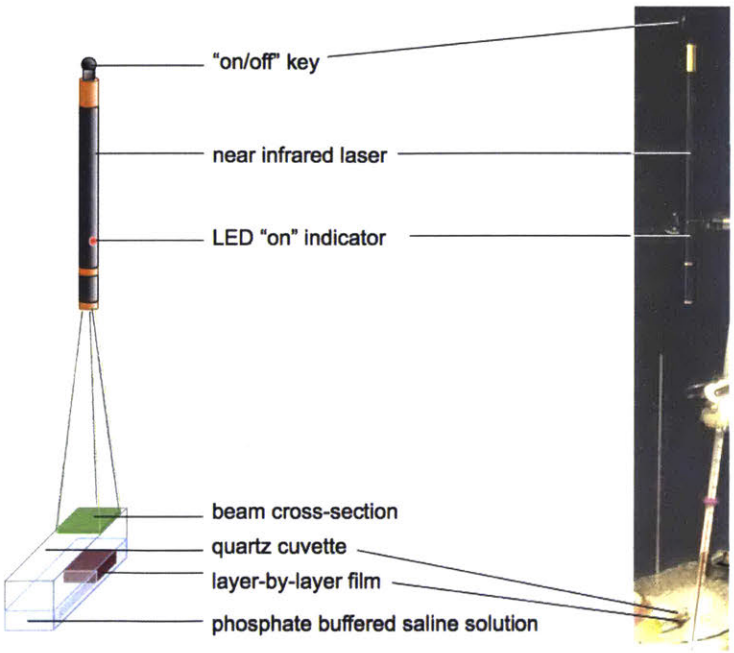

Scheme 2.3. Near-infrared irradiation of Layer-by-Layer films in bio-mimicking conditions (37°C, 10 mM phosphate buffered saline solution) took advantage of laser beam divergence to cover a significant area of the therapeutic-releasing film.

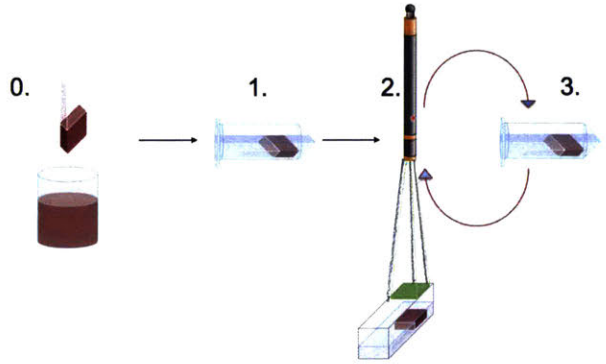

Scheme 2.4. All Layer-by-Layer films in this study underwent fabrication and post-fabrication treatments in this consistent order. 0. Films were built by dip Layer-by-Layer self-assembly. 1. Films were immersed in 1 mL of 10 mM phosphate buffered saline solution at 37°C overnight. 2. The release solution was changed out for fresh solution and irradiated in a quartz cuvette by a 980 nm laser at 0.697 W/cm^2 for 60 min. 3. The release solution was changed out for fresh solution and incubated at 37°C. 4. Steps 2 and 3 were cycled, in part to determine that the films remained functional after irradiation.

An initial comparison study was conducted to monitor the diclofenac release rate differences between forty-bilayer films (containing the prodrug but no nanorods) and twenty-hexalayer films (containing the prodrug and gold nanorods) fabricated on silica without base layers. Each of these film architectures contained forty layers of the polymeric prodrug poly(L-

glutamic acid-triethylene glycol-diclofenac) (PGA-Diclof) for equivalent initial loading of therapeutic. Both of the film types, $40BL_0$ and $20HL_0$ (Table 2.1), demonstrated enhanced release rates of diclofenac with near-infrared irradiation as evaluated by high performance liquid chromatography (HPLC) (Figure 2.3).

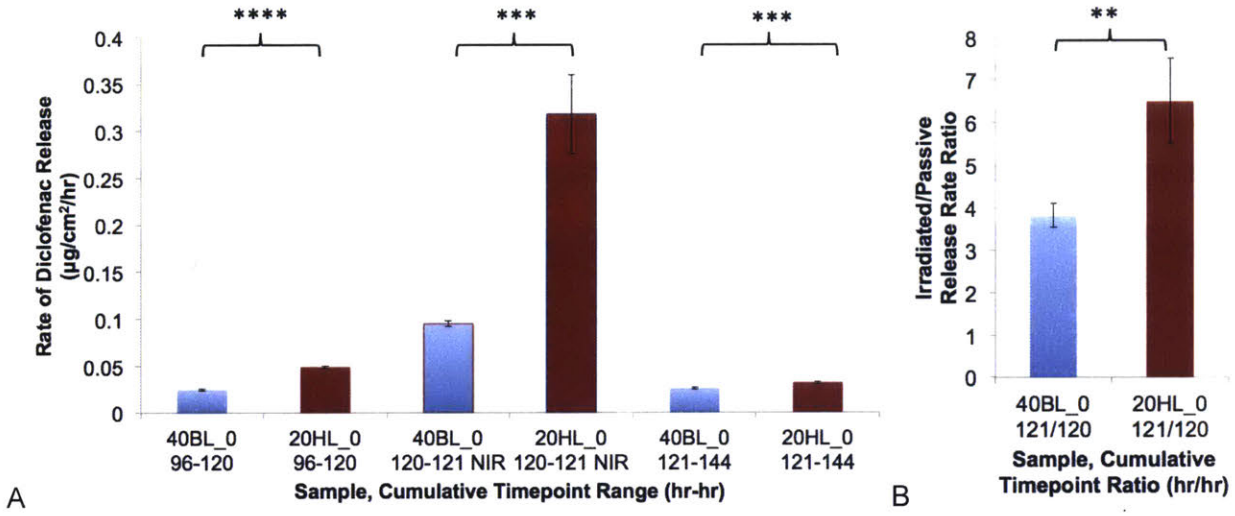

Figure 2.3. Comparison of diclofenac release rates from forty-bilayer ($40BL_0$) and twenty-hexalayer ($20HL_0$) Layer-by-Layer films (i.e. without base layers) quantified by high performance liquid chromatography showed the potential advantage of incorporating nanorods into films. A. For films not containing base layers, the passive release rates and near-infrared irradiated release rates of diclofenac were compared between films containing gold nanorods ($20HL_0$) and those not containing gold nanorods ($40BL_0$). B. To elucidate the effect of irradiation on the relative release rate of diclofenac from the Layer-by-Layer films, the ratio of the irradiated release rate to the passive release rate was taken for the bilayer control films and the hexalayer films. While the release rate was 3.8 times greater when irradiating films that did not contain gold nanorods, this enhanced release rate effect was significantly greater for gold-nanorod nano-blend films at 6.5 times the passive release rate. Analysis for statistical significance was determined by paired two-tailed t-tests assuming unequal variances (ns: $p > 0.05$; *: $p \leq 0.05$; **: $p \leq 0.01$; ***: $p < 0.001$; ****: $p < 0.0001$).

Both the passive release rate and the near-infrared irradiated release rate were significantly greater for the $20HL_0$ films than for the $40BL_0$ films (Figure 2.3A). To clarify the effect of the gold nanorods on the release rate of therapeutic from the films, the ratios of the irradiated release rate to the passive release rate for $40BL_0$ and $20HL_0$ were compared (Figure 2.3B). For both nanorod-containing films and bilayer control films, near-infrared irradiation caused a significant increase in therapeutic release rate during the timeframe of the irradiation. Therefore, the films responded to the near-infrared stimulus even without nanorods present.

Films containing nanorods demonstrated release rate enhancement by near infrared significantly greater than the bilayer control.

Following this promising first comparison, all subsequent films were built on top of non-degradable base layers to facilitate uniform adhesion of the films to the substrate and film growth.[39] These base layers consisted of ten bilayers of linear polyethylenimine with poly(sodium 4-styrenesulfonate) $(LPEI/SPS)_{10}$. A freeze-fractured scanning electron microscopy cross-section of a hexalayer film built on polymer base layers demonstrated the random distribution and dispersion of nanorods throughout the film thickness (Figure 2.4, Figure A.7).

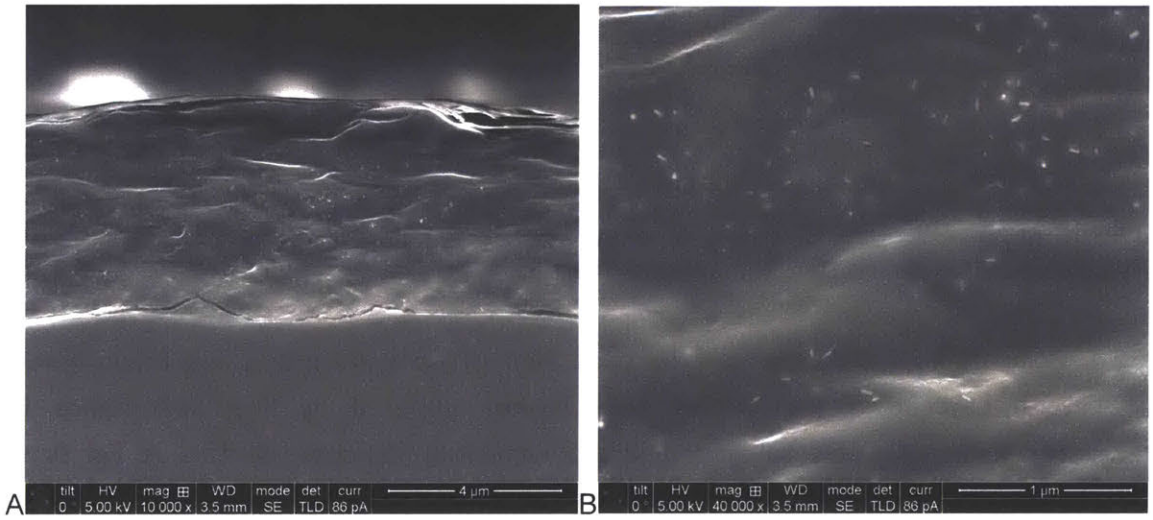

Figure 2.4. Gold nanorods were initially distributed in a nano-blend throughout the thickness of the hexalayer film. This hexalayer film was fabricated on top of polyelectrolyte base layers on un-polished silicon, flash-frozen by immersion in liquid nitrogen for 30 seconds, and fractured to reveal this freeze-fractured cross-section of the film. The film cross-section was then coated with 10 nm of carbon before imaging. Images obtained by scanning electron microscopy (Helios NanoLab™ DualBeam™). A. Scale bar: 4 µm. B. Scale bar: 1 µm.

Twenty-hexalayer and forty-bilayer films were investigated at release time points relevant to the 72-hr acute inflammatory phase of wound healing. The irradiated/passive release rate ratios demonstrated that for this particular twenty-hexalayer film architecture, there was no enhancement in the release rate above the control at the 24-hr mark (Figure 2.5). However, after three days the near-infrared-enhanced release rate ratio was significantly greater for the films containing nanorods than for the films that did not contain nanorods (Figure 2.5).

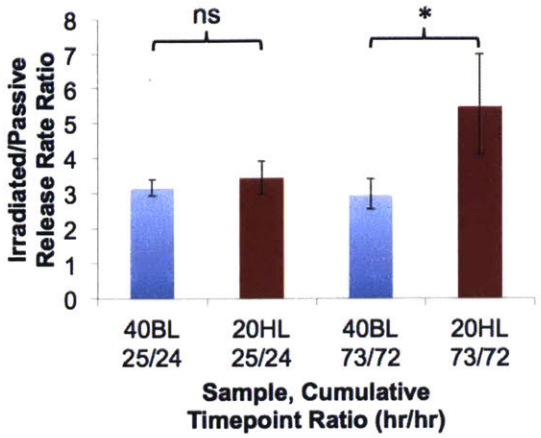

Figure 2.5. Comparison of the irradiated/passive release rate ratios for the forty-bilayer (40BL) and twenty-hexalayer (20HL) systems quantified by high performance liquid chromatography demonstrated kinetic effects on the relative efficacy of gold nanorod-containing films. At 24 hr, at the potential peak of the inflammatory stage of wound healing, the gold nanorods in the film did not add an additional increase in release rate above control. However, at the three-day mark, there was a significant increase in release rate above bilayer control. Analysis for statistical significance was determined by paired two-tailed t-tests assuming unequal variances (ns: $p > 0.05$; *: $p \leq 0.05$; **: $p \leq 0.01$; ***: $p < 0.001$; ****: $p < 0.0001$).

2.2.2. Mechanism of Kinetic Variation in Performance with Respect to the Gold Nanorod Component

The colloidal dispersion of gold nanorods in these films was not stable due to the type of coating on the nanorods. Gold nanorods non-covalently suspended with cetyltrimethyl-ammonium bromide (CTAB) were not stable against aggregation. During incubation in 10 mM phosphate buffered saline, the gold nanorods in the film were shuttled towards one another to form aggregates. Due to the swollen nature of the film (at least 38 ± 12%)[17] and the non-covalent interaction between the CTAB and the nanorods, in addition to the multiple interacting film components, the gold nanorods were mobile within the film. Through a shuttling mechanism involving exchange between for example the amine groups of poly(L-lysine) and CTAB interacting with the gold nanorod surface, plus attractive forces between the nanorods, aggregates formed over time. This aggregation phenomenon was observed by scanning electron microscopy for twenty-hexalayer films (Figure 2.6).

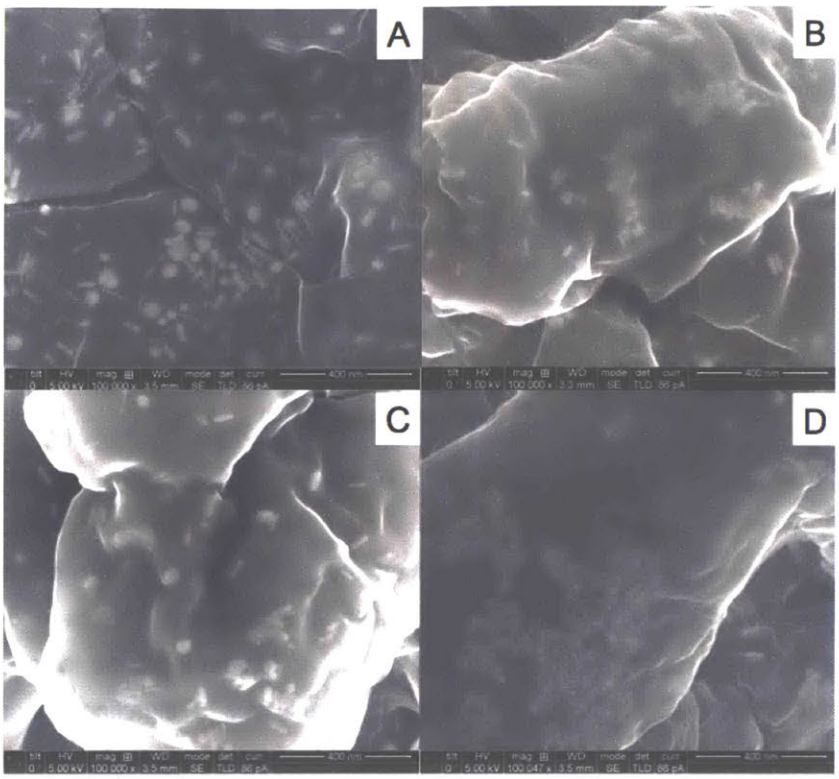

Figure 2.6. Scanning electron microscopy images of twenty-hexalayer (20HL) film surface after successive post-fabrication treatments illustrated progressive nanorod aggregation. Scale bar: 400 nm. A. Initially, gold nanorods were dispersed in the 20HL film at a high density, at close proximity and random orientations. B. After incubation of the film for 24 hr at 37°C in 10 mM phosphate buffered saline, aggregates of gold nanorods began to form. C. During the next stage of treatment for the film, i.e. near-infrared irradiation (980 nm, 0.697 W/cm^2, 60 min, 37°C, 1x PBS), the gold nanorod aggregates did not grow significantly in size. D. Subsequent incubation for an additional 24 hr at 37°C in 1x PBS yielded nanorod aggregates in the film consisting of at least one hundred nanorods.

The fact that the extent of nanorod aggregation varied with time explained how the gold nanorod-containing films did not perform better than the bilayer films at 24 hr after beginning release conditions, but improved in performance after 72 hr (Figure 2.5). This improved performance was postulated to be due to the increase in photothermal-responsive gold nanorod aggregates that absorbed in resonance with the 980 nm laser stimulus (Figure A.12).

2.2.3. Effect of Tissue Mimic Thickness on Therapeutic Release Rate During Near-Infrared Irradiation

The films in this study, whether containing nanorods or not, were active in the near infrared. Irradiation with a laser at 980 nm caused a contemporaneous enhancement in the release of therapeutic from these films. Due to the bio-transparent nature of the 980 nm wavelength, it was hypothesized that these enhanced release effects would be maintained even in the presence of a breast tissue mimic as a barrier between the laser and the sample (Figure 2.7). A breast tissue mimic was used for testing twenty-hexalayer films due to the projected application of these films in translation. The medicinal objective of these photo-responsive films with high therapeutic loading was the modulation of acute wound healing in deep tissue to prevent fibrosis, for example from a blast wound to the chest in battle.

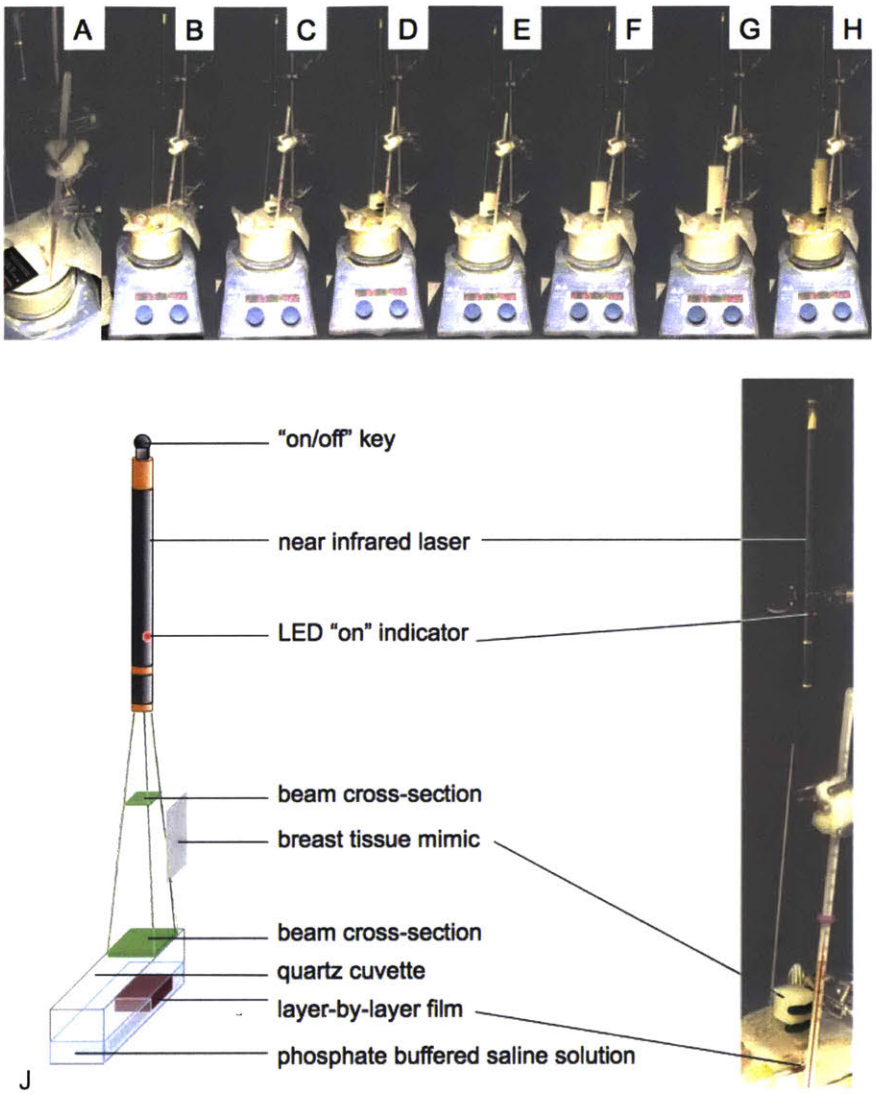

Figure 2.7. A-H. Photographs of near-infrared irradiation apparatus for twenty-hexalayer Layer-by-Layer films in 10 mM phosphate buffered saline held at 37°C in a sand bath. A. Alignment of near-infrared laser with Layer-by-Layer film sample using detector card. B. Near-infrared irradiation apparatus without any tissue mimic barrier (see also Scheme 2.3, Scheme 2.4). Breast tissue mimics were used as barriers between the irradiating laser and the film sample with thicknesses: C: 2 cm; D: 3 cm; E: 5 cm; F: 7 cm; G: 10 cm; H: 12 cm. J. Schematic diagram of the breast tissue mimic barrier apparatus.

Regardless of the tissue thickness down to at least 12 cm, which was a substantial tissue penetration depth, the twenty-hexalayer samples were photo-responsive to the same extent as when no breast tissue mimic barrier was present (Figure 2.8). These films therefore operated at high tissue penetration depths with a non-invasive stimulus.

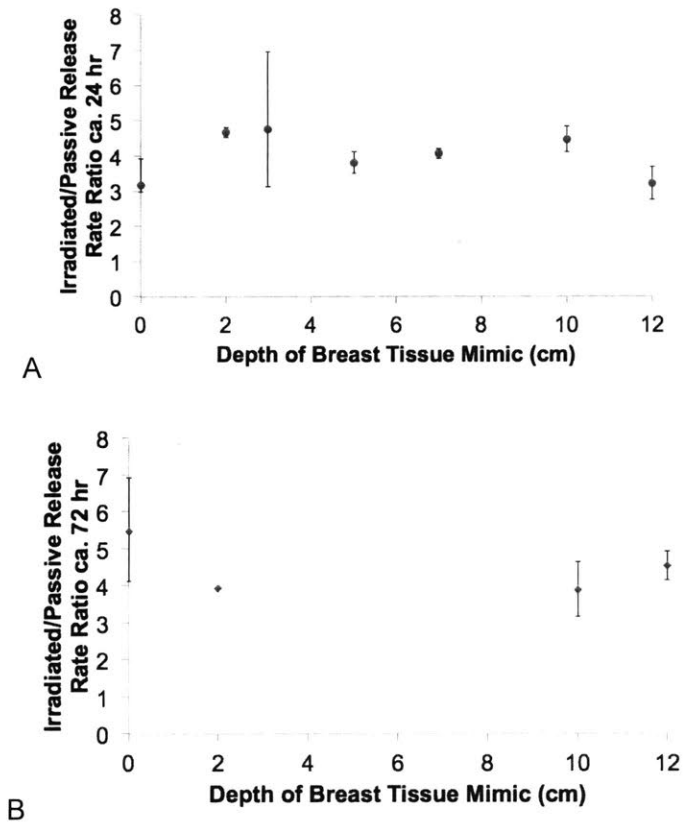

Figure 2.8. As the breast tissue mimic barrier thickness was increased up to 12 cm, there was no attenuation of near-infrared enhanced therapeutic release effects in twenty-hexalayer (20HL) films. This resulted from the bio-transparent nature of the 980 nm laser. This enhancement was maintained at both 24 hr (A) and 72 hr (B) cumulative release time points. Release rates were quantified by high performance liquid chromatography (HPLC).

2.2.4. Increased Diclofenac Loading in Films to Obtain Cyclooxygenase Inhibition Above the IC_{50} Value on a One-Hour Timescale During Near-Infrared Irradiation

The intended release profile from these films included slow passive release of diclofenac such that the hourly concentration eluted fell well below the IC_{50} value for cyclooxygenase, and release of diclofenac at least at the IC_{50} value during near-infrared irradiation. The IC_{50} value is the concentration of the inhibitory therapeutic (diclofenac) that inhibits the target activity (cyclooxygenase) by at least 50%. This functionality was targeted during the 72-hr time window representing acute inflammation during wound healing. It was determined that twenty-hexalayer and forty-bilayer films irradiated with near infrared had enhanced release rates of diclofenac

(Figure 2.3, Figure 2.5). However, the diclofenac concentration released with irradiation still fell below the IC_{50} value for cyclooxygenase (Figure A.10).

To improve the system, forty-hexalayer (40HL) and eighty-bilayer (80BL) films were fabricated with twice the therapeutic loading as in the 20HL and 40BL films. The films were successfully employed to remotely administer two doses of anti-inflammatory close to or above the IC_{50} value of cyclooxygenase *in vitro* during the first 72 hours of release, corresponding to the acute inflammatory phase of would healing (Figure 2.9). After the 72-hr time point, a low dose of anti-inflammatory continued to release at a declining rate on longer time scales with the objective of locally alleviating pain during the healing process for traumatic wounds.

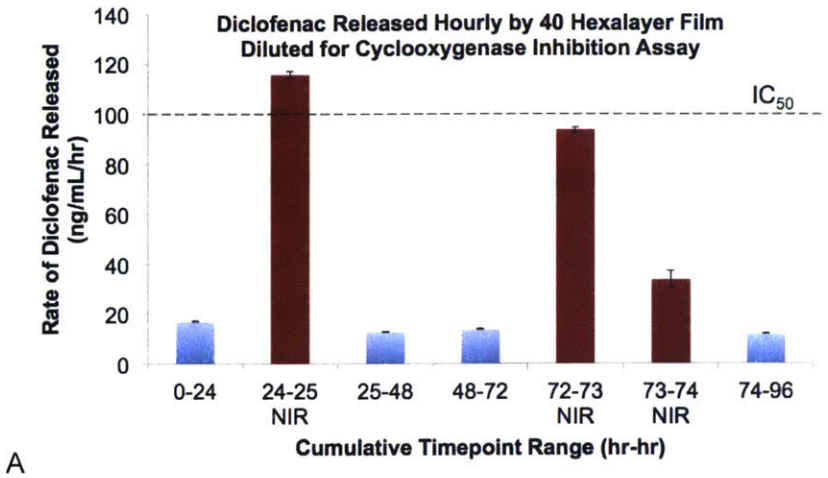

A

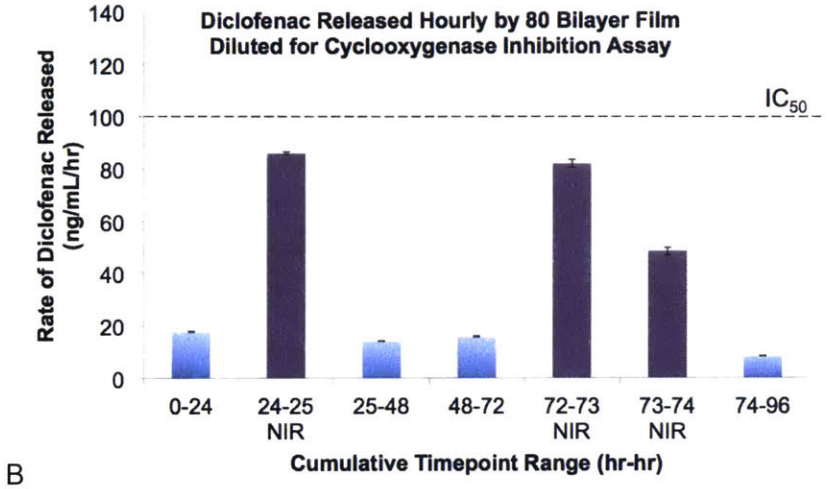

B

Figure 2.9. A. During the 72-hr timeframe corresponding to acute inflammation, forty-hexalayer films were utilized to successfully administer two on-demand doses of the non-steroidal anti-inflammatory therapeutic diclofenac at levels above or approaching the IC_{50} value for cyclooxygenase *in vitro*. These doses were dispensed remotely by irradiation with near-infrared laser. B. Eighty-bilayer films under identical treatment conditions released two laser-enhanced doses that approached but did not exceed the IC_{50} value for cyclooxygenase-1 *in vitro*. Due to cyclooxygenase-2 selectivity,[40] the irradiated doses all exceed the IC_{50} value of the induced enzyme.

The variation in performance of the forty-hexalayer (40HL) gold nanorod films over time (Figure 2.10) followed a pattern consistent with that observed in the 20HL films (Figure 2.5) that was similarly attributed to the gold nanorod aggregation phenomenon (Figure 2.6). In hexalayer films, there was a time-dependent distribution of absorbing entities that comprised clusters of gold nanorods at various orientations with respect to one another and to the irradiating laser

source (Figure 2.6). Due to plasmon coupling effects, the absorption spectra of the films were altered during the course of aggregation (Figure A.12). It was hypothesized that at the observed time points where the hexalayer films out-performed the bilayer films, the greatest number of aggregate entities absorbing in resonance with the 980 nm laser source existed.

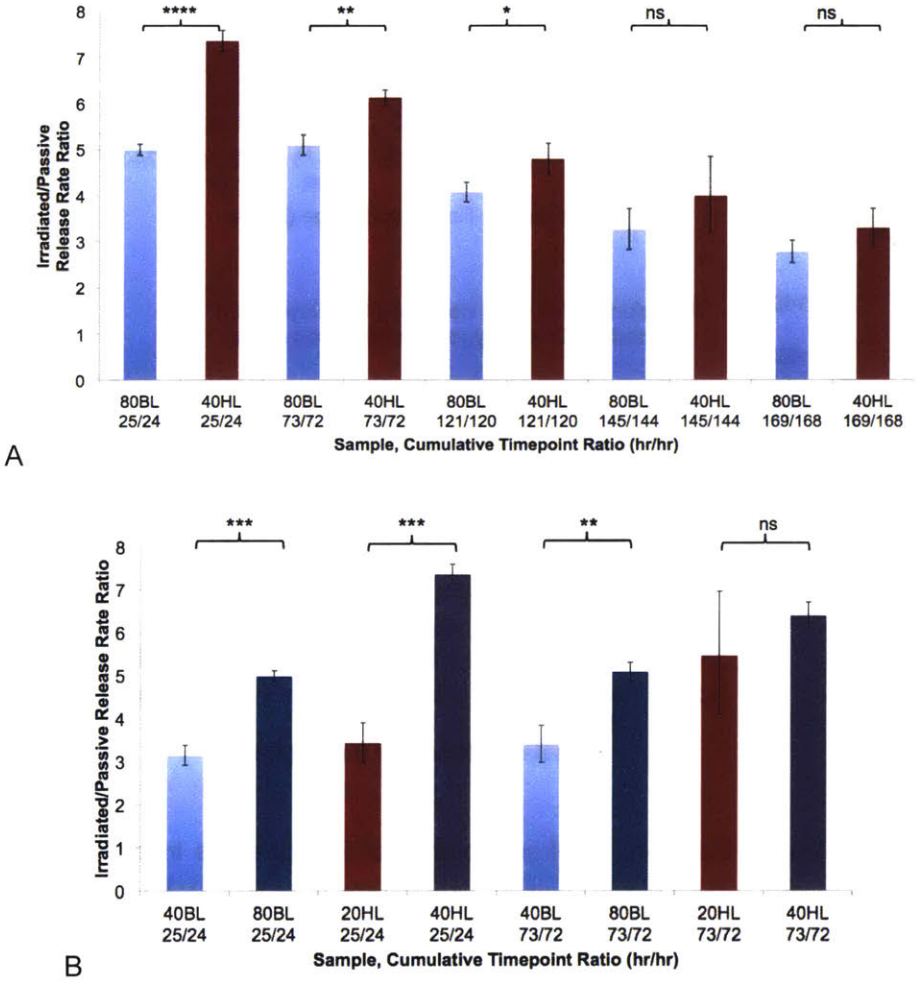

Figure 2.10. Comparison of therapeutic release rates demonstrated that due to the aggregation behavior of the gold nanorods (Figure 2.6), the hexalayer films were under more dramatic kinetic control than the bilayer films. A. 40HL films out-performed 80BL films during the 72-hr release timeframe. Irradiation by near infrared at later time-points demonstrated that the gold nanorod advantage disappeared over time in these films. B. Quantification by HPLC revealed that at both time-points examined in the range relevant to the inflammatory stage of wound healing, 80BL films exhibited a significantly greater irradiated/passive release rate ratio than 40BL films. Both film types 40BL and 80BL did not contain nanorods. On the other hand, while at 24 hr the 40HL film greatly out-performed the 20HL film during near-infrared irradiation, at 72 hr the 20HL film performed on par with the 40HL film.

2.2.5. Elucidation of the Mechanism of Enhanced Diclofenac Release *via* Near-Infrared Irradiation of Bilayer Films Alone

By examining more closely the feature of enhanced diclofenac release rates by near-infrared irradiation of bilayer films alone, the mechanism of enhanced release began to be elucidated. In particular, the results of treatments with repeated successive irradiations were informative (Figure 2.11).

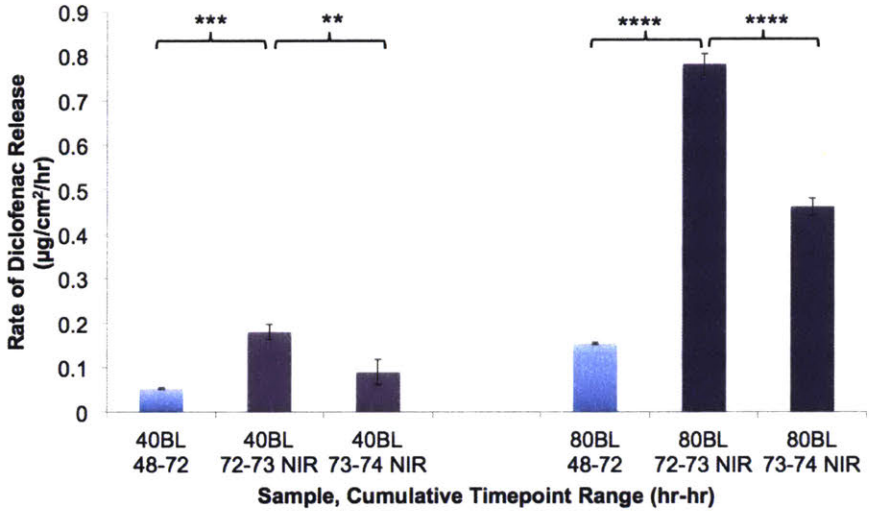

Figure 2.11. The diminishing diclofenac release rate enhancement from the first irradiation to the second successive irradiation of bilayer films implied depletion of free molecule stored within the film. If the main mechanism of enhancement were instead related to hydrolysis of diclofenac from the polymer-drug conjugate, the enhancement during the first irradiation would have been at least matched by the second successive irradiation since the rate of hydrolysis in aqueous media is an increasing function of temperature.

From this pattern of diminishing returns from irradiation over time, the primary mechanism was deduced to be an emptying of reservoirs of free diclofenac molecules stored in the film. A secondary mechanism was reasoned to be enhanced hydrolysis at an elevated temperature. If on the other hand enhanced hydrolysis had dominated, the mechanism would enable sustained enhanced release rates over time as opposed to the diminishing rates with continued irradiation that were observed (Figure 2.11). To determine how the free diclofenac molecules were stored in the film and exhibited delayed release behavior, the behavior of the polymer-drug conjugate poly(L-glutamic acid-triethylene glycol-diclofenac) (PGA-Diclof) was examined.

Due to the amphiphilic nature of PGA-Diclof, micellar aggregates consisting of several polymer molecules formed above the critical micelle concentration (CMC). Above the CMC, there was a thermodynamic equilibrium between micelles and unimers i.e. individual polymer chains. The micelle cores were comprised of associating hydrophobic diclofenac-triethylene glycol (Scheme 2.1) side groups, and the coronas were the hydrophilic anionic glutamic acid side groups along the polymer chains. The presence of micelles was macroscopically observable by the high viscosity of the PGA-Diclof Layer-by-Layer (LbL) precursor solution, and was confirmed by dynamic light scattering (DLS) measurements.

This polymer chain design, i.e. hydrophobic side chains with a triethylene glycol linker and ester linkages, can be considered for any application where a small molecule hydrophobic drug needs to be released locally at a slow timescale.[17] Other hydrophobic side chain polymer-drug conjugates with ester linkages but without a triethylene glycol linker released much more quickly.[41] The presence of the triethylene glycol linker was key to decreasing the critical micelle concentration of the polymer-drug conjugate. Micelle formation slowed hydrolysis by minimizing the interfacial area of the polymer-drug ester linkages with the aqueous phase. Temperature-responsive Layer-by-Layer films including block copolymer micelles and loaded with hydrophobic molecule pyrene showed similar diminishing-rate release profiles to those observed with the current bilayer films.[42]

When assembled into the LbL film, the polycation poly(L-Lysine) (PLL) electrostatically associated with the PGA-Diclof unimers facilitated hydrolysis of the ester linkages binding the diclofenac, but during the diffusion process out of the film a portion of free diclofenac became sequestered in PGA-Diclof micelles within the film. This sequestration slowed the passive release process considerably. This hypothesis of mechanism can initially be tested by incubation of films with pyrene[43] and performing fluorescence microscopy on the films to observe the pyrene elution behavior from the micelles. Diclofenac is also fluorescent so the drug itself might also be visible under fluorescence microscopy.

The partition coefficient is a quantity reflecting the relative concentrations of a molecule in the hydrophobic and hydrophilic phases in a system. Among other factors, the partition coefficient is a function of temperature and degree of ionization. The pK_a of diclofenac sodium at 37°C is 4.41,[44] so the assumption of near-complete ionization at pH 7.4 assembly and release solution conditions was made. The partition coefficient for diclofenac into octanol vs. water in its ionized form at 37°C is 1.9953,[45] meaning that twice the concentration of diclofenac was found in the hydrophobic phase vs. the hydrophilic phase. In a study of prodrugs made with diclofenac

attached by ester to different oligomer lengths of polyethylene oxide groups, triethylene glycol-diclofenac was found to have a significantly greater partition coefficient than diclofenac alone.[46] In addition, in the presence of protonated amine groups, hydrophobic interactions have been found to strengthen two-fold.[47] Therefore it is hypothesized that the diclofenac and triethylene glycol-diclofenac partition coefficients into the triethylene glycol-diclofenac hydrophobic cores are even higher in the Layer-by-Layer films than in solution.

Even in the ionized form, a significant fraction of hydrolyzed diclofenac therefore resided in the hydrophobic triethylene glycol-diclofenac phases within the film during passive release. The energy imparted by the near-infrared irradiation caused an emptying of free drug from the intra-film hydrophobic compartments and enabled diffusion of free diclofenac out of the film.

Over time, as more diclofenac was hydrolyzed from the poly(L-glutamic acid) unimers, more negative charges emerged along the polymer chain, repelling one another and increasing the swelling of the film. This increased swelling can be confirmed by spectroscopic ellipsometry. There were also fewer triethylene glycol-diclofenac moieties exposed for hydrolysis over time, resulting in a declining passive release rate as has been observed in this and previous study.[17]

One aspect of film assembly that may have contributed to the highly enhanced release rates in the 24-hr and 72-hr timeframes was the duration of dip Layer-by-Layer fabrication. The two-to-four day self-assembly process for forty-to-eighty bilayer films by near-continuous incubation in aqueous solutions allowed for hydrolysis of free diclofenac from unimers in the film and accumulation into the hydrophobic micelle cores within the film before commencing release studies. This may in part have explained why diclofenac release from 80BL films was enhanced five-fold, but only three-fold for 40BL films that were assembled in half the time. 80BL films also absorbed more strongly in the near infrared than 40BL films, as expected (Figure A.5).

Applying the spray Layer-by-Layer (LbL) deposition method to these films was hypothesized to produce films that are smooth[48] and lend themselves to coating by a clay barrier layer[21] to limit passive diclofenac release (Appendix B). Spray deposition also dramatically decreases film assembly time.[49] Upon fabrication of these polymer multilayer films by rapid spray-assisted LbL, the films can potentially be incubated with free hydrophobic drug to sequester it into the film. The drug would be incubated with the film rather than with a PGA-Diclof solution due to the hypothesized higher partition coefficient in the films, with protonated amines from PLL strengthening the hydrophobic interactions.[47] Both solution and film incubation

methods could be attempted and compared to support the hypothesis of film-enhanced diclofenac partition coefficient.

The micellar structure of the polymer-drug conjugate lends itself to delivery with multiple hydrophobic drug payloads simultaneously. Hydrophobic drugs of different identities can potentially be sequestered into the micelles. To build on this system further, hydrophobic small molecule drugs can be incorporated with spatiotemporal control by a clay barrier layer in between in order to have a staggered release profile.[21]

2.3 Conclusions

Near-infrared responsive behavior was observed in Layer-by-Layer films of biocompatible poly(L-lysine) (PLL) and polymer-drug conjugate poly(L-glutamic acid-triethylene glycol-diclofenac) (PGA-Diclof). Due to the amphiphilic nature of the PGA-Diclof and assembly above the critical micelle concentration, a mixture of unimers with accelerated hydrolysis due to proximal protonated amines and intact micellar aggregates were present in the film.

The protonated amine groups provided by the PLL served to strengthen the hydrophobic interactions of diclofenac-triethylene glycol pendant groups in the film and to partition hydrolyzed diclofenac preferentially into the micelle cores within the film, resulting in a slow passive elution of drug from the film. Energy imparted by near-infrared irradiation at 980 nm freed the untethered diclofenac molecules from the micelle reservoirs and allowed them to escape from the film by diffusion. Inhibition of cyclooxygenase by the near infrared-released diclofenac was maintained *in vitro.*

Inclusion in the film of gold nanorods coated with surfactant and polymer was found to increase the rate of release of diclofenac only at certain time points during incubation due to the progression of nanorod aggregation with time. The enhancement of release rate from gold nanorod-containing films was maintained to at least 12 cm tissue penetration depth. With high loading and slow release rates of diclofenac, near-infrared-activated therapeutic release rate was increased to reach the IC_{50} value of the target for inhibition of cyclooxygenase.

Clay barrier layers did not decrease the passive release profile of the diclofenac due to the micron-scale roughness of the films (Figure B.3). These films can potentially be improved by changing the mode of fabrication to spin-[49] or spray-assisted[50] Layer-by-Layer to result in smoother films that would allow modification of the release profile with clay barrier layers. These films could then be tested for increased activated/passive release rate ratios.

Due to the modular character of Layer-by-Layer assembly, is possible to build upon this technology for anti-fibrotic applications. There has been found to be a TGF-β-independent increase in collagen deposition in the progression towards pulmonary fibrosis in fibroblasts overexpressing lysosomal sialidase (NEU-1).[4] Due to the charged nature of ribonucleic acids, small interfering ribonucleic acids (siRNA) against NEU-1 expression can potentially be included in the Layer-by-Layer film from this work. More broadly, the use of near infrared as a tool to modulate release kinetics from hydrophobic compartments should be explored further for applications like remotely controlled enhanced release of therapeutics at high tissue penetration depth.

2.4 Acknowledgments

This work was supported in part by the National Science Foundation Graduate Research Fellowship Program, and by funding and core facilities provided by the U.S. Army Research Office under contract W911NF-07-D-0004 at the MIT Institute of Soldier Nanotechnologies. This work was also supported by the Massachusetts Institute of Technology Materials Processing Center, the Koch Institute for Integrative Cancer Research, and the MRSEC Program of the National Science Foundation under grant number DMR-14-19807. This work made use of the Center for Materials Science and Engineering Shared Experimental Facilities. Shiahn Chen assisted with scanning electron microscopy. Christian Soule and Jaime Cheah assisted with cyclooxygenase assay in The High Throughput Screening Core supported in part by funding provided to the Koch Institute from a National Cancer Institute Cancer Center Support Grant.

2.5 Materials and Methods

All materials were obtained from Sigma-Aldrich unless indicated otherwise.

Synthesis of gold nanorods: Based on the methods of Nikoobakht and El-Sayed,[51, 52] seed-mediated growth of gold nanorods was conducted at 25°C from freshly prepared aqueous solutions in 18.2 MΩ•cm Milli-Q® water. Stirring in a 50 mL Erlenmeyer flask, 2.75 mL of 1.00 mM Gold chloride trihydrate ($HAuCl_4 \bullet 3H_2O$) was added to 5.5 mL of 0.200 M cetyltrimethyl-ammonium bromide (CTAB). To this, 600 µL of ice-cold 10 mM sodium borohydride ($NaBH_4$) was added and this stirring mixture was allowed to react for several minutes and form the seed solution, pale brown-gold in color. To form the transparent growth solution, three batches were made in 250 mL Erlenmeyer flasks with the following in each: 100 mL of 1.00 mM $HAuCl_4$ was added to 100 mL of 0.200 M CTAB and 5.5 mL of 4.00 mM silver nitrate ($AgNO_3$), and then 1.4 mL of 78.8 mM L-ascorbic acid was added followed by gentle swirling until colorless.

Following the separate formation of seed and growth solutions, 160 μL of the seed solution was added to each non-stirring growth solution and allowed to react in stationary position for 2 hr. Nanorods synthesized by this method were approximately 12 nm in width and 50 nm in length (aspect ratio 4.0) (Figure A.1) and had a longitudinal plasmon absorption maximum at 865.5 nm (Figure A.2). Gold nanorods were centrifuged in 50-mL tubes at 3,100 RCF for 60 min and re-suspended in 16 mL of 18.2 MΩ•cm water to remove excess CTAB molecules. Gold nanorod solutions were stable in this form at room temperature for at least several months.

Coating the gold nanorods with poly(4-styrenesulfonic acid), sodium salt (PSS): Poly(4-styrenesulfonic acid), sodium salt (PSS, MW ~ 18 kDa, M_w/M_n ~ 1.10) was purchased from Polysciences, Inc. This protocol was adapted from that of Gole and Murphy.[36] PSS was dissolved at 5 mg/mL in 50 mL of 0.01x PBS. This solution was transferred into four 20-mL vials. The gold nanorod solutions were briefly and gently heated to 28°C (3-5 minutes) to re-dissolve CTAB crystallites. While stirring each of the 12.5 mL solutions, gold nanorod solution was added drop-wise until an optical density of about 0.1 was reached or until precipitates persisted for a few seconds. All three batches of purified gold nanorods were combined together for coating with PSS. These stirring suspensions were left for 60 min at room temperature. Centrifugation in two 50 mL tubes at 3,100 RCF for 15 min followed, and the supernatant was removed and stored at 4°C for possible later centrifugation to isolate more nanorods. The pellet was re-suspended in ~200 uL of 18.2 MΩ•cm water, bringing the total volume of the final AuNR solution to ~500 uL. Suspensions of AuNRs coated in PSS were stored at 4°C until further use. Within one week these suspensions were diluted to 0.5 nM in 0.01x PBS and used for Layer-by-Layer (LbL) assembly. These diluted solutions were stored at 4°C and reused post-LbL.

Synthesis of triethylene glycol-diclofenac prodrug: Synthesis of the triethylene glycol-diclofenac prodrug was carried out as described previously by Hsu et al.[17, 46] at a two-fold scale. The product was purified by flash silica gel column chromatography using 50:50 ethyl acetate:hexanes as the eluent solution. Solvent was removed under vacuum from the purified product. Triethylene glycol-diclofenac ^{1}H NMR (400 MHz, $CDCl_3$) δ 7.33 (d, *J* = 8.1 Hz, 2H), 7.24 (dd, *J* = 7.5, 1.3 Hz, 1H), 7.11 (td, *J* = 7.8, 1.4 Hz, 1H), 7.02 – 6.86 (m, 3H), 6.54 (d, *J* = 8.0 Hz, 1H), 4.31 (dd, *J* = 5.4, 4.1 Hz, 2H), 3.85 (s, 2H), 3.72 (dd, *J* = 5.3, 4.3 Hz, 4H), 3.66 – 3.48 (m, 6H), 2.49 (s, 1H). Triethylene glycol-diclofenac ^{13}C NMR (101 MHz, $CDCl_3$) δ 172.47 (s), 142.86 (s), 137.90 (s), 131.02 (s), 129.68 (s), 128.94 (s), 128.08 (s), 124.31 (s), 124.15 (s), 122.04 (s), 118.27 (s), 72.55 (s), 70.68 (s), 70.39 (s), 69.06 (s), 64.36 (s), 61.82 (s), 38.55 (s).

Synthesis and characterization of polymer-drug conjugate for therapeutic loading: Poly(L-glutamic acid) (PGA, molecular weight 50-100 kDa) was purchased from Sigma-Aldrich. Synthesis of the polymer-drug conjugate was carried out as described previously by Hsu et al.[17, 46, 53] at a three-fold scale. Poly(L-glutamic acid-triethylene glycol-diclofenac) ^{1}H NMR (400 MHz, D_2O) δ 7.39 – 6.38 (m, 7H), 6.20 (s, 1H), 4.50 – 3.87 (m, 6H), 3.87 – 3.11 (m, 13H), 2.76 – 1.68 (m, 7H).

The degree of diclofenac conjugation to the poly(L-glutamic acid) was determined by incubation of 400 μg/mL PGA-TriEG-Diclof in 500 μL of 0.1 M sodium hydroxide overnight at 37°C, quenching with 500 μL of 0.1M hydrochloric acid, and then quantification by HPLC. It was determined that 17.75 wt% of the polymer comprised repeat units functionalized with diclofenac (vs. 19.5% in the literature).

Materials for dip Layer-by-Layer assembly: Linear polyethylenimine (LPEI, molecular weight 25 kDa) was obtained from Polysciences, Inc. Poly(L-lysine) hydrobromide (PLL, molecular weight 30-70 kDa) and poly(sodium 4-styrenesulfonate) (SPS, molecular weight 1 MDa) were purchased from Sigma-Aldrich. Alkaline earth boro-aluminosilicate glass substrates (0.7 × 7 × 50 mm) were obtained from Delta Technologies, Ltd. All of the Layer-by-Layer assembly protocols took place at room temperature and ambient pressure.

Fabrication of Layer-by-Layer films without base layers: Glass substrates were plasma treated for 10 minutes and then immediately dipped into poly(L-lysine) solution at 1 mg/mL in 10 mM sodium phosphate buffer at pH 7.4. The glass substrates were incubated in the solution for 20 minutes, and then the regular dipping program was subsequently employed. This started with an additional 10 min in the poly(L-lysine) bath. Onto this base layer of PLL, films were built 20 bilayers or 10 hexalayers at a time, switching out polyelectrolyte solutions for fresh ones between rounds. One sequence in a bilayer program consisted of 10 min incubation in polycation (PLL); 30 s, 60 s, and then 90s-with-agitation rinses in 18.2 MΩ•cm Milli-Q® water; 10 min incubation in polyanion (PGA-Diclof) at 1 mg/mL in 10 mM sodium phosphate buffer at pH 7.4; and finally 18.2 MΩ•cm water rinses (30, 60, 90s). The hexalayer sequence contained the same dipping programs for the polymers and every sixth layer added a 30-minute dip in gold nanorod-poly(4-styrenesulfonic acid) (AuNR-PSS) at 0.5 nM in 0.01x PBS followed by 18.2 MΩ•cm water rinses (30s, 60s, 90s-with-agitation).

Fabrication of Layer-by-Layer films containing base layers: Following plasma treatment of glass substrates for ten minutes, the substrates were immediately immersed in

linear poly(ethyleneimine) (LPEI) at 10 mM in Milli-Q® water with resistivity 18 MΩ•cm at pH 4.25 and incubated at room temperature for 20 minutes before starting an alternating dip program. The base layer dip program consisted of repeating cycles of: 10 minutes in LPEI; rinses in Milli-Q® for 30s, 60s, and 90s-with-agitation; 10 minutes in poly(sodium 4-styrenesulfonate) (SPS) at 10 mM in Milli-Q® with resistivity 18 MΩ•cm at pH 4.75 for 10 minutes; and rinses in Milli-Q® for 30s, 60s, and 90s-with-agitation. This was followed with the bilayer or hexalayer dip protocol above.

Passive release of diclofenac from Layer-by-Layer films: Each fabricated film studied for diclofenac release was individually immersed in 1 mL of 10 mM phosphate buffered saline (1x PBS) in a cylindrical 2 mL centrifuge tube, suspended horizontally for the purpose of total immersion in the release solution. This setup was incubated at 37°C. After subsequently moving the sample to fresh 1x PBS solution, the release solution was stored at -20°C until characterization by high performance liquid chromatography (HPLC) and/or cyclooxygenase (COX) inhibition assay.

Near-infrared irradiation release of diclofenac from Layer-by-Layer films: In a laser housing, a sand bath was heated to 37°C until reading stable by thermocouple and thermometer. In a quartz cuvette, 1 mL of 1x PBS preheated to 37°C was prepared. The following steps were conducted efficiently to minimize error in therapeutic release rate results.

The sample to be irradiated was transferred from the previous release solution into the quartz cuvette with transparency in the near infrared. The cuvette was then sealed by polytetrafluoroethylene (PTFE) stopper and reinforced with laboratory tape and Parafilm M® to prevent leakage. The previous release solution was stored at -20°C. The cuvette was placed horizontally onto lens paper on top of the heated sand to prevent scratching of the quartz.

Associated near-infrared laser protective eyewear was employed. The portable near-infrared laser (980nm, 400mW) was loaded with new AAA batteries and positioned vertically with the aperture facing the sample, clamped at a pre-determined height to achieve a time-averaged power density of 0.697 W/cm^2 hitting the sample. The laser was switched on and using an infrared detector card, the laser cross-section was aligned with the Layer-by-Layer film. After alignment, the laser housing was closed and the timer set for 60 minutes.

Upon completion of the 60 min irradiation (980 nm, 0.697 W/cm^2), the sample was transferred to a cylindrical 2 mL centrifuge tube containing a fresh 1 mL of 1x PBS preheated to

37°C. This was replaced horizontally in the 37°C incubator for further passive release. The release solution from the 60 min laser irradiation was stored at -20°C until characterization.

Irradiation of samples was also attempted for durations of 15 and 30 minutes under the same conditions (980 nm, 0.697 W/cm^2, 37°C, 1x PBS). Resultant diclofenac concentrations in the release solutions fell below the detection limit of the HPLC fluorescence detector.

Analyzing diclofenac release rates from Layer-by-Layer films using high performance liquid chromatography (HPLC): Diclofenac standards at 0.2 mg/mL, 0.02 mg/mL, 0.002 mg/mL, and 0.0002 mg/mL in Milli-Q® water at resistivity 18 MΩ•cm were prepared and stored at -20°C until use. To facilitate initial dissolution of diclofenac sodium salt (TCI America) at 1 mg/mL to prepare the standards, 20 µL of 1 M sodium hydroxide was added to an approximately 30 mL solution in a 50 mL polypropylene centrifuge tube and the tube was inverted to dissolve the sample. Samples and standards were thawed from -20°C and 600 µL of each sample were filtered through HPLC-certified 13 mm nylon membrane syringe filters with 0.2 µm pore size (Minispike Acrodisc®, Pall Laboratory) into 2 mL HPLC-certified vials (Agilent). The nylon membrane material was chosen due to its hydrophilicity so as not to bind free diclofenac, its chemical compatibility with esters, and lack of pre-wetting required due to a small amount of sample.

The diclofenac concentrations in the release solutions were quantified by high performance liquid chromatography (HPLC) as described previously[17, 18, 54] using an Agilent 1100 series instrument suite and a reverse-phase Supelco Discovery® C18 HPLC Column (Sigma-Aldrich) with 5 µm particle size, length × inner diameter = 15 cm × 4.6 mm. The mobile phase employed was 70:30 of 1x PBS:acetonitrile (PBS:ACN) and the sample injection volume was 100 µL. Each sample was run for 15 min at 1 mL/min mobile phase. The fluorescence detector was used for quantification ($\lambda_{excitation}$ = 280 nm, $\lambda_{emission}$ = 355 nm). All samples were characterized in triplicate.

Preparation of hexalayer film for cross-sectional scanning electron microscopy (SEM): Silicon substrates were plasma-treated for 5 minutes before immersion in linear polyethylenimine for 20 minutes. Layer-by-Layer films were built on $(LPEI/SPS)_{10}$ base layers as described above. After completion of film fabrication, the silicon was scribed, the sample was flash-frozen by immersion in liquid nitrogen for 30 seconds, and then the scribe was propagated obtain a freeze-fractured cross-section. The sample was immediately mounted on a perpendicular SEM mount with carbon tape and stored at -20°C until use for SEM. Prior to

characterization by SEM, the film cross-section was carbon-coated with a 10-nm-thick coating using a vacuum evaporator (Denton) to prevent charging of the polymer matrix and allow contrast with the gold. SEM images were obtained with Helios NanoLab™ DualBeam™.

Preparation of twenty-hexalayer films for gold nanorod aggregation characterization by scanning electron microscopy (SEM): Twenty-hexalayer films were fabricated and treated with the same experimental conditions as those used to obtain high performance liquid chromatography and cyclooxygenase inhibition assay data. Following those treatments, each film was thoroughly rinsed with Milli-Q® by dipping for 1 and 2 minutes followed by flushing with a stream of Milli-Q® to remove salts from the 1x PBS release solution. Then each film was immersed in liquid nitrogen for 30 seconds, immediately mounted on a flat SEM stub with carbon tape and stored at -20°C until coating with 10 nm of carbon by vacuum evaporator and characterization by SEM.

Near-infrared irradiation for enhanced release of diclofenac from Layer-by-Layer films using a breast tissue mimic as a barrier: In addition to the standard irradiation protocol, alignment of the laser with a breast tissue mimic after alignment with the Layer-by-Layer film sample was conducted using an infrared detector card. The clamped breast tissue mimic was rotated and tightened into place while the laser and film sample remained stationary.

2.6 References

1. Wynn, T. A., Cellular and molecular mechanisms of fibrosis. *Journal of Pathology* **2008,** *214* (2), 199-210.
2. Leask, A.; Abraham, D. J., TGF-beta signaling and the fibrotic response. *Faseb Journal* **2004,** *18* (7), 816-827.
3. Daniels, C. E.; Wilkes, M. C.; Edens, M.; Kottom, T. J.; Murphy, S. J.; Limper, A. H.; Leof, E. B., Imatinib mesylate inhibits the profibrogenic activity of TGF-beta and prevents bleomycin-mediated lung fibrosis. *Journal of Clinical Investigation* **2004,** *114* (9), 1308-1316.
4. Luzina, I. G.; Lockatell, V.; Hyun, S. W.; Kopach, P.; Kang, P. H.; Noor, Z.; Liu, A. G.; Lillehoj, E. P.; Lee, C.; Miranda-Ribera, A.; Todd, N. W.; Goldblum, S. E.; Atamas, S. P., Elevated expression of NEU1 sialidase in idiopathic pulmonary fibrosis provokes pulmonary collagen deposition, lymphocytosis, and fibrosis. *American Journal of Physiology-Lung Cellular and Molecular Physiology* **2016,** *310* (10), L940-L954.
5. Mura, S.; Nicolas, J.; Couvreur, P., Stimuli-responsive nanocarriers for drug delivery. *Nature Materials* **2013,** *12* (11), 991-1003.
6. Huang, X. H.; Neretina, S.; El-Sayed, M. A., Gold Nanorods: From Synthesis and Properties to Biological and Biomedical Applications. *Advanced Materials* **2009,** *21* (48), 4880-4910.
7. Huang, X. H.; El-Sayed, I. H.; Qian, W.; El-Sayed, M. A., Cancer cell imaging and photothermal therapy in the near-infrared region by using gold nanorods. *Journal of the American Chemical Society* **2006,** *128* (6), 2115-2120.
8. Hribar, K. C.; Lee, M. H.; Lee, D.; Burdick, J. A., Enhanced Release of Small Molecules from Near-Infrared Light Responsive Polymer-Nanorod Composites. *Acs Nano* **2011,** *5* (4), 2948-2956.
9. Charati, M. B.; Lee, I.; Hribar, K. C.; Burdick, J. A., Light-Sensitive Polypeptide Hydrogel and Nanorod Composites. *Small* **2010,** *6* (15), 1608-1611.

10. Decher, G.; Hong, J. D., BUILDUP OF ULTRATHIN MULTILAYER FILMS BY A SELF-ASSEMBLY PROCESS .2. CONSECUTIVE ADSORPTION OF ANIONIC AND CATIONIC BIPOLAR AMPHIPHILES AND POLYELECTROLYTES ON CHARGED SURFACES. *Berichte Der Bunsen-Gesellschaft-Physical Chemistry Chemical Physics* **1991,** *95* (11), 1430-1434.
11. Decher, G., Fuzzy nanoassemblies: Toward layered polymeric multicomposites. *Science* **1997,** *277* (5330), 1232-1237.
12. Macdonald, M. L.; Samuel, R. E.; Shah, N. J.; Padera, R. F.; Beben, Y. M.; Hammond, P. T., Tissue integration of growth factor-eluting layer-by-layer polyelectrolyte multilayer coated implants. *Biomaterials* **2011,** *32* (5), 1446-1453.
13. Shah, N. J.; Macdonald, M. L.; Beben, Y. M.; Padera, R. F.; Samuel, R. E.; Hammond, P. T., Tunable dual growth factor delivery from polyelectrolyte multilayer films. *Biomaterials* **2011,** *32* (26), 6183-6193.
14. Shah, N. J.; Hong, J.; Hyder, M. N.; Hammond, P. T., Osteophilic Multilayer Coatings for Accelerated Bone Tissue Growth. *Advanced Materials* **2012,** *24* (11), 1445-1450.
15. Shah, N. J.; Hyder, M. N.; Quadir, M. A.; Courchesne, N. M. D.; Seeherman, H. J.; Nevins, M.; Spector, M.; Hammond, P. T., Adaptive growth factor delivery from a polyelectrolyte coating promotes synergistic bone tissue repair and reconstruction. *Proceedings of the National Academy of Sciences of the United States of America* **2014,** *111* (35), 12847-12852.
16. Smith, R. C.; Riollano, M.; Leung, A.; Hammond, P. T., Layer-by-Layer Platform Technology for Small-Molecule Delivery. *Angewandte Chemie-International Edition* **2009,** *48* (47), 8974-8977.
17. Hsu, B. B.; Park, M. H.; Hagerman, S. R.; Hammond, P. T., Multimonth controlled small molecule release from biodegradable thin films. *Proceedings of the National Academy of Sciences of the United States of America* **2014,** *111* (33), 12175-12180.
18. Shukla, A.; Avadhany, S. N.; Fang, J. C.; Hammond, P. T., Tunable Vancomycin Releasing Surfaces for Biomedical Applications. *Small* **2010,** *6* (21), 2392-2404.
19. Shukla, A.; Fuller, R. C.; Hammond, P. T., Design of multi-drug release coatings targeting infection and inflammation. *Journal of Controlled Release* **2011,** *155* (2), 159-166.
20. Shukla, A.; Fang, J. C.; Puranam, S.; Hammond, P. T., Release of vancomycin from multilayer coated absorbent gelatin sponges. *Journal of Controlled Release* **2012,** *157* (1), 64-71.
21. Min, J.; Braatz, R. D.; Hammond, P. T., Tunable staged release of therapeutics from layer-by-layer coatings with clay interlayer barrier. *Biomaterials* **2014,** *35* (8), 2507-2517.
22. Hsu, B. B.; Jamieson, K. S.; Hagerman, S. R.; Holler, E.; Ljubimova, J. Y.; Hammond, P. T., Ordered and Kinetically Discrete Sequential Protein Release from Biodegradable Thin Films. *Angewandte Chemie-International Edition* **2014,** *53* (31), 8093-8098.
23. Hsu, B. B.; Hagerman, S. R.; Jamieson, K.; Veselinovic, J.; O'Neill, N.; Holler, E.; Ljubimova, J. Y.; Hammond, P. T., Multi layer Films Assembled from Naturally-Derived Materials for Controlled Protein Release. *Biomacromolecules* **2014,** *15* (6), 2049-2057.
24. Castleberry, S.; Wang, M.; Hammond, P. T., Nanolayered siRNA Dressing for Sustained Localized Knockdown. *Acs Nano* **2013,** *7* (6), 5251-5261.
25. Wood, K. C.; Zacharia, N. S.; Schmidt, D. J.; Wrightman, S. N.; Andaya, B. J.; Hammond, P. T., Electroactive controlled release thin films. *Proceedings of the National Academy of Sciences of the United States of America* **2008,** *105* (7), 2280-2285.
26. Schmidt, D. J.; Moskowitz, J. S.; Hammond, P. T., Electrically Triggered Release of a Small Molecule Drug from a Polyelectrolyte Multilayer Coating. *Chemistry of Materials* **2010,** *22* (23), 6416-6425.
27. Kim, B. S.; Gao, H. F.; Argun, A. A.; Matyjaszewski, K.; Hammond, P. T., All-Star Polymer Multilayers as pH-Responsive Nanofilms. *Macromolecules* **2009,** *42* (1), 368-375.
28. Schmidt, D. J.; Hammond, P. T., Electrochemically erasable hydrogen-bonded thin films. *Chemical Communications* **2010,** *46* (39), 7358-7360.
29. Kozlovskaya, V.; Shamaev, A.; Sukhishvili, S. A., Tuning swelling pH and permeability of hydrogel multilayer capsules. *Soft Matter* **2008,** *4* (7), 1499-1507.
30. Radt, B.; Smith, T. A.; Caruso, F., Optically addressable nanostructured capsules. *Advanced Materials* **2004,** *16* (23-24), 2184-+.
31. Angelatos, A. S.; Radt, B.; Caruso, F., Light-responsive polyelectrolyte/gold nanoparticle microcapsules. *Journal of Physical Chemistry B* **2005,** *109* (7), 3071-3076.

32. Skirtach, A. G.; Dejugnat, C.; Braun, D.; Susha, A. S.; Rogach, A. L.; Parak, W. J.; Mohwald, H.; Sukhorukov, G. B., The role of metal nanoparticles in remote release of encapsulated materials. *Nano Letters* **2005,** *5* (7), 1371-1377.
33. Javier, A. M.; del Pino, P.; Bedard, M. F.; Ho, D.; Skirtach, A. G.; Sukhorukov, G. B.; Plank, C.; Parak, W. J., Photoactivated Release of Cargo from the Cavity of Polyelectrolyte Capsules to the Cytosol of Cells. *Langmuir* **2008,** *24* (21), 12517-12520.
34. Carregal-Romero, S.; Ochs, M.; Rivera-Gil, P.; Ganas, C.; Pavlov, A. M.; Sukhorukov, G. B.; Parak, W. J., NIR-light triggered delivery of macromolecules into the cytosol. *Journal of Controlled Release* **2012,** *159* (1), 120-127.
35. Bao, Y.; Vigderman, L.; Zubarev, E. R.; Jiang, C. Y., Robust Multi layer Thin Films Containing Cationic Thiol-Functionalized Gold Nanorods for Tunable Plasmonic Properties. *Langmuir* **2012,** *28* (1), 923-930.
36. Gole, A.; Murphy, C. J., Polyelectrolyte-coated gold nanorods: Synthesis, characterization and immobilization. *Chemistry of Materials* **2005,** *17* (6), 1325-1330.
37. Jiang, C. Y.; Markutsya, S.; Tsukruk, V. V., Collective and individual plasmon resonances in nanoparticle films obtained by spin-assisted layer-by-layer assembly. *Langmuir* **2004,** *20* (3), 882-890.
38. Jo, Y. S.; Gantz, J.; Hubbell, J. A.; Lutolf, M. P., Tailoring hydrogel degradation and drug release via neighboring amino acid controlled ester hydrolysis. *Soft Matter* **2009,** *5* (2), 440-446.
39. Wood, K. C.; Chuang, H. F.; Batten, R. D.; Lynn, D. M.; Hammond, P. T., Controlling interlayer diffusion to achieve sustained, multiagent delivery from layer-by-layer thin films. *Proceedings of the National Academy of Sciences of the United States of America* **2006,** *103* (27), 10207-10212.
40. Mitchell, J. A.; Akarasereenont, P.; Thiemermann, C.; Flower, R. J.; Vane, J. R., SELECTIVITY OF NONSTEROIDAL ANTIINFLAMMATORY DRUGS AS INHIBITORS OF CONSTITUTIVE AND INDUCIBLE CYCLOOXYGENASE. *Proceedings of the National Academy of Sciences of the United States of America* **1993,** *90* (24), 11693-11697.
41. Kondo, S.; Murase, K.; Kuzuya, M., MECHANOCHEMICAL SOLID-STATE POLYMERIZATION .7. THE NATURE OF HYDROLYSIS OF NOVEL POLYMERIC PRODRUGS PREPARED BY MECHANOCHEMICAL COPOLYMERIZATION. *Chemical & Pharmaceutical Bulletin* **1994,** *42* (12), 2412-2417.
42. Zhu, Z. C.; Sukhishvili, S. A., Temperature-Induced Swelling and Small Molecule Release with Hydrogen-Bonded Multilayers of Block Copolymer Micelles. *Acs Nano* **2009,** *3* (11), 3595-3605.
43. Seo, J.; Lutkenhaus, J. L.; Kim, J.; Hammond, P. T.; Char, K., Development of surface morphology in multilayered films prepared by layer-by-layer deposition using poly(acrylic acid) and hydrophobically modified poly(ethylene oxide). *Macromolecules* **2007,** *40* (11), 4028-4036.
44. Meloun, M.; Bordovska, S.; Galla, L., The thermodynamic dissociation constants of four non-steroidal anti-inflammatory drugs by the least-squares nonlinear regression of multiwavelength spectrophotometric pH-titration data. *Journal of Pharmaceutical and Biomedical Analysis* **2007,** *45* (4), 552-564.
45. Balon, K.; Riebesehl, B. U.; Muller, B. W., Drug liposome partitioning as a tool for the prediction of human passive intestinal absorption. *Pharmaceutical Research* **1999,** *16* (6), 882-888.
46. Bonina, F. P.; Puglia, C.; Barbuzzi, T.; de Caprariis, P.; Palagiano, F.; Rimoli, M. G.; Saija, A., In vitro and in vivo evaluation of polyoxyethylene esters as dermal prodrugs of ketoprofen, naproxen and diclofenac. *European Journal of Pharmaceutical Sciences* **2001,** *14* (2), 123-134.
47. Ma, C. D.; Wang, C. X.; Acevedo-Velez, C.; Gellman, S. H.; Abbott, N. L., Modulation of hydrophobic interactions by proximally immobilized ions. *Nature* **2015,** *517* (7534), 347-U443.
48. Krogman, K. C.; Lyon, K. F.; Hammond, P. T., Metal Ion Reactive Thin Films Using Spray Electrostatic LbL Assembly. *Journal of Physical Chemistry B* **2008,** *112* (46), 14453-14460.
49. Seo, J.; Lutkenhaus, J. L.; Kim, J.; Hammond, P. T.; Char, K., Effect of the layer-by-layer (LbL) deposition method on the surface morphology and wetting behavior of hydrophobically modified PEO and PAA LbL films. *Langmuir* **2008,** *24* (15), 7995-8000.
50. Hsu, B. B.; Hagerman, S. R.; Hammond, P. T., Rapid and efficient sprayed multilayer films for controlled drug delivery. *Journal of Applied Polymer Science* **2016,** *133* (25), 8.
51. Nikoobakht, B.; El-Sayed, M. A., Preparation and growth mechanism of gold nanorods (NRs) using seed-mediated growth method. *Chemistry of Materials* **2003,** *15* (10), 1957-1962.

52. Dickerson, E. B.; Dreaden, E. C.; Huang, X. H.; El-Sayed, I. H.; Chu, H. H.; Pushpanketh, S.; McDonald, J. F.; El-Sayed, M. A., Gold nanorod assisted near-infrared plasmonic photothermal therapy (PPTT) of squamous cell carcinoma in mice. *Cancer Letters* **2008,** *269* (1), 57-66.
53. Li, C.; Yu, D. F.; Newman, R. A.; Cabral, F.; Stephens, L. C.; Hunter, N.; Milas, L.; Wallace, S., Complete regression of well-established tumors using a novel water-soluble poly(L-glutamic acid) paclitaxel conjugate. *Cancer Research* **1998,** *58* (11), 2404-2409.
54. Kim, B. S.; Park, S. W.; Hammond, P. T., Hydrogen-bonding layer-by-layer assembled biodegradable polymeric micelles as drug delivery vehicles from surfaces. *Acs Nano* **2008,** *2* (2), 386-392.

Chapter 3:

Improved Synthesis and Optimized Composition of a Multi-Responsive Spiropyran Methacrylate Copolymer for Externally Triggered Therapeutic Release Applications

Chapter 3. Improved Synthesis and Optimized Composition of a Multi-Responsive Spiropyran Methacrylate Copolymer for Externally Triggered Therapeutic Release Applications

It is a challenge to produce dynamic materials that can be introduced locally into the body and respond to an external stimulus like light in a way that does not produce any adverse health effects and releases a therapeutic payload. This innocuous response behavior would be beneficial for non-invasive modulation of healing processes. Spiropyrans present strong changes in properties in response to various stimuli including light, and their covalent incorporation into polymer chains provides enhanced photo-stability and aqueous solubility. In this work the synthesis by atom transfer radical polymerization of a copolymer with multi-responsive constituents 2-(dimethylamino)ethyl methacrylate and 1,3',3'-trimethylspiro[chromene-2,2'-indolin]-6-yl methacrylate was improved for control over kinetics and resultant product composition. The improved synthesis was applied to different monomer feed ratios to achieve a composition with dramatically varying solubility properties across 37°C with different isomeric states of the spiropyran pendant groups. This multi-responsive system can be improved by introducing biodegradable ester linkages along the polymer backbone before progressing to *in vitro* therapeutic release studies.

3.1 Introduction

Photo-responsive materials that produce a biologically orthogonal chemical change in response to light have potential benefits for biomedical applications involving healing. By contrast, materials that produce heat[1] and free radicals[2] in response to light are more relevant for intentional cell killing as in chemotherapeutic applications. One set of biologically orthogonal photochemical responsive candidates is a group of molecules that act as photo-switches and isomerize in response to light, including for example azobenzenes,[3, 4] diarylethenes,[5, 6] and spiropyrans.[7, 8]

Spiropyrans hold as an advantage over other photoswitches the ability to access isomeric states with dramatically different properties with respect to one another. Reversible isomerization of spiropyrans can be instigated by a variety of stimuli including light, mechanical force, and metal ions, as well as variation of solvent polarity, pH, temperature, and redox potential.[9] Covalent attachment of spiropyrans along a biocompatible polymer chain in a minority mole fraction of units[10] confers many benefits

for their utilization in biomedical applications, notably aqueous solubility,[11] biocompatibility,[12] and reduced photo-degradation.[10]

Localized delivery of therapeutics at a high loading and degree of control over release profile can be accomplished by self-assembling the therapeutic molecule with polymeric materials Layer-by-Layer (LbL).[13] Polyelectrolytes have been used in electrostatic LbL assemblies that can release therapeutic in response to stimuli including voltage.[14] LbL assemblies incorporating star polymers of poly(2-dimethylamino)ethyl methacrylate) have been found to undergo dramatic film thickness changes in response to change in pH.[15]

Thermo-responsive polymers such as the well-studied biocompatible poly(N-isopropylacrylamide)[16] (polyNIPAM) undergo dramatic solubility transitions under the right environmental conditions of pH, temperature, and other factors. PolyNIPAM has been covalently modified with spiropyran functionality to add another handle of control for polymer solubility, with a 35°C cloud point when the spiropyran side groups were in the open-ring hydrophilic merocyanine isomeric state and a 30°C cloud point when spiropyran side groups were in the closed-ring hydrophobic state.[17]

Copolymers of 2-(dimethylamino)ethyl methacrylate (DMAEMA) and 1,3',3'-trimethylspiro[chromene-2,2'-indolin]-6-yl methacrylate (spiropyran methacrylate, SP) have been examined in previous work for responsiveness to pH, temperature, and light.[18] These copolymers presented a solubility transition at 37°C in aqueous media induced by isomerization of the photo-switchable spiropyran from the hydrophobic closed-ring form to the hydrophilic open-ring form by ultraviolet light (λ = 365 nm) or vice versa by green light (λ = 532 nm). Use of this functionality at core body temperature could be beneficial for remotely triggered release of therapeutics by an external stimulus.

In this work, the synthesis of a copolymer of 2-(dimethylamino)ethyl methacrylate and a spiropyran methacrylate by atom transfer radical polymerization was improved to achieve tighter control over kinetics and composition. The improved synthetic protocol was utilized to achieve a copolymer composition such that a solubility transition occurred surrounding 37°C. A second solubility transition was also observed in a higher temperature regime. These solubility transitions corresponded to ring-opening/ring-closing isomerization and protonation/de-protonation of the spiropyran moieties along the copolymer chain.

3.2 Results and Discussion

3.2.1. Improvements to the Atom Transfer Radical Copolymerization of 2-(Dimethylamino)ethyl Methacrylate and Spiropyran Methacrylate to Enhance Control Over Composition and Kinetics

Experimental principles of atom transfer radical polymerization (ATRP) developed in the Matyjaszewski group were utilized to improve the copolymerization process for two stimuli-responsive methacrylate comonomers of interest (Scheme 3.1, Scheme 3.2).

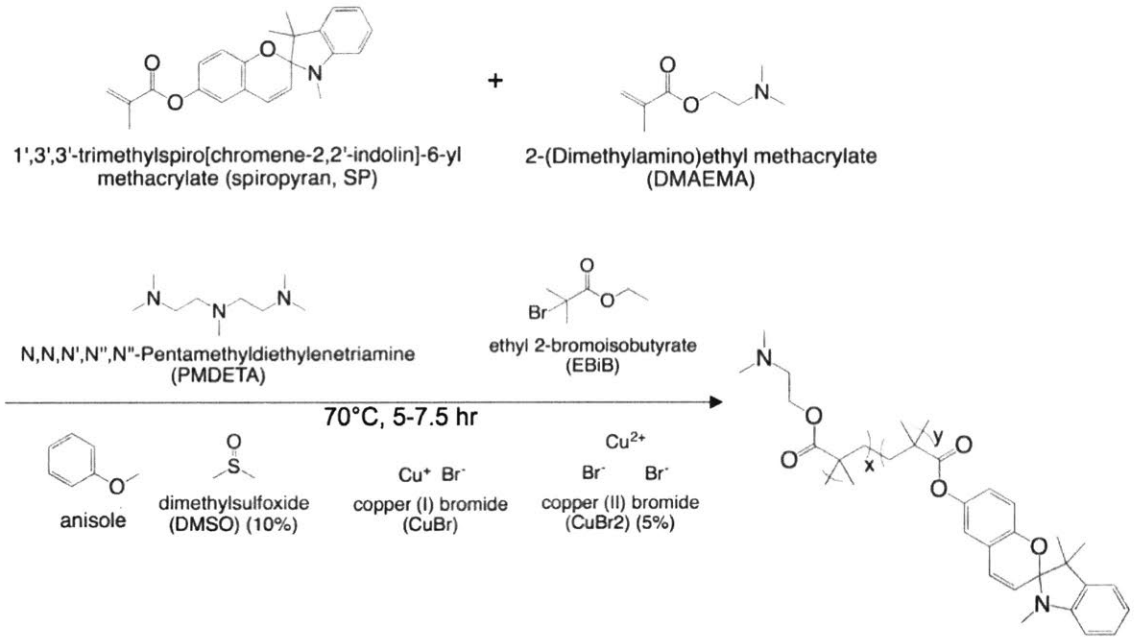

Scheme 3.1. The improved synthetic scheme of spiropyran methacrylate copolymer by atom transfer radical polymerization (ATRP) is shown here. Anisole, used in a 1:1 mass ratio with the total mass of the comonomers, was found to have favorable solubilizing properties and low volatility to maintain a homogeneous constant-volume copolymerization solution. Copper (II) bromide was introduced to control the development of the radical activation-deactivation equilibrium. Dimethylsulfoxide was added to solubilize the copper (II) bromide and to serve as the reference in ^{1}H NMR spectroscopy.

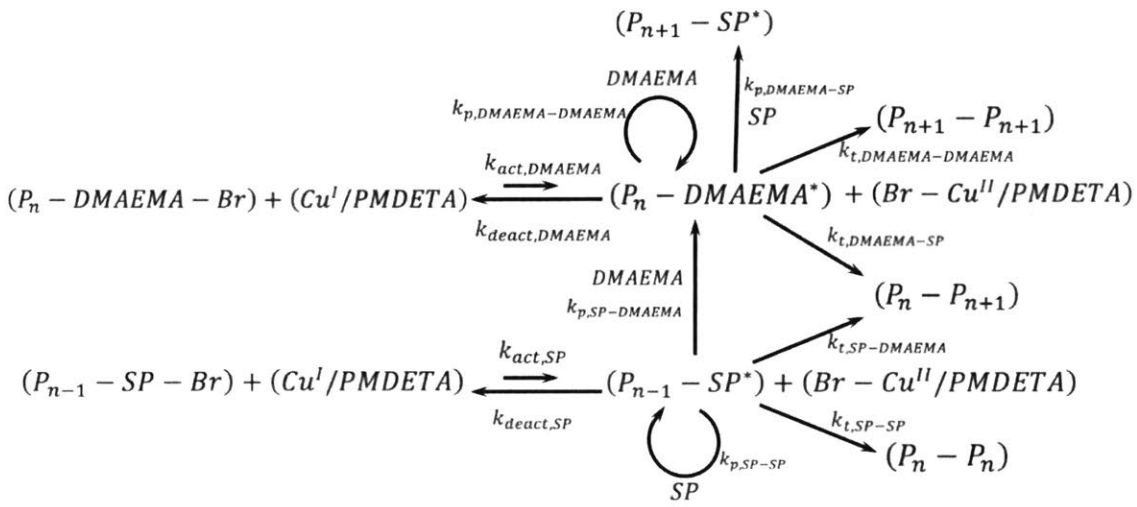

Scheme 3.2. Atom transfer radical polymerization (ATRP) mechanism for the controlled copolymerization of 2-(dimethylamino)ethyl methacrylate (DMAEMA) and spiropyran methacrylate (SP) after all initiator has been consumed.[19] P_n-DMAEMA-Br and P_{n-1}-SP-Br are the dormant macromolecular species once all of the initiator ethyl 2-bromoisobutyrate (EBiB) has been consumed. P_{n-1}, P_n, and P_{n+1} are the copolymer chains with degrees of polymerization n-1, n, and n+1. Cu^I/PMDETA is the activator, the transition-metal complex in the low oxidation state. P_n-DMAEMA* and P_{n-1}-SP* are the propagating radicals ending with DMAEMA or SP respectively. Br-Cu^{II}/PMDETA is the deactivator, the transition-metal complex in the higher oxidation state coordinated with the halide ligand. Activation rate constants with SP and DMAEMA at the end of the propagating copolymer chain are respectively $k_{act,SP}$ and $k_{act,DMAEMA}$, and deactivation rate constants are $k_{deact,SP}$ and $k_{deact,DMAEMA}$. Homopropagation rate constants for SP and DMAEMA are respectively $k_{p,SP-SP}$ and $k_{p,DMAEMA-DMAEMA}$. Cross-propagation rate constants for SP and DMAEMA respectively are $k_{p,SP-DMAEMA}$ and $k_{p,DMAEMA-SP}$. Termination rate constants are $k_{t,SP-SP}$, $k_{t,SP-DMAEMA}$, $k_{t,DMAEMA-SP}$, and $k_{t,DMAEMA-DMAEMA}$ where two propagating polymer chains with the indicated end species identities react to form a completed polymer chain.

The overall apparent rate equation for ATRP with the catalyst and ligand specific to the system described in this work is:[19]

$$R_p = k_p K_{ATRP} \left(\frac{[P_n Br][Cu^I/PMDETA][M]}{[Br-Cu^{II}/PMDETA]} \right) \qquad \text{Equation 3.1}$$

R_p is the rate of chain propagation, k_p is the propagation rate constant, K_{ATRP} is the activation-deactivation rate constant ratio k_{act}/k_{deact}, $[P_nBr]$ is the concentration of inactive polymer chains, [Cu^I/PMDETA] is the activator concentration, [M] is the concentration of monomer in the system, and [Br-Cu^{II}/PMDETA] is the deactivator concentration.

For greater control over copolymerization kinetics, a higher solvent-to-monomer volume ratio was established and a different solvent was employed than had been used in the literature.[18] Since methacrylate polymerization is relatively rapid, the slowing of the reaction by dilution (Equation 3.1) creates more kinetic control. It was also observed that tetrahydrofuran, used as the solvent in the previous work, was evaporating significantly during the polymerization. Anisole was therefore used instead of tetrahydrofuran as the solvent. The higher boiling point of anisole keeps the solvent volume and consequently the polymerization volume closer to constant throughout the reaction.

As another improvement to the copolymerization system, ten volume percent of dimethylsulfoxide was introduced for two reasons: first, to dissolve the copper (II) bromide, which does not dissolve well in anisole; and second, to act as a reference in nuclear magnetic resonance spectroscopy (^{1}H NMR) when performing kinetics studies.

Finally, a small amount of copper (II) bromide (equivalent to 5% of the added CuBr) was introduced to stabilize the development of the radical activation-deactivation equilibrium. By examining Equation 3.1, it becomes apparent that the initial rate of polymerization would be infinite if the system began without any Cu^{II} present, so the addition of copper (II) bromide addresses this issue. The initial presence of copper in its higher oxidation state was also hypothesized to decrease the polydispersity index of the copolymer products:[19]

$$\frac{M_w}{M_n} = 1 + \left(\frac{k_p[P_nBr]}{k_{deact}[Br-Cu^{II}/PMDETA]}\right)\left(\frac{2}{p} - 1\right) \qquad \text{Equation 3.2}$$

The weight- and number-average molecular weights of the copolymer chains are M_w and M_n, respectively. The monomer conversion fraction is p.

The molar feed ratio for the initial copolymerization with the new synthetic approach was 4.2:1 [DMAEMA]:[SP] (Figure 3.1A). Kinetics studies of a small-scale reaction (5 mL) using nuclear magnetic resonance (^{1}H NMR) spectroscopy were used to determine the approximate relative rates of incorporation of each monomer into the copolymer chains (Figure 3.1B).

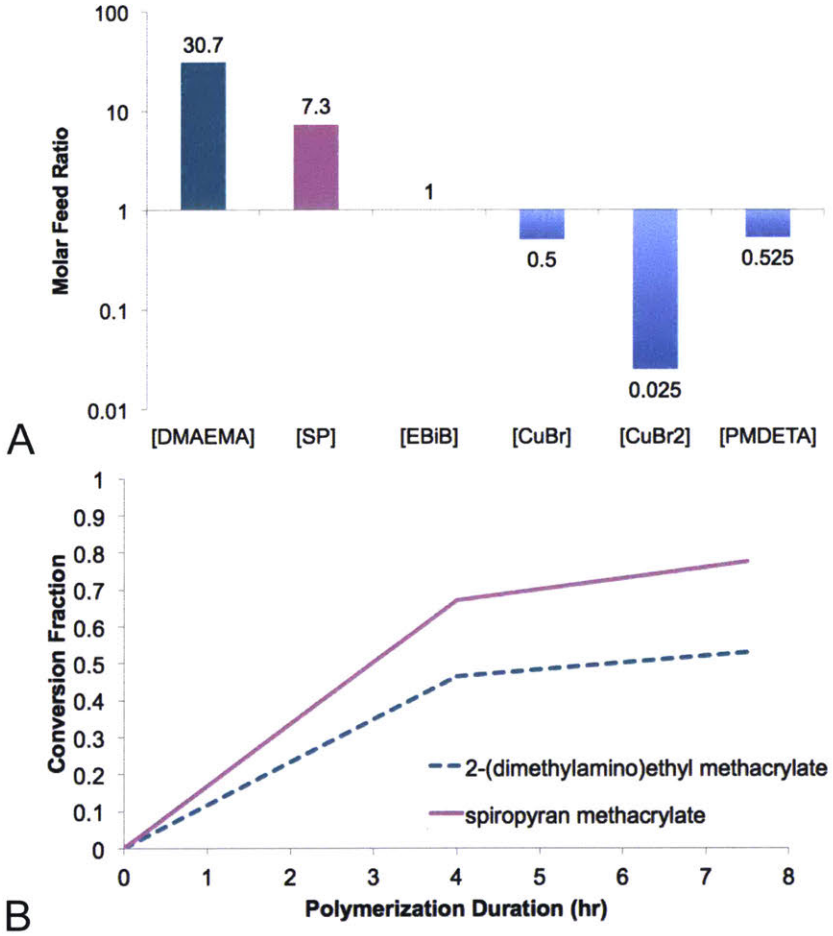

Figure 3.1. A. The molar feed ratios for the different non-solvent components of the first improved small batch ATRP synthesis of the spiropyran methacrylate copolymer: comonomer 2-(dimethylamino)ethyl methacrylate (DMAEMA), comonomer 1',3',3'-trimethylspiro [chromene-2,2'-indolin]-6-yl methacrylate (spiropyran methacrylate, SP), initiator ethyl 2-bromoisobutyrate (EBiB), catalyst copper (I) bromide (CuBr), copper (II) bromide ($CuBr_2$), and ligand N,N,N',N'',N''-Pentamethyldiethylenetriamine (PMDETA). B. Copolymerization was found to progress with the spiropyran methacrylate comonomer having a greater reactivity with the propagating chain ends (^{1}H NMR). The nonlinearity of the conversion rate points to a not fully living system.

The resulting copolymer composition of this first product by the improved synthetic route was 25.7 mol% spiropyran (Table 3.1, SP1).

Table 3.1. Compositions and Molecular Weights of Different Spiropyran Methacrylate Copolymer Products

			Data Acquisition Method			
			GPC	GPC	LS/RI	LS/RI
	f_{SP}	F_{SP}	Rel. M_n (g/mol)	PDI	Abs. M_n (g/mol)	PDI
SP1	0.1921	0.2568	2320	1.13	7795	1.135
SP3	0.0090	(0.0091)	10800	1.20	24700	1.099
SP4	0.0138	(0.0162)	11000	1.19	[25100]	[1.1]

GPC: gel permeation chromatography
LS/RI: light scattering/refractive index
f_{SP}: SP comonomer feed mole fraction
F_{SP}: SP mole fraction in copolymer chains
Rel. M_n: relative number-average molecular weight
Abs. M_n: absolute number-average molecular weight
PDI: polydispersity index = M_w/M_n = weight-average molecular weight/M_n
( ): low degree of accuracy
[ ]: predicted

Copolymer product (SP1) at this composition proved unable to dissolve in aqueous solution at 5 mg/mL for cloud point evaluation. Due to the high orange coloration of the solid polymer, this insolubility could not be attributed to predominance of the hydrophobic closed-ring spiropyran isomeric state. The orange coloration indicated the presence of the open-ring merocyanine isomer of the spiropyran (Figure 3.3B). Above a threshold percentage of spiropyran side groups along the polymer chains, merocyanine rings can π-π stack with one another within and between macromolecules, resulting in aggregates that cannot be solubilized.[20] The copolymer at this high spiropyran content was therefore determined not to be conducive to photo-switching capabilities in biological environments. The kinetics information obtained by ^{1}H NMR (Figure 3.1B) was leveraged to estimate the monomer feed ratios required to obtain an intended copolymer composition with less spiropyran content.

3.2.2. Confirmation of the Thermoresponsive Capability of a Spiropyran Methacrylate Copolymer by Cloud Point Measurement and Assumption of Monomer Reactivity Ratios

The kinetic data obtained from the first copolymerization under improved synthesis conditions (Figure 3.1B) was then utilized under the assumption of ideal copolymerization as a starting point to predict the monomer feed ratio that would yield a 1.3 mol% spiropyran methacrylate (SP) copolymer. This copolymer composition had

been shown previously to possess favorable biologically relevant photo-switching properties.[18] The 1.3 mol% SP copolymer with open-ring merocyanine moieties in their hydrophilic state was soluble in aqueous solution at core body temperature (37°C) and above, and the same copolymer with closed-ring spiropyran moieties in their hydrophobic state was insoluble in aqueous solution at body temperature (37°C) and slightly below.[18] It is this solubility transition on either side of core body temperature that can be of use in biomedical applications for therapeutic delivery.

For the copolymerization of these two comonomers, four propagation reactions are possible under the assumption that the reactivity of the propagating polymer chain depends only on the monomer unit at the growing chain end:

$$SP^* + SP \xrightarrow{k_{p,SP-SP}} SP^* \qquad \text{Equation 3.3}$$

$$SP^* + DMAEMA \xrightarrow{k_{p,SP-DMAEMA}} DMAEMA^* \qquad \text{Equation 3.4}$$

$$DMAEMA^* + SP \xrightarrow{k_{p,DMAEMA-SP}} SP^* \qquad \text{Equation 3.5}$$

$$DMAEMA^* + DMAEMA \xrightarrow{k_{p,DMAEMA-DMAEMA}} DMAEMA^* \qquad \text{Equation 3.6}$$

In these relations, $k_{p,SP-SP}$ is the rate constant for homopropagation of SP, i.e. a propagating chain end SP* reacting with monomer SP. The homopropagation of monomer DMAEMA is characterized by rate constant $k_{p,DMAEMA-DMAEMA}$. The rate constants $k_{p,SP-DMAEMA}$ and $k_{p,DMAEMA-SP}$ describe the rates of cross-propagation.

Monomer reactivity ratios are defined as:

$$r_{SP} = \frac{k_{p,SP-SP}}{k_{p,SP-DMAEMA}} \; ; \; r_{DMAEMA} = \frac{k_{p,DMAEMA-DMAEMA}}{k_{p,DMAEMA-SP}} \qquad \text{Equation 3.7}$$

The copolymerization equation (Equation 3.8) can be used with experimental data from at least two runs with different starting mole fractions of comonomers to de-convolute the values of r_{SP} and r_{DMAEMA}:

$$F_{SP} = \frac{r_{SP} f_{SP}^2 + f_{SP} f_{DMAEMA}}{r_{SP} f_{SP}^2 + 2 f_{SP} f_{DMAEMA} + r_{DMAEMA} f_{DMAEMA}^2} \qquad \text{Equation 3.8}$$

F_{SP} is the mole fraction of SP in the copolymer. In this study, F_{SP} can be determined by calculating changes in the integration values of vinyl peaks in the ^{1}H NMR spectra of the copolymerization solution corresponding to the two monomers. F_{DMAEMA} =

$1 - F_{SP}$ is the mole fraction of DMAEMA in the copolymer. The mole fractions of monomers in the feed are f_{SP} and $f_{DMAEMA} = 1 - f_{SP}$, which are directly measured at the start of the experiment. The copolymerization equation holds under the same assumption of the propagation equations (Equations 3.3-3.6), provided that there are no depropagation events and high molecular weight polymer is formed.

Under conditions of ideal copolymerization:

$$r_{SP} r_{DMAEMA} = 1 \qquad \text{Equation 3.9}$$

Ideal copolymerization refers to the propagating radical (*) species DMAEMA* and SP* showing the same preference for adding one monomer over another. This means that the rate at which each monomer is incorporated into the polymer chains is independent of the identity of the unit at the propagating chain end. By this assumption, 0.9 mol% SP monomer and 99.1 mol% DMAEMA monomer were added as the starting feed ratio (Table 3.1, SP3; Figure 3.2A).

This attempt resulted in a copolymer composition of approximately 0.91 mol% spiropyran in the copolymer (based on ^{1}H NMR) rather than the predicted 1.3 mol% under the assumption of ideal copolymerization. One caveat was that the integral of the spiropyran vinyl peak at the polymerization halt point reached the limits of detection for NMR, so the conversion was imprecise. The copolymer was soluble in aqueous solution in its hydrophobic closed-ring spiropyran form up to the cloud point of 48.1°C (Figure 3.2C). The closed-ring form was inferred by the absence of absorbance in the visible spectrum. This 48.1°C cloud point exceeded core body temperature, which meant that the same copolymer with the spiropyran moieties switched over to the hydrophilic open-ring merocyanine isomer would have an even higher cloud point. In order to achieve at least two distinct cloud points surrounding 37°C, a greater spiropyran methacrylate composition was required.

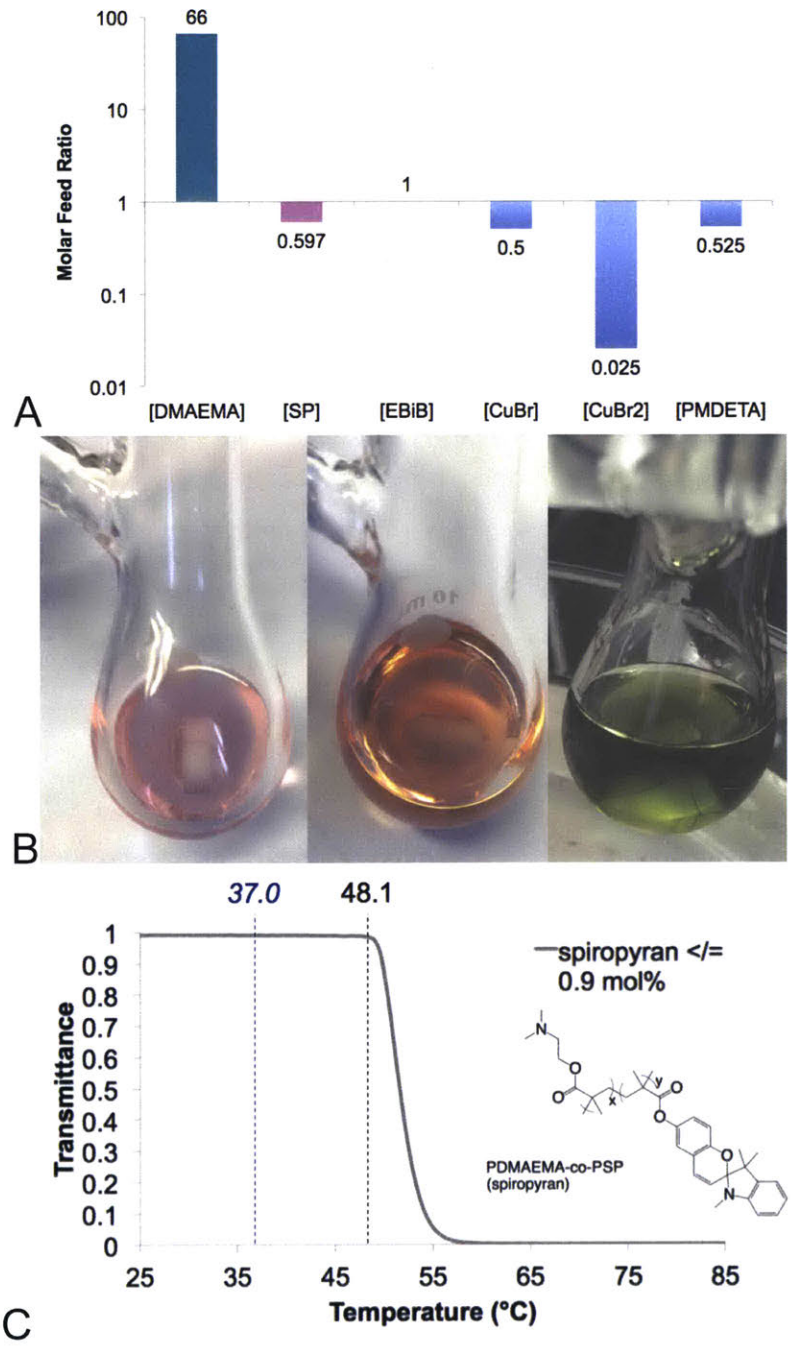

Figure 3.2. A. Molar feed ratios for the comonomer, initiator, catalyst, and ligand for the attempt to achieve 1.3 mol% copolymer based on the assumption of ideal copolymerization. B. Left: spiropyran methacrylate (SP) monomer in anisole. Pink color connotes the presence of the open-ring merocyanine (MC) isomer. Center: comonomers SP and DMAEMA in anisole. Right: polymerization solution, with the green color confirming the predominant copper (I) oxidation state in the activation-deactivation equilibrium of the atom transfer radical polymerization (ATRP). C. The cloud point of the copolymer at this composition exceeded 37°C with the spiropyran moieties in their

hydrophobic closed-ring form. If the spiropyran rings were to isomerize into their hydrophilic open-ring merocyanine form, the copolymer solubility would extend to an even higher temperature. The isomer-dependent solubility shift property around body temperature was not achieved with this spiropyran methacrylate copolymer composition (SP3, Table 3.1).

Using the two sets of copolymerization results (Table 3.1, SP1 and SP3), without a robust value for the second copolymer composition, estimates were determined for the r_{SP} and r_{DMAEMA} values as 1.01 and 3.44 respectively. This $r_{SP} > 1$, $r_{DMAEMA} > 1$ reflects a tendency towards block copolymer structure which is a rare occurrence in copolymerization. Therefore this result was taken with caution. A third copolymerization was undertaken using these tentative monomer reactivity ratios to determine the comonomer feed composition for the 1.3 mol% spiropyran (Figure 3.3A).

3.2.3. Optimized Spiropyran Methacrylate Copolymer Composition for Triggered Therapeutic Release Applications

For this next copolymer composition (Table 3.1, SP4), which was estimated by ^{1}H NMR to be 1.6 mol% SP, three distinct states of the spiropyran moieties (Figure 3.3B) were detectable by absorption spectroscopy (Figure 3.3C) and by eye (Figure 3.3D). The monomer reactivity ratios could not be reliably determined due end-of-polymerization peak integrations approaching the detection limits of ^{1}H NMR for both SP3 and SP4. The closed-ring hydrophobic spiropyran form present in aqueous solution was detected as colorless. The open-ring hydrophilic protonated merocyanine isomer present in acidic solution was detected as orange. The open-ring hydrophilic zwitterionic merocyanine isomer present in neutral salt solution was detected as bright fuchsia.

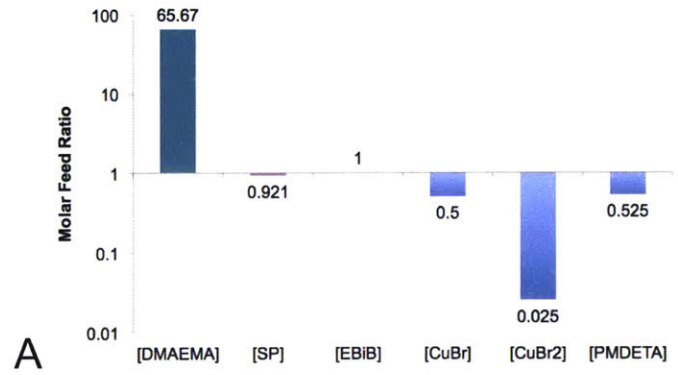
100
10
1
0.1
0.01
Molar Feed Ratio
65.67
0.921
1
0.5
0.025
0.525
[DMAEMA]
[SP]
[EBiB]
[CuBr]
[CuBr2]
[PMDETA]

A

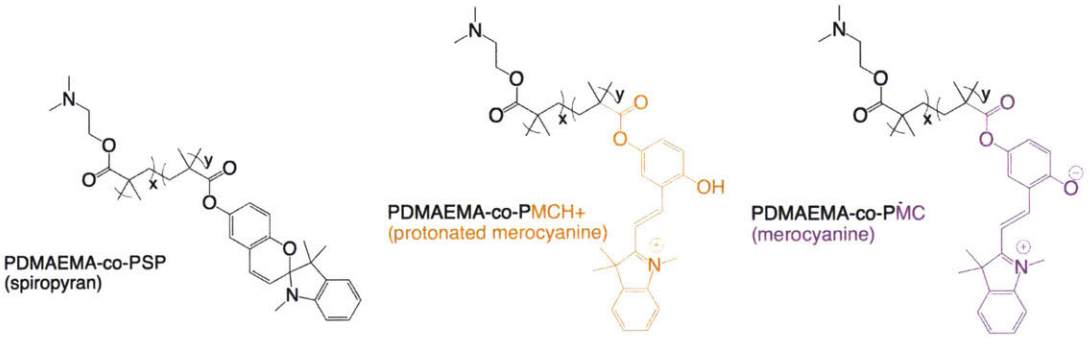
PDMAEMA-co-PSP
(spiropyran)
PDMAEMA-co-PMCH+
(protonated merocyanine)
PDMAEMA-co-PMC
(merocyanine)

B

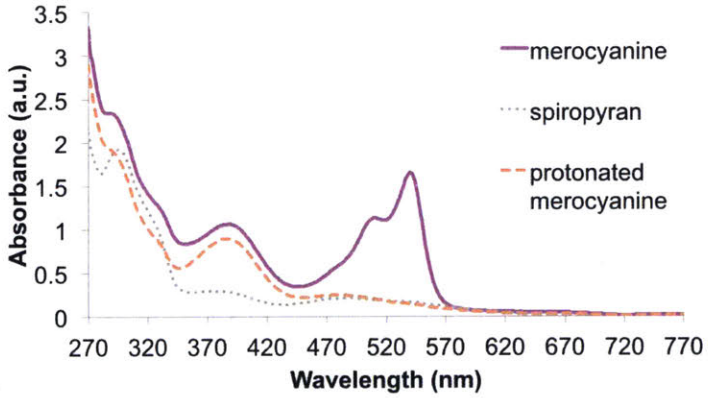
3.5
3
2.5
2
1.5
1
0.5
0
Absorbance (a.u.)
merocyanine
spiropyran
protonated
merocyanine
270 320 370 420 470 520 570 620 670 720 770
Wavelength (nm)

C

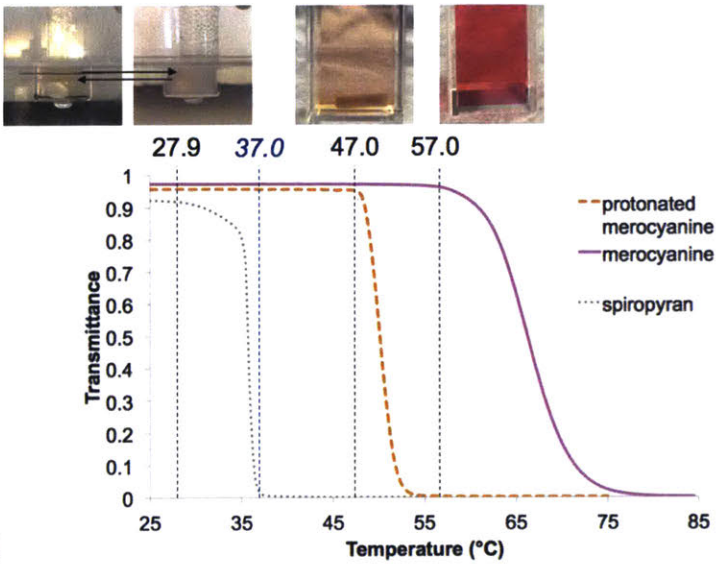
27.9
37.0
47.0
57.0
1
0.9
0.8
0.7
0.6
0.5
0.4
0.3
0.2
0.1
0
Transmittance
protonated
merocyanine
merocyanine
spiropyran
25 35 45 55 65 75 85
Temperature (°C)

D

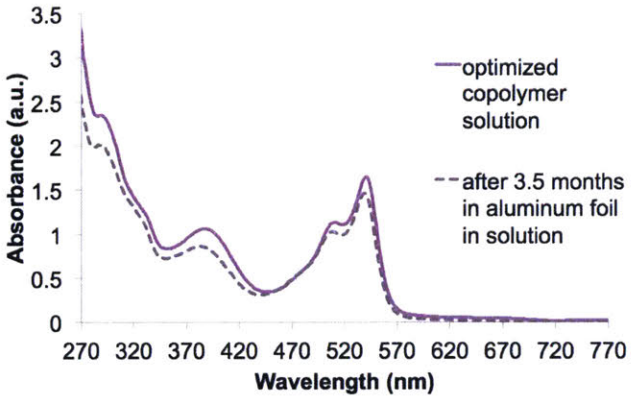

E

Figure 3.3. A. Molar feed ratios of the non-solvent components of the spiropyran methacrylate copolymerization for optimal composition. B. The three isomeric states of spiropyran detected for the copolymer by absorption spectroscopy and cloud point measurements. C. Absorption spectra of the merocyanine, spiropyran, and protonated merocyanine copolymer states. D. Superposition of cloud point determinations for the three forms of the copolymer investigated. Associated photograph(s) for each is aligned with the corresponding cloud point temperature at the 5mg/mL aqueous solution condition. The cloud points surround core body temperature (37°C), making this copolymer composition a promising candidate for triggered therapeutic delivery applications. E. The copolymer with merocyanine groups is stable in aqueous solution in darkness for months.

Each isomeric form of the copolymer presented a different thermal transition (Figure 3.3D). In the hydrophobic spiropyran isomeric state the copolymer began to lose its solubility above room temperature. The protonated merocyanine form was soluble out to 47°C, and the zwitterionic merocyanine form was soluble to 57°C. The merocyanine and spiropyran states of this copolymer switch the aqueous solubility of the chains from soluble to insoluble at 37°C respectively. This solubility switch also applies at the elevated temperatures of injured tissue, since the first transition is from 27.9°C to 47°C.

The copolymer is highly stable with merocyanine groups in aqueous salt solution in relative darkness, maintaining its absorption spectrum at least three months after dissolution (Figure 3.3E). This is consistent with previous reporting that the 2-(dimethylamino)ethyl methacrylate comonomer provides a hydrophilic nano-environment for the spiropyran methacrylate such that the spiropyran spontaneously isomerizes to its open-ring hydrophilic merocyanine form in aqueous solution.[18]

3.3 Conclusions

Improvements in the synthesis of a copolymer of a multi-responsive spiropyran methacrylate comonomer with thermoresponsive 2-(dimethylamino)ethyl methacrylate were accomplished by modifying the solvent identity and ratio and by introducing a stabilizing quantity of higher oxidation state catalyst in the atom transfer radical polymerization solution. The first improved synthesis resulted in aqueous-insoluble product. Under assumed monomer reactivity ratios, two more copolymerizations with low molar feed ratio spiropyran were conducted. One resulted in a thermo-responsive system outside of the range of internal body temperatures. Another yielded the copolymer composition with optimal solubility shift properties for use in biomedical applications, with the solubility shift occurring well above or well below 37°C depending on the isomeric state of the spiropyran moieties.

This highly controlled synthesis could be conducted for varied comonomer feed ratios to determine the nature of the copolymerization and have a more predictive approach towards choosing the monomer feed ratios to attain the optimal copolymer for a given application. The polymer composition can be further improved by introducing biodegradable ester linkages along the backbone to increase biocompatibility,[21-23] bearing in mind that the resultant copolymer properties would be affected.

3.4 Materials and Methods

All materials were obtained from Sigma-Aldrich unless indicated otherwise.

Synthesis of the spiropyran methacrylate monomer: A 250 mL flask was prepared by flame drying. One equivalent of 1',3',3'-trimethylspiro[chromene-2,2'-indolin]-6-ol (HBPS, 1.0 g, 3.4 mmol, pre-monomer) was transferred into the flask and dried under vacuum for 2 hours. The reaction vessel was maintained under inert gas from this point. Dry ethyl acetate (29 mL, solvent) was injected into the reaction vessel, followed by 1.2 equivalents of N,N-diisopropylethylamine (DIPEA, base). To this mixture, 1.2 equivalents of methacryloyl chloride (reagent) were added dropwise. Another 0.4 equivalents of methacryloyl chloride were added after 2 days due to an observation of incomplete conversion by thin layer chromatography (TLC). The total reaction time was 3-4 days.

The DIPEA hydrochloride salt was filtered off, followed by liquid removal from the product by rotary evaporation. Next the product was further purified by chromatography column on silica gel with 30% ethyl acetate, 70% hexanes as eluent. The product (~1.2 g) was dried under high vacuum overnight, and at this stage one spot was observed on TLC. The monomer was re-dissolved in dichloromethane (DCM) and evaporated in DCM to remove the ethyl acetate. The monomer was then lyophilized using benzene to aid the process. NMR shows approx. 90% conversion. The monomer is hygroscopic, so the material was stored in a vacuum desiccator until polymerization. ^{1}H NMR (400 MHz, $CDCl_3$) δ 7.18 (td, *J* = 7.6, 1.3 Hz, 1H), 7.07 (dd, *J* = 7.2, 0.8 Hz, 1H), 6.88 – 6.74 (m, 4H), 6.70 (d, *J* = 8.4 Hz, 1H), 6.52 (d, *J* = 7.7 Hz, 1H), 6.35 – 6.25 (m, 1H), 5.72 (dd, *J* = 6.6, 5.0 Hz, 2H), 2.73 (s, 3H), 2.05 (dd, *J* = 1.5, 1.0 Hz, 3H), 1.31 (s, 3H), 1.16 (s, 3H).

Copolymer synthesis by atom transfer radical polymerization: The following protocol is specific to SP1 but is consistent with the protocols for SP3 and SP4 with only amounts of reagents and solvents changed. The copolymerization was conducted in a ventilation hood equipped with a heat/stir plate with a silicone oil bath, bubbler, and at least one line on the N_2/vacuum dual manifold. Into the bottom of a 10 mL Schlenk flask containing an egg-shaped stir bar, 0.750 g of spiropyran methacrylate (SP, 1 equivalent) monomer (solid light orange powder) was funneled using weigh paper. To the bottom of the flask, 3.75 mL of anisole was injected. The flask was sealed, the flow of nitrogen to the Schlenk flask was initiated and the mixture was stirred at room temperature. The SP monomer dissolved well into the anisole to form a light orange solution.

While the SP was dissolving, comonomer 2-(dimethylamino)ethyl methacrylate (DMAEMA, contained 700-1000 ppm monomethyl ether hydroquinone as inhibitor) was passed through a basic alumina (Al_2O_3, activated, basic, Brockmann I) column and 0.2 μm polytetrafluoroethylene (PTFE) filter to remove inhibitor. To the anisole solution under nitrogen was then added 1.3745 g of DMAEMA (4.22 equivalents) weighed by tared syringe, purged of air before adding. Into a 20 mL vial was weighed 1.1 mg of copper (II) bromide ($CuBr_2$) (part of deactivator), and to this 0.375 mL of dimethylsulfoxide (DMSO, anhydrous) was added by syringe to dissolve the powder. $CuBr_2$ dissolved well in DMSO but not in anisole. Once fully dissolved, this solution was added to the stirring solution in the Schenk flask under nitrogen by syringe purged of air before injection.

Using a glass micro-syringe purged of air before injection, 22.9 µL of N,N,N',N'',N''-Pentamethyldiethylenetriamine (PMDETA, ligand) was added to the stirring solution. The micro-syringe was cleaned three times by acetone and then used to add 29.3 µL of ethyl 2-bromoisobutyrate (EBiB, initiator), purged of air first. The silicone oil bath was then heated to 70 °C using the same hot/stir plate. At this point two ~40 µL samples were taken by Pasteur pipette into 2 mL vials for ^{1}H NMR. The Schlenk flask was sealed and equilibrated under nitrogen for 30 min.

Into the bulb end of a Pasteur pipette (i.e. a narrow glass tube) was weighed 14.3 mg of copper (I) bromide (CuBr, catalyst) and tapped into the stirring solution after inserting the pipette deep into the flask through the addition neck. The solution turned green, signaling the predominance of the low oxidation state of the copper (I, vs. blue for II). Rubber stopper with Parafilm sealed the addition neck of the flask and the reaction ran at 70°C for 4 hours. At the 4-hour mark two more samples were collected for ^{1}H NMR in deuterated chloroform ($CDCl_3$) (Figure 3.1B) by nitrogen-purged syringe. The solution remained green/brown. The polymerization was run for 3.5 more hours, and two samples were collected for NMR from this final time point.

Final conversions from ^{1}H NMR for SP1, SP3, SP4: DMAEMA 0.53, 0.847, 0.7356; SP 0.77, (0.857), (0.8632). Conversions obtained by monitoring disappearance of vinyl proton peaks for SP (δ 6.29 ppm) and DMAEMA (δ 6.18 ppm). DMSO was used as a reference with integration set to 1 (δ 2.63 ppm).

Workup for the copolymer: The copolymer solution was filtered through a neutral alumina (Al_2O_3, Type WN-6, Neutral, Activity Grade Super I) column and 0.2 µm PTFE filter into a 20 mL vial to remove the copper. Tetrahydrofuran (THF) was added at the head of the column following the copolymer solution to increase yield. A stratum of green/blue indicating the copper resided in the column above the bottom of the column, indicating successful filtration. The filtered copolymer solution was then precipitated in hexanes (HPLC Plus) at a 10:1 volume ratio of hexanes (50 mL) to copolymer solution (5 mL) by adding the solution drop-wise to the stirring hexanes at room temperature. The precipitation was rapid. The hexanes were poured away from the polymer pellet, and the polymer was dried under vacuum overnight at room temperature. ^{1}H NMR (400 MHz, $CDCl_3$, δ in ppm): 4.1 (t, 2H), 2.6 (t, 2H), 2.3 (s, 6H), 1.9 (s, 2H), 1.0 (s, 3H).

Copolymer molecular weight characterization: Relative molecular weights were obtained by gel permeation chromatography (GPC) with poly(methyl methacrylate) (PMMA) standards using mobile phase dimethylformamide (DMF) at a flow rate of 1 mL/min. Absolute molecular weights were obtained by DMF GPC with light scattering and refractive index detection (Optilab T-rEX) to determine the refractive index increment (dn/dc) from samples 1, 2, 3, 4, and 5 mg/mL in DMF.

Absorption spectra measurements and cloud point experiments: Absorption spectra were obtained prior to and following cloud point experiments to determine that the copolymer isomeric state was maintained. Spectra were measured 200-800nm at 600 nm/min (Agilent Cary 60). The copolymer was dissolved at 5 mg/mL in 18.2 MΩ•cm Milli-Q® water for 30 min. Adding hydrochloric acid (aq.) to 0.0265 M induced the protonated merocyanine form. Adding to this sodium hydroxide (aq.) to 0.0265 M (26.5 mM sodium chloride) induced the merocyanine form. Cloud point experiments were run using a temperature-controlled cuvette holder and circulator (Quantum), collecting absorption measurements at 750 nm every second for 160 min. A program ran equilibration for 5 min and then a temperature ramp 25°C to 90°C and back to 25°C at 1°C/min.

3.5 Acknowledgments

This work was supported in part by the National Science Foundation Graduate Research Fellowship Program, and by funding and core facilities provided by the U.S. Army Research Office under contract W911NF-07-D-0004 at the MIT Institute of Soldier Nanotechnologies. This work was also supported by the Massachusetts Institute of Technology (MIT) Materials Processing Center, the Koch Institute for Integrative Cancer Research, and the MRSEC Program of the National Science Foundation under grant number DMR-14-19807. This work made use of the instrumentation in the laboratory of Professor Bradley D. Olsen, and in the MIT Department of Chemistry Instrumentation Facility.

3.6 References

1. Shen, S.; Tang, H. Y.; Zhang, X. T.; Ren, J. F.; Pang, Z. Q.; Wang, D. G.; Gao, H. L.; Qian, Y.; Jiang, X. G.; Yang, W. L., Targeting mesoporous silica-encapsulated gold nanorods for chemo-photothermal therapy with near-infrared radiation. *Biomaterials* **2013,** *34* (12), 3150-3158.
2. Punjabi, A.; Wu, X.; Tokatli-Apollon, A.; El-Rifai, M.; Lee, H.; Zhang, Y. W.; Wang, C.; Liu, Z.; Chan, E. M.; Duan, C. Y.; Han, G., Amplifying the Red-Emission of Upconverting Nanoparticles for Biocompatible Clinically Used Prodrug-Induced Photodynamic Therapy. *Acs Nano* **2014,** *8* (10), 10621-10630.
3. Henzl, J.; Mehlhorn, M.; Gawronski, H.; Rieder, K. H.; Morgenstern, K., Reversible cis-trans isomerization of a single azobenzene molecule. *Angewandte Chemie-International Edition* **2006,** *45* (4), 603-606.
4. Bandara, H. M. D.; Burdette, S. C., Photoisomerization in different classes of azobenzene. *Chemical Society Reviews* **2012,** *41* (5), 1809-1825.
5. Matsuda, K.; Irie, M., Diarylethene as a photo switching unit. *Journal of Photochemistry and Photobiology C-Photochemistry Reviews* **2004,** *5* (2), 169-182.
6. Kudernac, T.; van der Molen, S. J.; van Wees, B. J.; Feringa, B. L., Uni- and bi-directional light-induced switching of diarylethenes on gold nanoparticles. *Chemical Communications* **2006,** (34), 3597-3599.
7. Berkovic, G.; Krongauz, V.; Weiss, V., Spiropyrans and spirooxazines for memories and switches. *Chemical Reviews* **2000,** *100* (5), 1741-1753.
8. Minkin, V. I., Photo-, thermo-, solvato-, and electrochromic spiroheterocyclic compounds. *Chemical Reviews* **2004,** *104* (5), 2751-2776.
9. Klajn, R., Spiropyran-based dynamic materials. *Chemical Society Reviews* **2014,** *43* (1), 148-184.
10. Bell, N. S.; Piech, M., Photophysical effects between spirobenzopyran-methyl methacrylate-functionalized colloidal particles. *Langmuir* **2006,** *22* (4), 1420-1427.
11. Ivanov, A. E.; Eremeev, N. L.; Wahlund, P. O.; Galaev, I. Y.; Mattiasson, B., Photosensitive copolymer of N-isopropylacrylamide and methacryloyl derivative of spyrobenzopyran. *Polymer* **2002,** *43* (13), 3819-3823.
12. Chan, Y. H.; Gallina, M. E.; Zhang, X. J.; Wu, I. C.; Jin, Y. H.; Sun, W.; Chiu, D. T., Reversible Photoswitching of Spiropyran-Conjugated Semiconducting Polymer Dots. *Analytical Chemistry* **2012,** *84* (21), 9431-9438.
13. Hammond, P. T., Building biomedical materials layer-by-layer. *Materials Today* **2012,** *15* (5), 196-206.
14. Wood, K. C.; Zacharia, N. S.; Schmidt, D. J.; Wrightman, S. N.; Andaya, B. J.; Hammond, P. T., Electroactive controlled release thin films. *Proceedings of the National Academy of Sciences of the United States of America* **2008,** *105* (7), 2280-2285.
15. Kim, B. S.; Gao, H. F.; Argun, A. A.; Matyjaszewski, K.; Hammond, P. T., All-Star Polymer Multilayers as pH-Responsive Nanofilms. *Macromolecules* **2009,** *42* (1), 368-375.
16. Schild, H. G., POLY (N-ISOPROPYLACRYLAMIDE) - EXPERIMENT, THEORY AND APPLICATION. *Progress in Polymer Science* **1992,** *17* (2), 163-249.
17. Sumaru, K.; Kameda, M.; Kanamori, T.; Shinbo, T., Characteristic phase transition of aqueous solution of poly(N-isopropylacrylamide) functionalized with spirobenzopyran. *Macromolecules* **2004,** *37* (13), 4949-4955.
18. Achilleos, D. S.; Vamvakaki, M., Multiresponsive Spiropyran-Based Copolymers Synthesized by Atom Transfer Radical Polymerization. *Macromolecules* **2010,** *43* (17), 7073-7081.
19. Matyjaszewski, K., Atom Transfer Radical Polymerization: From Mechanisms to Applications. *Israel Journal of Chemistry* **2012,** *52* (3-4), 206-220.
20. Eckhardt, H.; Bose, A.; Krongauz, V. A., FORMATION OF MOLECULAR H-STACKS AND J-STACKS BY THE SPIROPYRAN MEROCYANINE TRANSFORMATION IN A POLYMER MATRIX. *Polymer* **1987,** *28* (11), 1959-1964.
21. Agarwal, S.; Ren, L. Q.; Kissel, T.; Bege, N., Synthetic Route and Characterization of Main Chain Ester-Containing Hydrolytically Degradable Poly(N,N-dimethylaminoethyl

methacrylate)-Based Polycations. *Macromolecular Chemistry and Physics* **2010,** *211* (8), 905-915.
22. Ren, L. Q.; Speyerer, C.; Agarwal, S., Free-radical copolymerization behavior of 5,6-benzo-2-methylene-1,3-dioxepane and methacrylic acid via the in situ generation of 3-methyl-1,5-dihydrobenzo e 1,3 dioxepin-3-yl methacrylate and 2-(acetoxymethyl)benzyl methacrylate. *Macromolecules* **2007,** *40* (22), 7834-7841.
23. Ganda, S.; Jiang, Y. Y.; Thomas, D. S.; Eliezar, J.; Stenzel, M. H., Biodegradable Glycopolymeric Micelles Obtained by RAFT-controlled Radical Ring-Opening Polymerization. *Macromolecules* **2016,** *49* (11), 4136-4146.

Chapter 4:
Conclusions and Recommendations

Chapter 4. Conclusions and Recommendations

4.1 Thesis Summary

Overall, this thesis presented responsive materials for biomedical applications resulting from the synthesis and self-assembly of amphiphilic copolymers. These copolymers each contained a majority of hydrophilic pH-responsive side groups and a minority of labile and/or isomerizable hydrophobic side groups. In both cases, these copolymers demonstrated thermo-responsive capabilities, either in solution or in the form of Layer-by-Layer electrostatic assemblies. Each system was undertaken with the intention of utilization in localized triggered therapeutic delivery vehicles at high tissue penetration depth.

In Chapter 2, a polyelectrolyte multilayer system consisting of bilayers of biocompatible poly(L-Lysine) and polymer-drug conjugate poly(L-glutamic acid-triethylene glycol-diclofenac) with hydrolytically degradable ester linkages was investigated for near infrared-responsive properties. It was determined that these Layer-by-Layer films containing micelles and unimers of the polymer-drug conjugate were near-infrared responsive, increasing diclofenac release rates by up to five-fold. Based on diminishing returns from immediately successive irradiations, a near-infrared enhanced release mechanism was postulated whereby hydrolyzed diclofenac that accumulated in the hydrophobic domains within the film was freed by the near-infrared irradiation. Gold nanorods were also incorporated into the films for enhanced heating by photothermal conversion. Due to the non-covalent suspension of nanorods in the film, progressive nanorod aggregation caused a time-dependent enhancement of diclofenac release relative to the bilayer control.

In Chapter 3, the synthesis of a copolymer of multi-responsive 2-(dimethylamino)ethyl methacrylate and a spiropyran methacrylate was improved using principles of atom transfer radical polymerization. Its composition was optimized for solubility shift properties across 37°C for use in light-triggered therapeutic delivery applications. The shift in solubility was a consequence of the reversible ring-opening transition of the spiropyran groups from an uncharged hydrophobic to a cationic or zwitterionic hydrophilic isomeric state.

4.2 Recommendations for Future Directions

4.2.1 Polymer-Drug Conjugate Layer-by-Layer System

The hypothesis of the mechanism for delayed release of small-molecule hydrophobic therapeutics from Layer-by-Layer films of poly(L-lysine) (PLL) with poly(L-glutamic acid-triethylene glycol-diclofenac) (PGA-Diclof) by sequestration of hydrolyzed drug into PGA-Diclof intra-film micelles should be tested. First, loading hydrophobic fluorescent probe pyrene into the film and conducting fluorescence microscopy can confirm the presence of intact micelles in the film.[1] The hypothesis of the presence of the protonated amines strengthening the hydrophobic interactions in the system[2] can also be tested by incubating either the Layer-by-Layer film or the amphiphilic polymer alone in solution with pyrene and comparing resultant probe loading under these two conditions. By comparing the fluorescence results of the resultant Layer-by-Layer films prepared with pyrene under these two assembly conditions, it may be possible to see higher loading of film-incubated pyrene than polymer solution-incubated pyrene.

To support the postulated near infrared-enhanced release rate mechanism, fluorescence microscopy on the films can be performed on the Layer-by-Layer films *in situ* during irradiation with near infrared. Due to the fluorescent properties of diclofenac, diclofenac may be observed leaving the film by a decrease in fluorescence in intra-film micelles. If diclofenac does not fluoresce strongly enough, this experiment can be conducted with a more strongly fluorescent analog of diclofenac containing a carboxylic acid moiety.

Once the mechanism of release has been established, fabrication of smoother films can be attempted by first using spin-assisted Layer-by-Layer (LbL) since this involves facile optimization of experimental parameters. Root mean square roughness of the spin-fabricated films can be determined by profilometry. Roughness can be compared to the micron-scale roughness observed in the same $(PLL/PGA\text{-}Diclof)_n$ polymer multilayers fabricated by dip LbL assembly.

If spin-assembled films are found to be significantly smoother, they should be assessed for intact micelles using the same fluorescence microscopy method to be employed for the dip-assembled films. The therapeutic release properties should also be tested and compared to those from the dip-assembled films. If the micelles are still intact, then the hydrophobic interaction-mediated delayed release and accumulation of

free drug in the film should still occur. If however the micelles are disrupted during spin-assisted fabrication, the free drug may just diffuse directly out of the film. The free diclofenac would slow slightly as it approached tethered drug pendant groups, but would be unable to be sequestered in a hydrophobic minority phase since the kinetics of spin-assisted LbL precluded micelles from staying intact during film formation.

Provided that the release mechanism holds after spin-assisted deposition and smooth films have been achieved, clay platelets can then be layered on top of the smoother films[3] to decrease the rate of passive release and test the effects of near infrared. Once the spin LbL system is working, the next step for scalability of the system is to optimize the assembly parameters for spray LbL.[4]

Due to the modular nature of Layer-by-Layer assemblies, materials with other therapeutic functionalities can be incorporated with potentially synergistic effects.[5, 6] These anti-inflammatory-releasing films can be combined with more specific anti-fibrotic factors that can be made highly charged for electrostatic assembly like small interfering ribonucleic acids (siRNA)[7-9] and tested with pro-fibrotic induced tissues.

The search is ongoing for a potent anti-inflammatory without adverse health effects. It has been demonstrated that diclofenac and other non-steroidal anti-inflammatory drugs present gastrointestinal[10] and cardiovascular risks.[11] A new family of molecules called pyrazolylthiazole carboxylic acids has been synthesized and tested *in vivo*.[12] These molecules presented promising high anti-inflammatory activity, with varied antimicrobial capabilities. One molecule in the family had the optimal intersection of high antimicrobial activity and high anti-inflammatory activity (Figure 4.1).

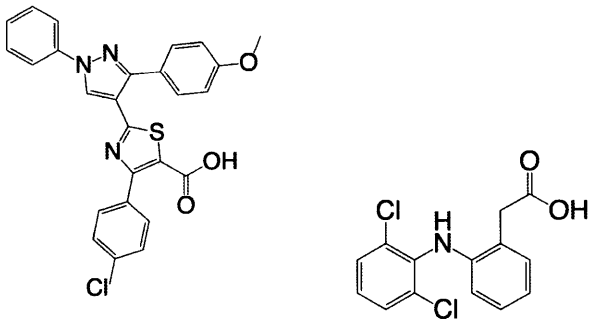

Figure 4.1. Novel anti-inflammatory pyrazolylthiazole carboxylic acids can be similarly covalently attached to a polymer-drug conjugate analogous to poly(L-glutamic acid-triethylene glycol-diclofenac). The particular chemical identity 2h also presented with strong antimicrobial activity.

This molecule contains a carboxylic acid moiety that can be reacted with triethylene glycol (or another short oligomer of polyethylene glycol) and ester-linked to poly(L-glutamic acid) in an analogous way to diclofenac to produce a polymer-drug conjugate. This therapeutic-eluting amphiphilic polyelectrolyte analogous to PGA-Diclof is hypothesized to also have micellization and electrostatic layering capabilities.

The dual mode of release demonstrated in this work, with both hydrolysis and hydrophobic-originated near-infrared responsive capability, can theoretically be extended to any hydrophobic small molecule therapeutic that can form an ester linkage.

4.2.2 Gold Nanorods for 980nm-Responsive Deep Tissue Biomedical Applications

A more kinetically stable formulation of the nanorod-containing films described in this work would include gold nanorods that absorb as individual entities exactly in resonance with the 980 nm laser stimulus and maintain their individual extinction properties and dispersion within the Layer-by-Layer film.

Coating the nanorods in silica could potentially enable many improvements to the system. First, a silica coating at least as thick as the diameter of the nanorods has been shown to more closely preserve the individual absorption properties of the nanorods even under conditions of aggregation.[13] Second, a silica coating at least 20 nm thick provided thermal and/or irradiation stability to gold nanorods.[14] However, there is a trade-off between stability and heat transport through the silica such that there may be an optimal coating thickness for this application. Third, gold nanorods with silica shells are biocompatible[15] and would reduce the toxicity of the system by eliminating

cytotoxicity from free CTAB.[16] The silica coating on the gold nanorods can also be covalently modified with materials terminating in crosslinking agents to immobilize the gold nanorods in the film. As a result, nanorod dispersion would be maintained and thereby individual rod plasmonic properties in the film.

While the commonly employed method of surfactant exchange with a thiol, for example heterobifunctional polyethylene glycol with thiol and carboxyl termini, eliminated the CTAB toxicity issue and reduced or eliminated gold nanorod aggregation,[17] it did not solve the problem of gold nanorod performance instability in response to near-infrared irradiation as did silica.[14] However, if heat transport through the silica proves to be an issue then the thiol coating can be employed instead.

In the ideal implementation, the nanorods would all be oriented perpendicular to the film surface (i.e. parallel to the laser source polarization direction) to allow maximum efficiency of photothermal conversion from the 980 nm laser source. However, 980 nm-absorbing entities maintaining individual properties and well-dispersed, even at random orientations, are projected to have more favorable performance than the current system.

4.2.3 Spiropyran Copolymer for Triggered Therapeutic Delivery by a Solubility-Shift Gating Mechanism with High Tissue Penetration Depth

The spiropyran copolymer synthesized in this work is demonstrative of the power of spiropyran to dramatically change the properties of a polymer to which it is covalently bound depending on its isomeric state. The strong solubility shifts observed with the copolymer can be applied towards photo-triggered therapeutic delivery applications by a gating mechanism.

In the current formulation, the polymer underwent a hydrophobic transition by photo-isomerization at 532 nm from merocyanine to spiropyran. Direct use of light at this wavelength is not practical for stimulating release from drug depots located deep within the body. Upconversion nanoparticles[18] can convert near infrared light at 980 nm to visible and ultraviolet light, with great potential utility in drug delivery systems.[19] Spiropyran has been combined with upconversion nanoparticles by covalent[20] or non-covalent[21] attachment to trigger delivery of large hydrophilic polyelectrolyte macromolecules[20] or small hydrophobic molecules.[21]

The copolymer synthesized in the current work can potentially be used to coat upconversion nanoparticles for triggered release. The visible light-stimulated ring closing

of merocyanine moieties has actuated release of large hydrophilic polyelectrolyte macromolecules from an upconversion nanoparticle coating.[20] Ultraviolet-stimulated ring opening of spiropyran moieties has actuated delivery of small hydrophobic molecules.[21] Upconversion nanoparticles coated with the copolymer from the current work can potentially be incorporated into Layer-by-Layer films by electrostatic forces for implant coatings with near-infrared triggerable high therapeutic payload.

4.3 Concluding Remarks

This thesis has contributed to the development of polymer-based exogenously responsive therapeutic delivery systems using amphiphilic copolymers. The intended end use for these systems is that of localized release at an on-demand time point at high tissue penetration depth, where direct or indirect use would be made of near-infrared light at 980 nm. With the current range of controlled polymerization techniques available to develop macromolecules, these majority hydrophilic-minority hydrophobic design principles can be carried forward for other specific delivery systems. The scientific community is encouraged to use the fundamental principles of responsive polymers involving hydrophobic interactions applied in this thesis to pursue non-invasive approaches to remotely triggered localized delivery of therapeutics deep within the body.

4.4 References

1. Seo, J.; Lutkenhaus, J. L.; Kim, J.; Hammond, P. T.; Char, K., Development of surface morphology in multilayered films prepared by layer-by-layer deposition using poly(acrylic acid) and hydrophobically modified poly(ethylene oxide). *Macromolecules* **2007,** *40* (11), 4028-4036.
2. Ma, C. D.; Wang, C. X.; Acevedo-Velez, C.; Gellman, S. H.; Abbott, N. L., Modulation of hydrophobic interactions by proximally immobilized ions. *Nature* **2015,** *517* (7534), 347-U443.
3. Min, J.; Braatz, R. D.; Hammond, P. T., Tunable staged release of therapeutics from layer-by-layer coatings with clay interlayer barrier. *Biomaterials* **2014,** *35* (8), 2507-2517.
4. Hsu, B. B.; Hagerman, S. R.; Hammond, P. T., Rapid and efficient sprayed multilayer films for controlled drug delivery. *Journal of Applied Polymer Science* **2016,** *133* (25), 8.
5. Shah, N. J.; Hong, J.; Hyder, M. N.; Hammond, P. T., Osteophilic Multilayer Coatings for Accelerated Bone Tissue Growth. *Advanced Materials* **2012,** *24* (11), 1445-1450.
6. Min, J. H.; Choi, K. Y.; Dreaden, E. C.; Padera, R. F.; Braatz, R. D.; Spector, M.; Hammond, P. T., Designer Dual Therapy Nanolayered Implant Coatings Eradicate Biofilms and Accelerate Bone Tissue Repair. *Acs Nano* **2016,** *10* (4), 4441-4450.
7. Castleberry, S. A.; Golberg, A.; Abu Sharkh, M.; Khan, S.; Almquist, B. D.; Austen, W. G.; Yarmush, M. L.; Hammond, P. T., Nanolayered siRNA delivery platforms for local silencing of CTGF reduce cutaneous scar contraction in third-degree burns. *Biomaterials* **2016,** *95*, 22-34.
8. Castleberry, S.; Wang, M.; Hammond, P. T., Nanolayered siRNA Dressing for Sustained Localized Knockdown. *Acs Nano* **2013,** *7* (6), 5251-5261.
9. Castleberry, S. A.; Almquist, B. D.; Li, W.; Reis, T.; Chow, J.; Mayner, S.; Hammond, P. T., Self-Assembled Wound Dressings Silence MMP-9 and Improve Diabetic Wound Healing In Vivo. *Advanced Materials* **2016,** *28* (9), 1809-1817.

10. de Abajo, F. J.; Gil, M. J.; Bryant, V.; Timoner, J.; Oliva, B.; Garcia-Rodriguez, L. A., Upper gastrointestinal bleeding associated with NSAIDs, other drugs and interactions: a nested case-control study in a new general practice database. *European Journal of Clinical Pharmacology* **2013,** *69* (3), 691-701.
11. Patrono, C., Cardiovascular Effects of Nonsteroidal Anti-inflammatory Drugs. *Current Cardiology Reports* **2016,** *18* (3), 8.
12. Khloya, P.; Kumar, S.; Kaushik, P.; Surain, P.; Kaushik, D.; Sharma, P. K., Synthesis and biological evaluation of pyrazolylthiazole carboxylic acids as potent anti-inflammatory-antimicrobial agents. *Bioorganic & Medicinal Chemistry Letters* **2015,** *25* (6), 1177-1181.
13. Vial, S.; Pastoriza-Santos, I.; Perez-Juste, J.; Liz-Marzan, L. M., Plasmon coupling in layer-by-layer assembled gold nanorod films. *Langmuir* **2007,** *23* (8), 4606-4611.
14. Chen, Y. S.; Frey, W.; Kim, S.; Homan, K.; Kruizinga, P.; Sokolov, K.; Emelianov, S., Enhanced thermal stability of silica-coated gold nanorods for photoacoustic imaging and image-guided therapy. *Optics Express* **2010,** *18* (9), 8867-8877.
15. Shen, S.; Tang, H. Y.; Zhang, X. T.; Ren, J. F.; Pang, Z. Q.; Wang, D. G.; Gao, H. L.; Qian, Y.; Jiang, X. G.; Yang, W. L., Targeting mesoporous silica-encapsulated gold nanorods for chemo-photothermal therapy with near-infrared radiation. *Biomaterials* **2013,** *34* (12), 3150-3158.
16. Alkilany, A. M.; Nagaria, P. K.; Hexel, C. R.; Shaw, T. J.; Murphy, C. J.; Wyatt, M. D., Cellular Uptake and Cytotoxicity of Gold Nanorods: Molecular Origin of Cytotoxicity and Surface Effects. *Small* **2009,** *5* (6), 701-708.
17. Rostro-Kohanloo, B. C.; Bickford, L. R.; Payne, C. M.; Day, E. S.; Anderson, L. J. E.; Zhong, M.; Lee, S.; Mayer, K. M.; Zal, T.; Adam, L.; Dinney, C. P. N.; Drezek, R. A.; West, J. L.; Hafner, J. H., The stabilization and targeting of surfactant-synthesized gold nanorods. *Nanotechnology* **2009,** *20* (43), 10.
18. Wang, F.; Liu, X. G., Recent advances in the chemistry of lanthanide-doped upconversion nanocrystals. *Chemical Society Reviews* **2009,** *38* (4), 976-989.
19. Bagheri, A.; Arandiyan, H.; Boyer, C.; Lim, M., Lanthanide-Doped Upconversion Nanoparticles: Emerging Intelligent Light-Activated Drug Delivery Systems. *Advanced Science* **2016,** *3* (7), 25.
20. Zhou, L.; Chen, Z. W.; Dong, K.; Yin, M. L.; Ren, J. S.; Qu, X. G., DNA-mediated Construction of Hollow Upconversion Nanoparticles for Protein Harvesting and Near- Infrared Light Triggered Release. *Advanced Materials* **2014,** *26* (15), 2424-2430.
21. Chen, S.; Gao, Y. J.; Cao, Z. Q.; Wu, B.; Wang, L.; Wang, H.; Dang, Z. M.; Wang, G. J., Nanocomposites of Spiropyran-Functionalized Polymers and Upconversion Nanoparticles for Controlled Release Stimulated by Near-Infrared Light and pH. *Macromolecules* **2016,** *49* (19), 7490-7496.
22. vandeWetering, P.; Cherng, J. Y.; Talsma, H.; Hennink, W. E., Relation between transfection efficiency and cytotoxicity of poly(2-(dimethylamino)ethyl methacrylate)/plasmid complexes. *Journal of Controlled Release* **1997,** *49* (1), 59-69.
23. Agarwal, S.; Ren, L. Q.; Kissel, T.; Bege, N., Synthetic Route and Characterization of Main Chain Ester-Containing Hydrolytically Degradable Poly(N,N-dimethylaminoethyl methacrylate)-Based Polycations. *Macromolecular Chemistry and Physics* **2010,** *211* (8), 905-915.
24. Kozlovskaya, V.; Ok, S.; Sousa, A.; Libera, M.; Sukhishvili, S. A., Hydrogen-bonded polymer capsules formed by layer-by-layer self-assembly. *Macromolecules* **2003,** *36* (23), 8590-8592.
25. Ganachaud, F.; Monteiro, M. J.; Gilbert, R. G.; Dourges, M. A.; Thang, S. H.; Rizzardo, E., Molecular weight characterization of poly(N-isopropylacrylamide) prepared by living free-radical polymerization. *Macromolecules* **2000,** *33* (18), 6738-6745.
26. Ifuku, S.; Kadla, J. F., Preparation of a Thermosensitive Highly Regioselective Cellulose/N-Isopropylacrylamide Copolymer through Atom Transfer Radical Polymerization. *Biomacromolecules* **2008,** *9* (11), 3308-3313.
27. Sumaru, K.; Kameda, M.; Kanamori, T.; Shinbo, T., Characteristic phase transition of aqueous solution of poly(N-isopropylacrylamide) functionalized with spirobenzopyran. *Macromolecules* **2004,** *37* (13), 4949-4955.

28. Zhu, M. Q.; Zhang, G. F.; Li, C.; Aldred, M. P.; Chang, E.; Drezek, R. A.; Li, A. D. Q., Reversible Two-Photon Photoswitching and Two-Photon Imaging of Immunofunctionalized Nanoparticles Targeted to Cancer Cells. *Journal of the American Chemical Society* **2011,** *133* (2), 365-372.

Appendices

Appendix A: Synthesis and Self-Assembly of Gold Nanorods Into Hexalayer Films Capable of Near Infrared-Stimulated Anti-Inflammatory Activity

A.1 Synthesis of Gold Nanorods and Layer-by-Layer Film Characterization

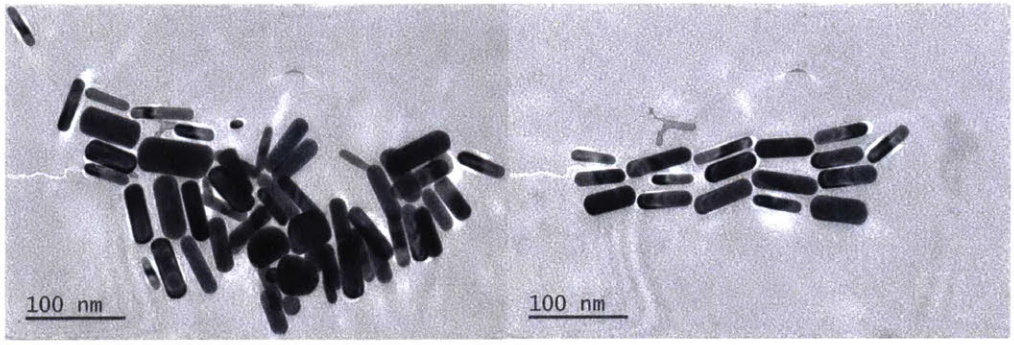

Figure A.1. Representative transmission electron microscopy (TEM) images of synthesized gold nanorods precipitated from 0.5 nM solutions indicated variation in rod diameter and aspect ratio. Image analysis was used to determine aspect ratio 3.591 ± 0.746 (ImageJ). Images captured by Matthew Klug (FEI Tecnai^{TM} G2 Spirit). Self-assembly into side-by-side nanorod assemblies resulted from capillary forces during drying on the TEM grid.[1]

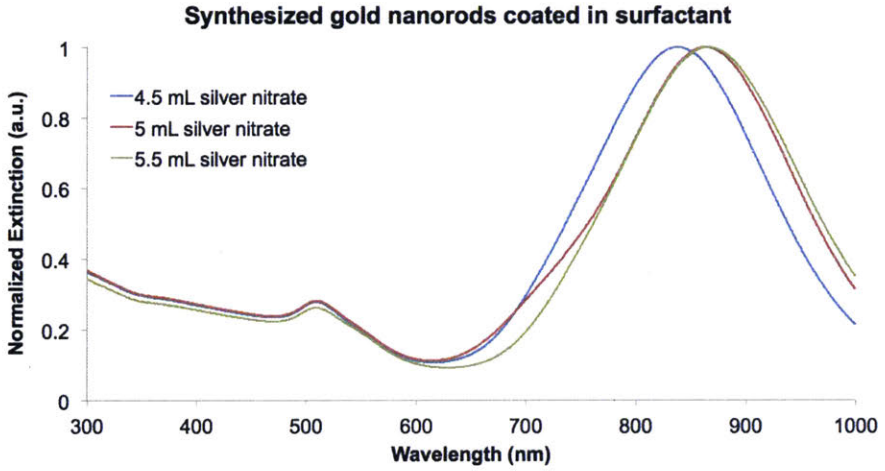

Figure A.2. Absorption spectra confirmed that the longitudinal surface plasmon resonance (LSPR) wavelength of gold nanorods increased as the amount of silver nitrate in the synthesis growth solution increased.[2] Peak wavelength increased from 836.5 for 4.5 mL of silver nitrate to 861 nm and 865.5 nm for 5 mL and 5.5 mL silver nitrate respectively.

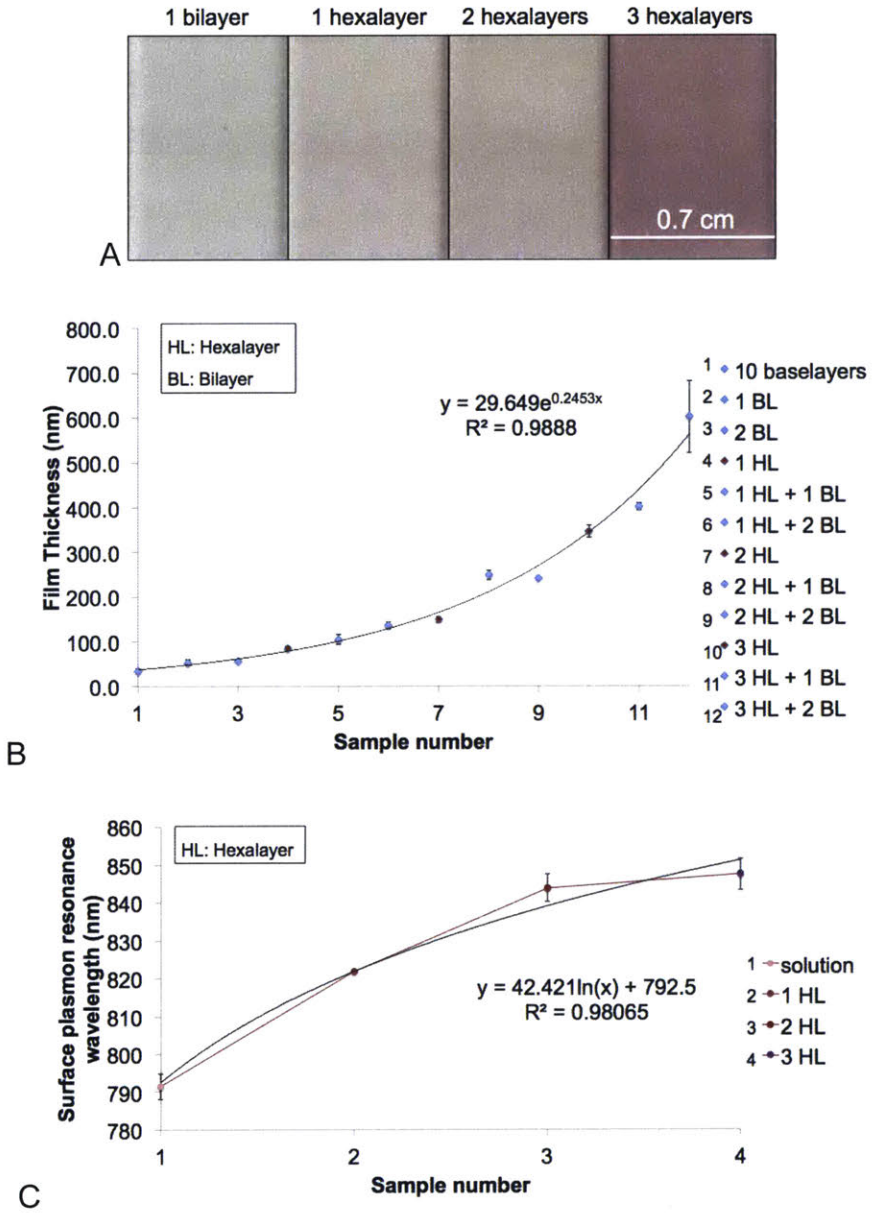

Figure A.3. Analysis of early growth stages of hexalayer films on top of base layers revealed uniform film deposition and exponential growth with the number of layers adsorbed. A. Films fabricated using dip Layer-by-Layer assembly containing gold nanorods deposited every sixth layer grew with a high degree of uniformity. Photograph with superimposed outlines and scale bar. B. The initial growth rate during the first three hexalayers was exponential. C. The initial longitudinal surface plasmon resonance (LSPR) wavelength red-shifting pattern was logarithmic.

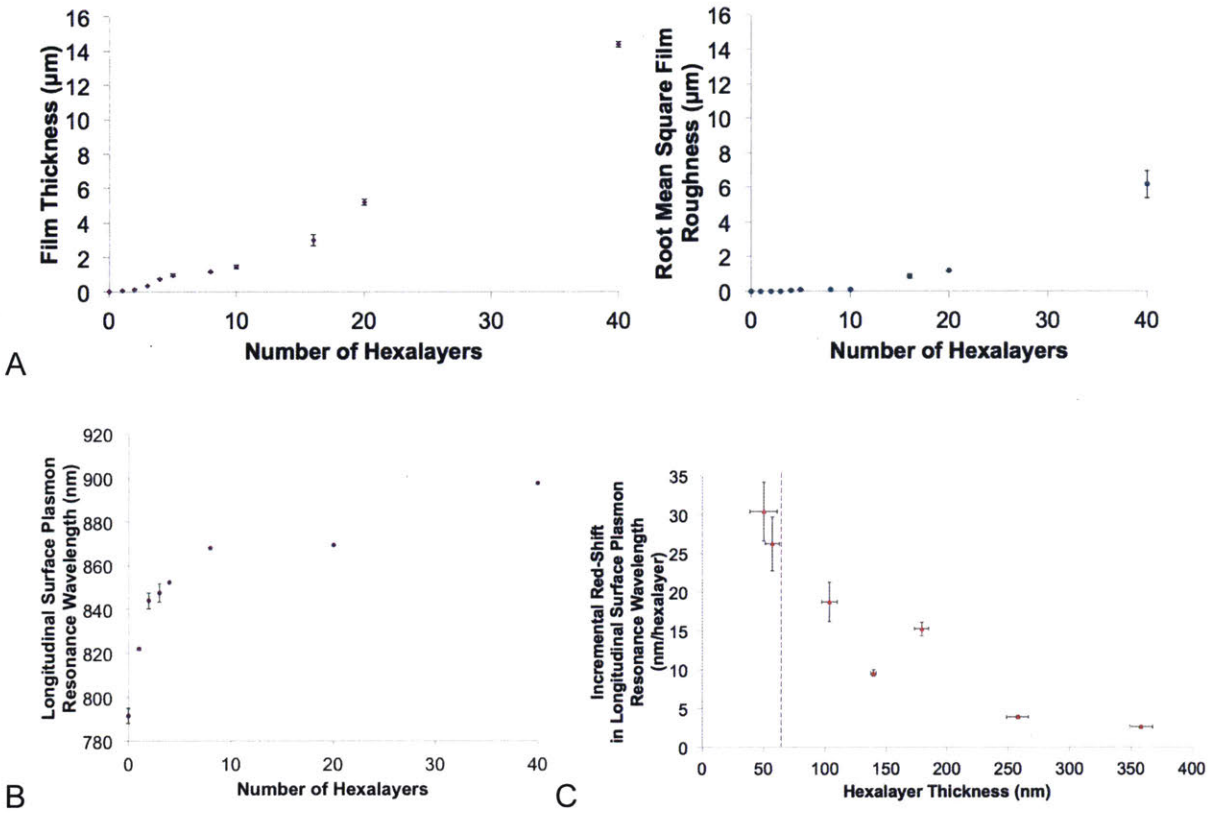

Figure A.4. Growth properties of the 20HL and 40HL films were monitored by profilometry and absorption spectroscopy. A. Initially the films grew exponentially, and then the growth rate slowed starting at the fifth hexalayer, as determined by profilometry. Film roughness was nanoscale initially during film growth, but for the films studied for therapeutic release the roughness was micron-scale. This growth pattern has been observed for hydrogen bonded Layer-by-Layer films with one amphiphilic component.[3, 4] B. Plasmon coupling interactions between nanorods red-shifted the absorption spectrum with each successive layer. C. There was found to be an inverse relationship between hexalayer thickness and the incremental red shift in the longitudinal surface plasmon resonance wavelength. The nanorod absorption spectrum in the films monotonically red-shifted even with hexalayers 360 nm thick, six times the length of a rod. The strongest red shifting occurred as the hexalayer thickness approached the length of a nanorod, i.e. 60 nm, indicated by the vertical dashed line. The two highest incremental red shifts and smallest hexalayer thicknesses corresponded to the first and second hexalayer deposited.

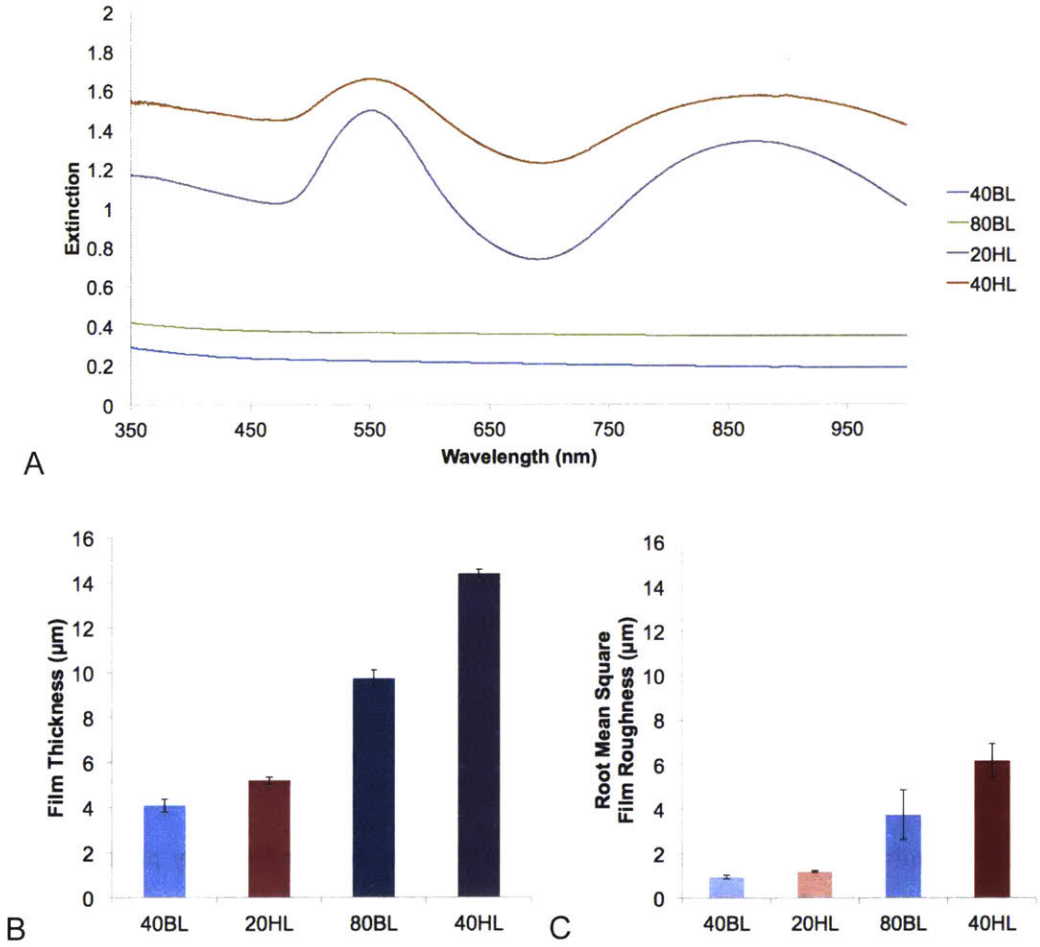

Figure A.5. A. Hexalayer films absorbed significantly in the near infrared, with the absorption peak wavelength out of phase with the 980 nm laser used for irradiation. Forty-hexalayer (40HL) films absorbed more strongly than did 20HL films. Eighty-bilayer (80BL) films absorbed more strongly than 40BL films. The extinction magnitudes measured for the 20HL and 40HL films were not proportional to the numbers of layers of material deposited. This was in part due to a high concentration of scattering entities, i.e. nanorods, and their interactions precluding the applicability of the Beer-Lambert Law. B. All films were microns in thickness, with double the number of layers yielding more than double the film thickness. C. All films had micron-scale roughness, with or without nanorods present. In all cases the roughness originated from layering behavior of micellar aggregates of the polymer-drug conjugate along with unimers.[3, 4] The film roughness approached one half of the total film thickness for the thickest films.

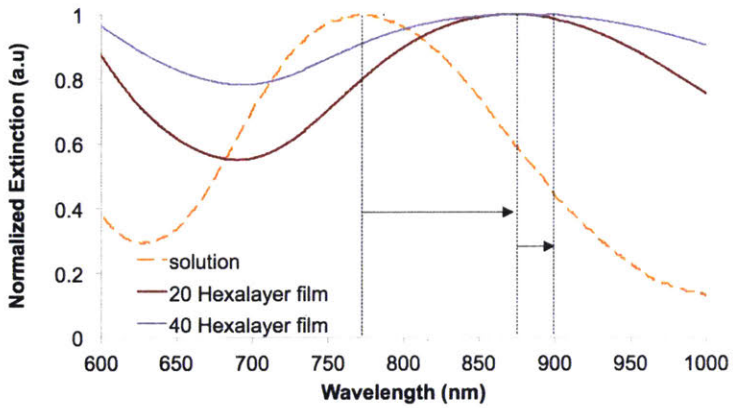

Figure A.6. A comparison of normalized extinction spectra demonstrated that the longitudinal surface plasmon resonance (LSPR) peak of the spectrum for the gold nanorods red shifted and the shape of the spectrum broadened upon incorporation into films and with increasing film thickness. The LSPR peak wavelength red shifted from 773.5 nm for rods coated in poly(4-styrenesulfonic acid) in solution to 869.5 nm for 20-hexalayer films and further to 897.5 for 40-hexalayer films. Note that coating the nanorods in poly(4-styrenesulfonic acid) blue-shifted the LSPR peak from CTAB-coated rods due to a refractive index shift (refer to Figure A.2).

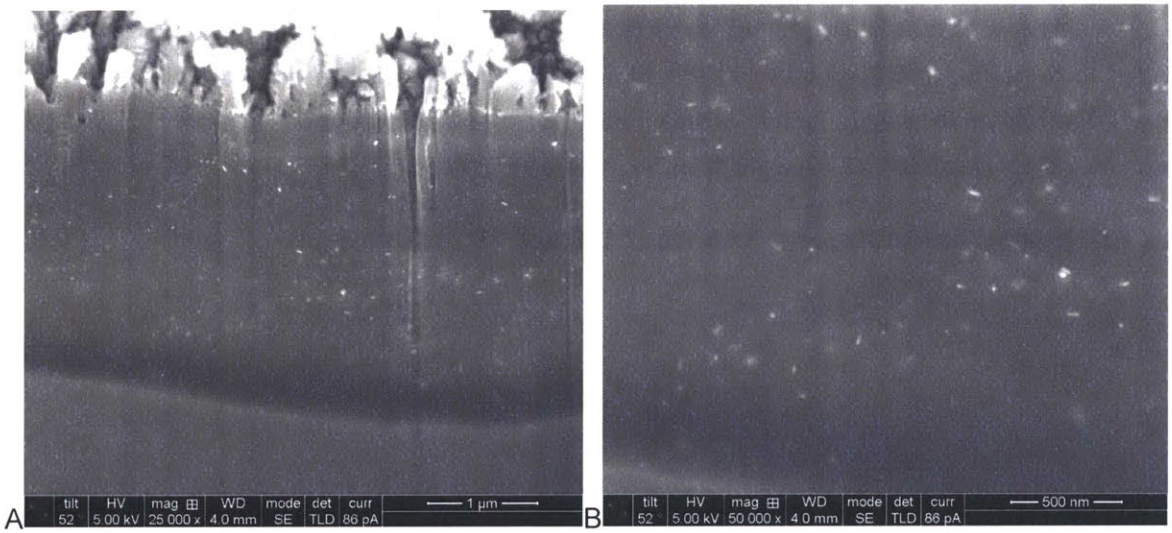

Figure A.7. Hexalayer films formed a nano-blend of gold nanorods throughout the film cross-section, with nanorods present from the substrate to the outer film surface. Nanorods were suspended at random orientations and were not stratified in the film. The film shown was coating the rough side of the silicon substrate. A. Scale bar: 1 µm. B. Scale bar: 500 nm. Images obtained by scanning electron microscopy (Helios). This 17-hexalayer-film cross-section was obtained by focused ion beam milling (FIB, ^{69}Ga source) after electron beam-induced platinum deposition (5 kV, 11 nA, approx. 0.5 µm thick). See Figure 2.4 for an alternative cross-section visualization that involved less processing to the sample than did this FIB preparation.

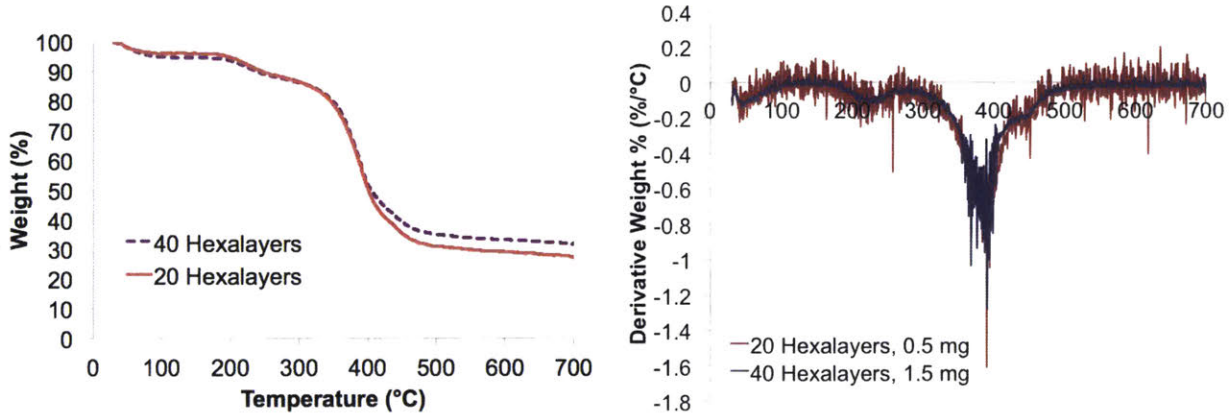

Figure A.8. Thermogravimetric analysis of hexalayer films involved three main weight loss events. First, weight loss from ambient temperature through 85°C corresponded to desorption of water from the film. Slight weight loss 100°C-185°C resulted from dehydration, i.e. removal of water more strongly bound within the film due to the presence of metal cations, e.g. Na^+. The second major weight loss from 185°C to 260°C involved decomposition of oligomers, i.e. shorter chains of polymer electrolytes, and loosely held physically adsorbed surfactant.[5-7] The third weight loss from 260°C to 500°C was the decomposition of polymers,[5, 6] free and covalently held diclofenac,[8, 9] and remaining electrostatically bound surfactant.[7] The slow mass loss 500-700°C can be attributed to remaining poly(L-glutamic acid).[6] After all organic matter was burned off from the sample, 20-hexalayer films were found to contain 23.45 weight % gold nanorods in a dry film, and 40-hexalayer films contained 27.4 weight % gold nanorods in a dry film.

A.2 Film Response to Incubation and Near-Infrared Irradiation

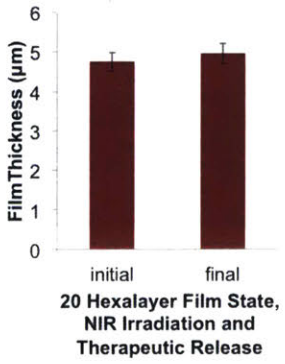

Figure A.9. Twenty-hexalayer film thickness was not altered by therapeutic release and near infrared irradiation, demonstrating that diclofenac was released during these treatments without macroscopic degradation of the film (profilometry).

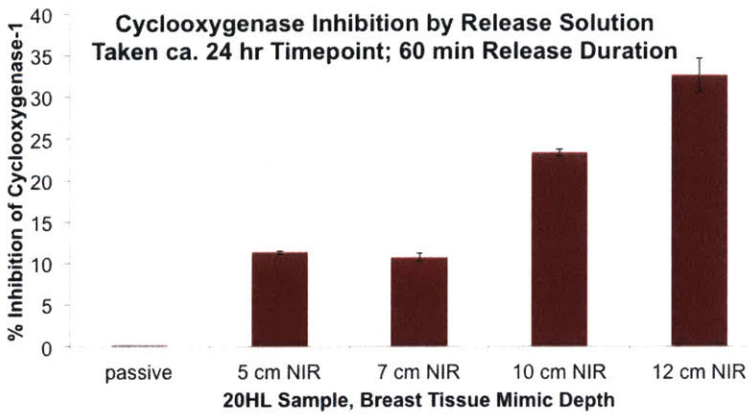

A

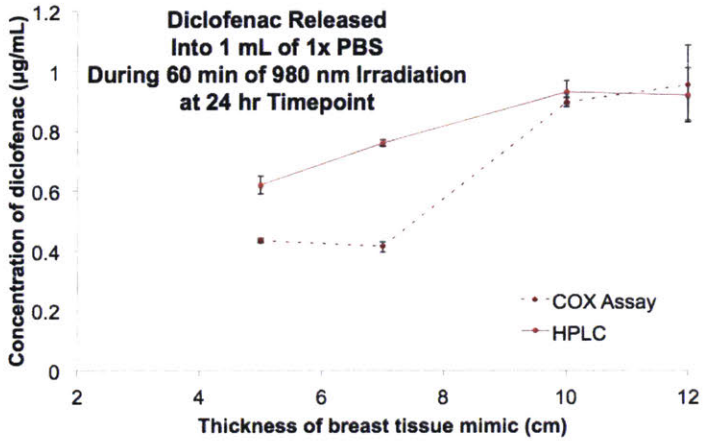

B

Figure A.10. A. The diclofenac released from films during near infrared irradiation retained its anti-inflammatory activity, as determined by cyclooxygenase (COX) fluorescent inhibitor screening assay (Cayman Chemical).[10] B. Release solution with diclofenac concentration 0.9 µg/mL or greater showed better quantitative agreement between COX assay and HPLC data than release solution at a concentration less than 0.9 µg/mL. This was due to a dearth of standard curve concentration measurements in the low concentration range for the COX assay, and therefore a less accurate estimate of concentration by interpolation.

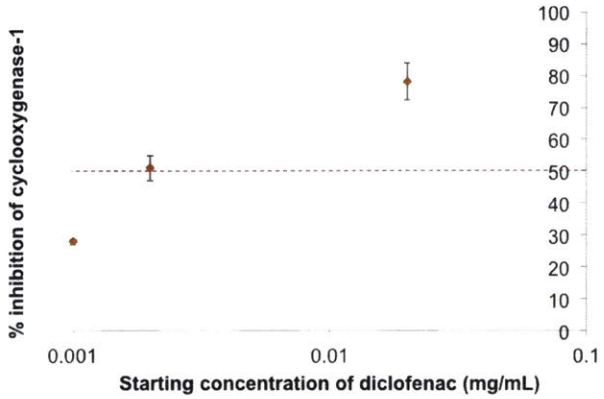

Figure A.11. The IC_{50} condition of free diclofenac was found from cyclooxygenase fluorescent inhibitor screening assay (Cayman Chemical) to be 0.002 mg/mL i.e. 2 µg/mL diclofenac in starting solution. This is equivalent to an IC_{50} value of 100 ng/mL due to dilution of 10 µL into a total of 200 µL solution for the assay. This IC_{50} value of 100 ng/mL is greater and therefore a more stringent condition on inhibition than the approx. 25 ng/mL found in the literature[10, 11] but 100 ng/mL was used in this study for consistency. Cyclooxygenase-2, responsible for prostaglandin synthesis under acute inflammatory conditions, is inhibited to a greater degree than cyclooxygenase-1 at the same concentration of diclofenac.[11, 12]

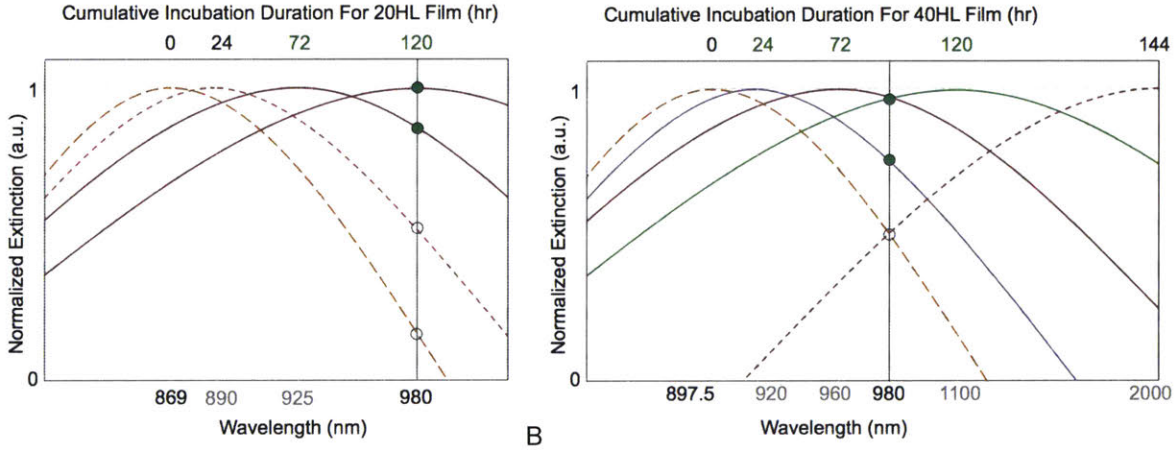

Figure A.12. Based on experimental extinction spectra, high performance liquid chromatography, and scanning electron microscopy data, the time progressions of the normalized extinction spectra during incubation for therapeutic release from 20HL (A) and 40HL (B) films were approximated. The absorption spectra were expected to red shift and broaden during nanorod aggregation. Open circles along the vertical 980 nm line and dashed curves intersecting the circles indicate that the fraction of photothermal conversion entities in the film in resonance with the near infrared irradiation wavelength were insufficient to produce enhanced release rates of diclofenac above bilayer controls (A: Figure 2.5; B: Figure 2.10).

Green filled circles along the 980 nm line and continuous curves intersecting them indicate that the fraction of in-resonance photothermal conversion aggregates of nanorods was sufficient to produce significantly enhanced diclofenac release rates above the control (A: Figure 2.5, Figure 2.3; B: Figure 2.10). LSPR peak wavelength values in gray were estimated, and those in black were measured.

A.3 The Effect of Film Thickness on Surface Morphology Response to Irradiation

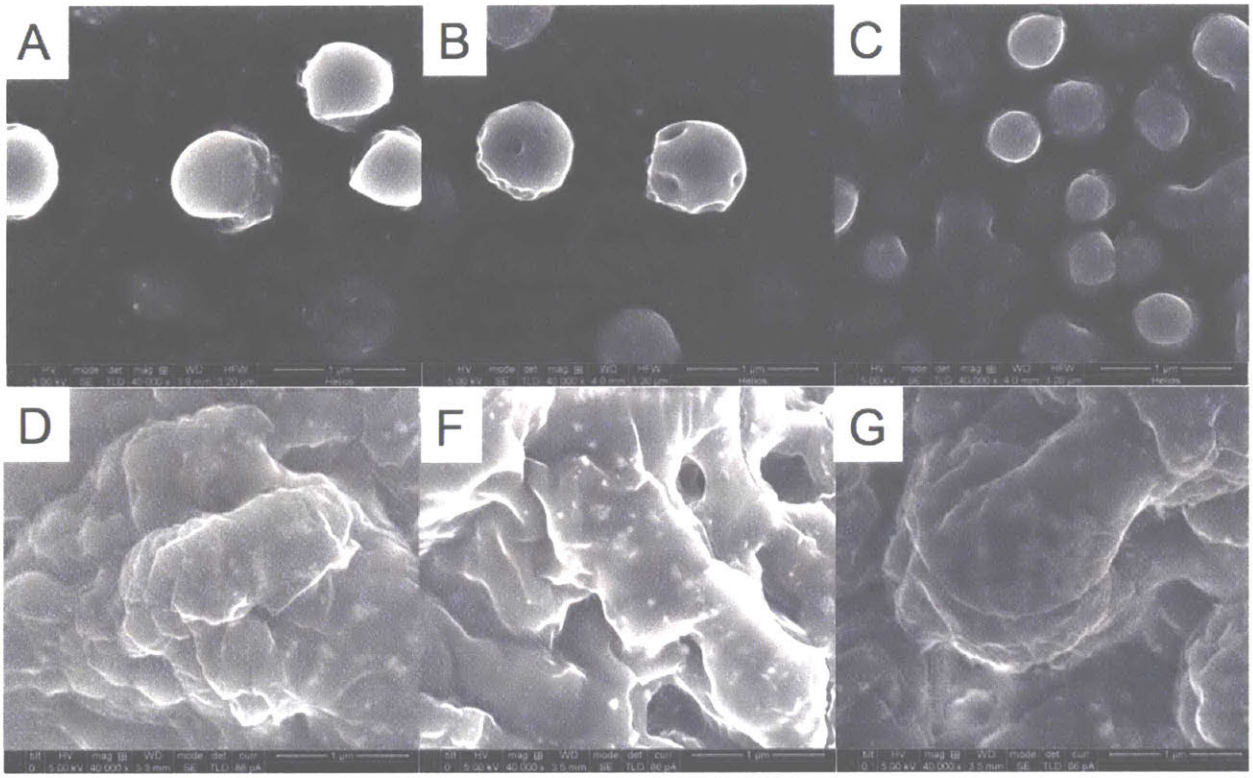

Figure A.13. Scanning electron microscopy on three and twenty-hexalayer film surfaces demonstrates the effect of film thickness on response to near infrared irradiation. Scale bar 1 μm for all. A. Three-hexalayer (3HL) film surface after incubation (24 hr, 1x PBS, 37°C) before irradiation. B. 3HL just after irradiation (980 nm, 0.2 W/cm^2, 60 min) developed nanocavitations at the surface. C. 3HL after post-irradiation incubation (24 hr, 1x PBS, 37°C) demonstrated self-healing. D. Twenty-hexalayer (20HL) film surface after incubation (24 hr, 1x PBS, 37°C) before irradiation. F. 20HL just after irradiation (980 nm, 0.2 W/cm^2, 60 min) did not change in surface morphology. G. 20HL after post-irradiation incubation (24 hr, 1x PBS, 37°C). 3HL films were 0.346 μm thick, the irradiating wavelength was 0.980 μm, and the 20HL films were 5.188 μm thick. This result underscores the importance of the relationship between the film thickness and the wavelength of impinging irradiation *in vitro*. The 3HL result viewed in isolation could be misinterpreted as film disruption by nanorod photothermal conversion, when in fact the origin of the disruption is the relation between film thickness and the wavelength of impinging irradiation.

A.4 Materials and Methods

Variation of silver nitrate incorporation into gold nanorod synthesis to control aspect ratio: Gold nanorod synthesis proceeded as usual[13] with the exception of varying the volume of silver nitrate added to the growth solution (4.5 mL, 5.0 mL, 5.5 mL).

Characterization of gold nanorod extinction spectra in solution and in Layer-by-Layer films: Gold nanorod extinction spectra were determined for gold nanorods suspended in solutions of 0.01x PBS at pH 7.4 and incorporated into LbL films every sixth layer. A DU800 spectrophotometer was used with wavelength range 300-1000nm at 600 nm/min.

Film thickness, film roughness, and absorption spectroscopy characterization of bilayer and hexalayer films: Films were built and characterized by photographic comparison, absorption spectroscopy, and then profilometry. Absorption spectra were obtained from the DU800 (300-1000 nm, 600 nm/min) and from these spectra the longitudinal surface plasmon resonance wavelength in the films was determined as the wavelength of peak absorption in the near infrared. Profilometry to determine film thickness and root mean square roughness was carried out on razor-scored films using the Dektak 150 Surface Profiler.

Focused ion beam cross-section for scanning electron microscopy (SEM): The hexalayer film was assembled Layer-by-Layer, followed by immersion in liquid nitrogen for 30 sec, then immediately mounting the sample on an SEM mount with carbon tape, and then storing the sample at -20°C. The sample was coated with 10 nm of carbon by vacuum evaporator (Denton) before placement in the SEM sample chamber.

To achieve the focused ion beam milled cross-section for imaging, first, 5 kV of 11 nA electron beam Platinum deposition was directed at 20 µm by 2 µm dimensions on the film surface, with approx. 0.5 µm thickness at 0° tilt. The ion beam with a ^{69}Ga source was initiated for the cross-section. Next, at 52° tilt, a regular cross-section was carved out at 9.3 nA with dimensions 20 µm by 20 µm by 5 µm thick. A cleaning cross-section was afterwards conducted with 0.92 nA. Finally, a second cleaning cross-section was used at 93 pA.

Thermogravimetric analysis (TGA) of hexalayer films: Each film sample was scraped off from its glass substrate into a high temperature platinum TGA pan using a fresh razor blade. TGA (Discovery) was carried out with the sample under nitrogen. The program began with equilibration at 30°C, followed by a temperature ramp at 20°C/minute to 700°C, and concluding isothermal for 1 minute.

Determination of therapeutic efficacy of released drug by cyclooxygenase (COX) fluorescent inhibition assay: COX-1 inhibition activity by diclofenac released from LbL films was quantified using a plate reader with the COX fluorescent inhibitor screening assay kit (Cayman Chemical) according to the manufacturer's directions. All samples were measured in triplicate.

Film thickness vs. irradiation response observation: therapeutic release incubation (37°C, 1x PBS, 24 hr) and irradiation (37°C, 1x PBS, 980 nm, 0.2 W/cm^2, 60 min) protocols were maintained for three- and twenty-hexalayer films on glass substrates. The surface morphological changes were studied by scanning electron microscopy (Helios).

A.5 References

1. Nikoobakht, B.; Wang, Z. L.; El-Sayed, M. A., Self-assembly of gold nanorods. *Journal of Physical Chemistry B* **2000,** *104* (36), 8635-8640.
2. Feng, L. L.; Xuan, Z. W.; Ma, J. B.; Chen, J.; Cui, D. X.; Su, C. W.; Guo, J. M.; Zhang, Y. J., Preparation of gold nanorods with different aspect ratio and the optical response to solution refractive index. *Journal of Experimental Nanoscience* **2015,** *10* (4), 258-267.
3. Seo, J.; Lutkenhaus, J. L.; Kim, J.; Hammond, P. T.; Char, K., Development of surface morphology in multilayered films prepared by layer-by-layer deposition using poly(acrylic acid) and hydrophobically modified poly(ethylene oxide). *Macromolecules* **2007,** *40* (11), 4028-4036.
4. Sung, C.; Hearn, K.; Reid, D. K.; Vidyasagar, A.; Lutkenhaus, J. L., A Comparison of Thermal Transitions in Dip- and Spray-Assisted Layer-by-Layer Assemblies. *Langmuir* **2013,** *29* (28), 8907-8913.
5. Krikorian, V.; Kurian, M.; Galvin, M. E.; Nowak, A. P.; Deming, T. J.; Pochan, D. J., Polypeptide-based nanocomposite: Structure and properties of poly(L-lysine)/Na+-montmorillonite. *Journal of Polymer Science Part B-Polymer Physics* **2002,** *40* (22), 2579-2586.
6. Dai, Z. Z.; Yin, J. B.; Yan, S. F.; Cao, T.; Ma, J.; Chen, X., Polyelectrolyte complexes based on chitosan and poly(L-glutamic acid). *Polymer International* **2007,** *56* (9), 1122-1127.
7. Ni, R. J.; Huang, Y.; Yao, C., Thermogravimetric analysis of organoclays intercalated with the gemini surfactants. *Journal of Thermal Analysis and Calorimetry* **2009,** *96* (3), 943-947.
8. Tudja, P.; Khan, M. Z. I.; Mestrovic, E.; Horvat, M.; Golja, P., Thermal behaviour of diclofenac sodium: Decomposition and melting characteristics. *Chemical & Pharmaceutical Bulletin* **2001,** *49* (10), 1245-1250.
9. Pasquali, I.; Bettini, R.; Giordano, F., Thermal behaviour of diclofenac, diclofenac sodium and sodium bicarbonate compositions. *Journal of Thermal Analysis and Calorimetry* **2007,** *90* (3), 903-907.
10. Hsu, B. B.; Park, M. H.; Hagerman, S. R.; Hammond, P. T., Multimonth controlled small molecule release from biodegradable thin films. *Proceedings of the National Academy of Sciences of the United States of America* **2014,** *111* (33), 12175-12180.
11. Kato, M.; Nishida, S.; Kitasato, H.; Sakata, N.; Kawai, S., Cyclooxygenase-1 and cyclooxygenase-2 selectivity of non-steroidal anti-inflammatory drugs: investigation using human peripheral monocytes. *Journal of Pharmacy and Pharmacology* **2001,** *53* (12), 1679-1685.
12. Mitchell, J. A.; Akarasereenont, P.; Thiemermann, C.; Flower, R. J.; Vane, J. R., SELECTIVITY OF NONSTEROIDAL ANTIINFLAMMATORY DRUGS AS INHIBITORS OF CONSTITUTIVE AND INDUCIBLE CYCLOOXYGENASE. *Proceedings of the National Academy of Sciences of the United States of America* **1993,** *90* (24), 11693-11697.
13. Nikoobakht, B.; El-Sayed, M. A., Preparation and growth mechanism of gold nanorods (NRs) using seed-mediated growth method. *Chemistry of Materials* **2003,** *15* (10), 1957-1962.

Appendix B: An Approach To Decrease Passive Release From Near-Infrared Responsive Films and Enhance Efficacy

B.1 Introduction of Clay Barrier Layers onto Layer-by-Layer Films

One potential improvement to the diclofenac-eluting system would have been to decrease the passive release rate of free diclofenac from the film. By slowing the release of the free drug from the film, which in itself would be beneficial, the near-infrared activated release could also potentially be increased as a result. As an approach to accomplish this objective, fifteen bilayers of Laponite clay platelets with poly(L-lysine) were layered on top of both forty bilayer (40BL) films and twenty hexalayer (20HL) films (Figure B.1).

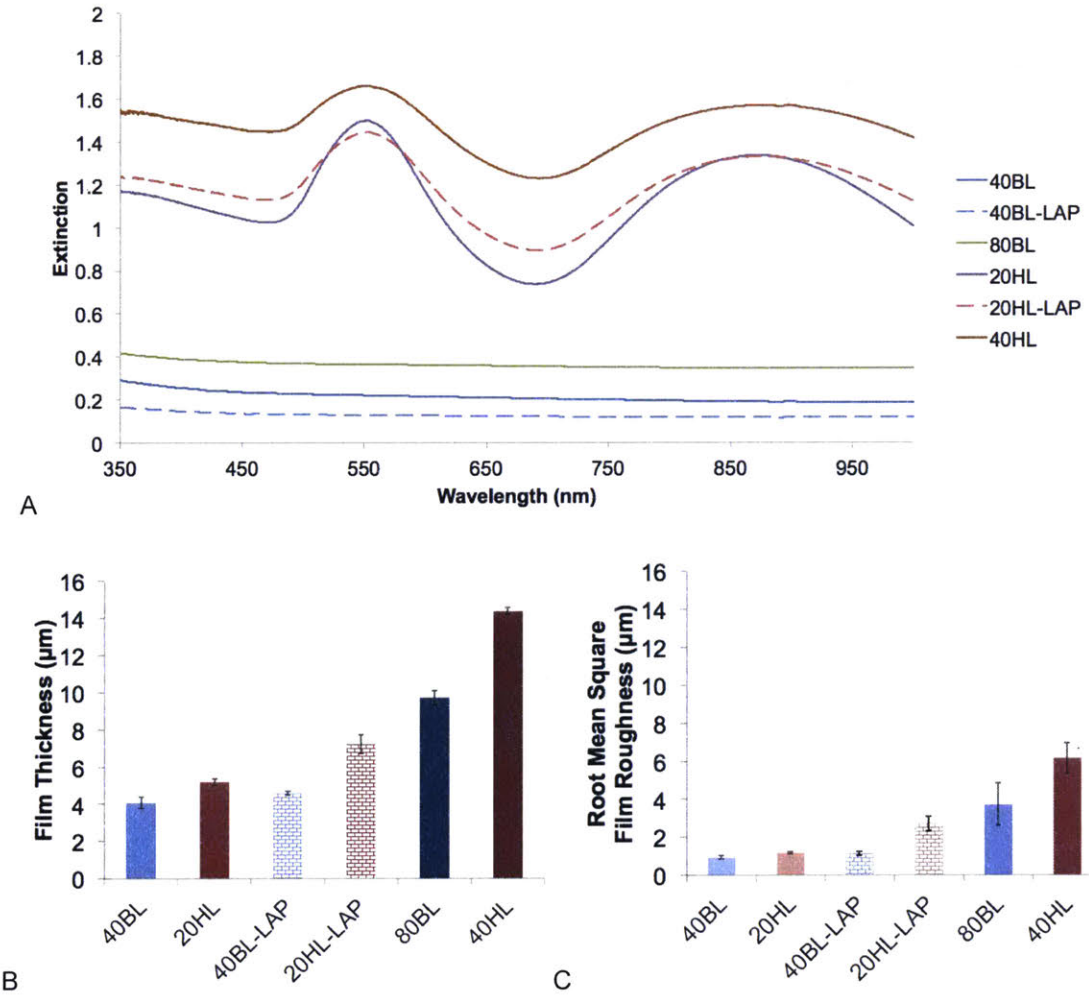

Figure B.1. A. Layering clay platelets on top of bilayer and hexalayer films did not substantially alter the absorption spectra of the films. B. Laponite clay (LAP) barrier layers increased the film thickness of 40BL and 20HL films. C. Films capped with clay layers had film roughness at the micron scale.

B.2 Performance of the Clay-Capped Films

This barrier layer method had been used previously to slow the passive release of gentamycin sulfate from films.[1] Upon comparing the molecular structures, it was predicted that the clay would slow the diclofenac diffusion to a lesser extent than it did gentamicin sulfate (Figure B.2).

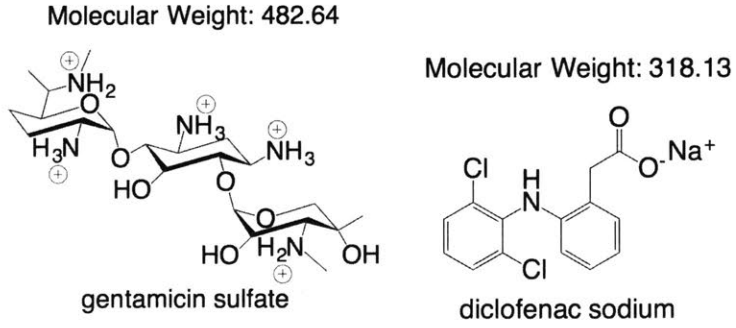

Figure B.2. Comparison of the molecular structures of gentamicin sulfate and diclofenac sodium revealed that the gentamicin molecule is more massive and highly charged under film assembly conditions. Molecular size and electrostatic forces are among many factors that play a role in the rate of diffusion of small molecules through a hydrogel. Ideally the film would be capped with a tortuous barrier created by the clay-polymer nanocomposite. Diclofenac and the clay platelets both had negative charge density under film assembly conditions. Gentamicin sulfate from the previous study was deposited with a highly positive charge density.[1] Due to the size difference, a given spacing between clay platelets that would allow the passage of gentamicin at a slowed rate would more easily accommodate diclofenac. Therefore, with all conditions being equal, it was hypothesized that a clay barrier layer would decrease the diffusion coefficient to a lesser extent for diclofenac than for gentamicin.

There was no decrease in the passive release rate of diclofenac from these films (Figure B.3.A). The clay did not provide a barrier sufficient to reduce the diffusion rate of diclofenac out of the film. Profilometry on the films revealed that the films had root mean square roughness on the micron scale (Figure B.1.C), which could prevent the clay from stacking in continuous brick-wall morphology.[1] This high micron-scale roughness explained, at least in part, why the clay did not serve as a sufficient barrier. A comparison of film surface morphologies by scanning electron microscopy corroborated the conclusion that the high film roughness frustrated the formation of a continuous clay barrier layer (Figure B.4).

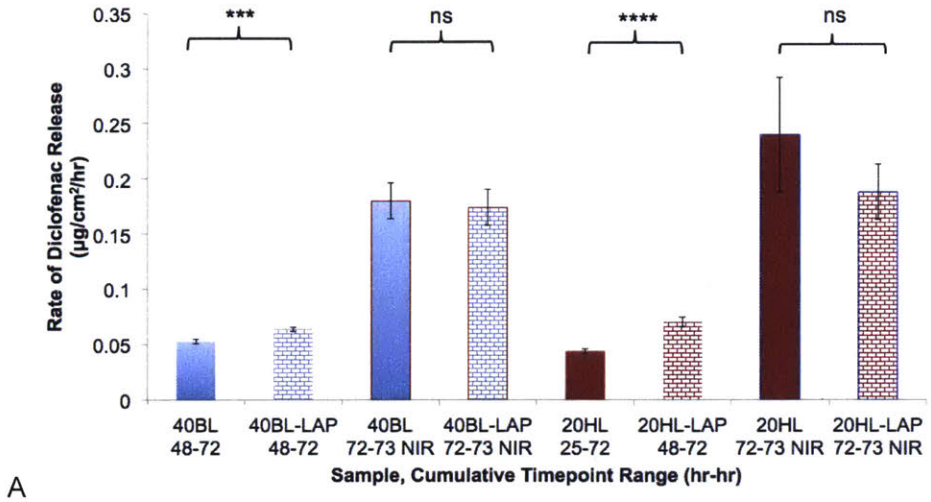

A

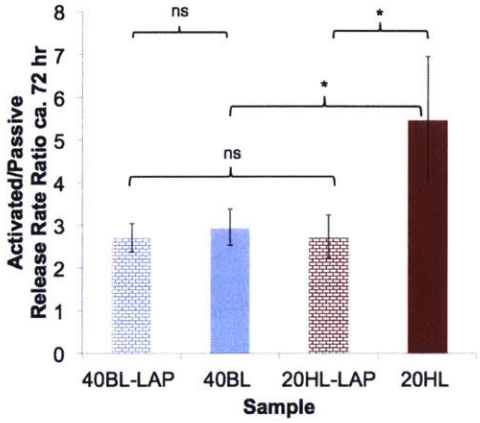

B

Figure B.3. A. The passive release rate of diclofenac was found to increase rather than decrease upon addition of fifteen bilayers of Laponite clay (LAP) platelets with poly(L-Lysine). Therefore, as no additional free diclofenac was withheld from release within the film, the release rate of diclofenac during near infrared irradiation did not increase. B. As a direct consequence, the irradiated/passive release rate ratio was not significantly different for bilayer films with (40BL-LAP) vs. without (40BL) clay platelets layered at the surface. Gold nanorod-containing films without clay (20HL) out-performed hexalayer films with a clay barrier layer (20HL-LAP). Analysis for statistical significance for paired data sets was determined by two-tailed t-tests assuming unequal variances (ns: $p > 0.05$; *: $p \leq 0.05$; **: $p \leq 0.01$; ***: $p < 0.001$; ****: $p < 0.0001$). Release rates of diclofenac from Layer-by-Layer films were quantified by high performance liquid chromatography.

As expected, a result of the diclofenac being able to pass freely out of the film was that the release rate of diclofenac from the film during irradiation was not increased relative to that for films without the clay barrier. In the case of twenty-hexalayer (20HL) films, the irradiated-to-passive release rate ratio was greater for the film without the barrier layer than with the clay

(Figure B.3.B). Since the performance of the bilayer films was not affected, this was not likely due to the clay serving as an obstruction in the irradiation path to the nanorods. More reasonably, it was the result of the nanorod aggregation kinetics. The nanorods were allowed additional time to migrate and aggregate during assembly of the clay barrier layers, decreasing film performance.

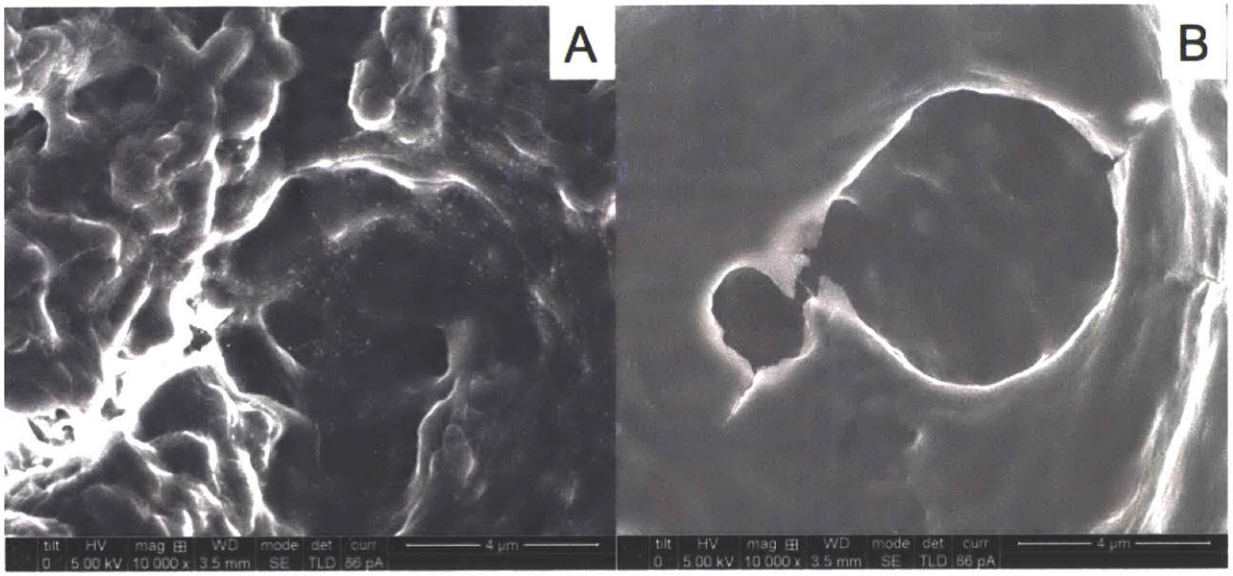

Figure B.4. Scanning electron microscopy images of twenty-hexalayer film surfaces without (A, 20HL) and with (B, 20HL-LAP) clay barrier layer demonstrate that the roughness of the film inhibited continuous barrier coverage by the clay. Scale bar: 4 µm. A. Gold nanorods were readily visible throughout the 20HL film surface. B. Gold nanorods were not visible at the outermost surface of 20HL-LAP (outer part of image) due to the clay barrier, but could be resolved inside of the microns-wide crevices (center of image), indicating a lack of coverage by the clay within the crevices. Despite the ~20 nm clay platelet size,[1] the clay deposited preferentially on the hills rather than the valleys of the film. The micron-scale roughness of the film frustrated the formation of a continuous barrier by the clay from the film to the surrounding medium. Defects in the clay layers enabled escape of diclofenac from the film during passive release. This same result applies to 40BL and 40BL-LAP films.

To form an effective clay barrier layer on these films, the film surface must be smooth. Due to the amphiphilic nature of poly(L-glutamic acid-triethylene glycol-diclofenac) (PGA-Diclof), micron-scale surface roughness was induced in both bilayer and hexalayer films due to hydrophobic interactions between the triethylene glycol-diclofenac side chains producing micelle-like structures that present roughening film growth characteristics. This has been observed in hydrogen-bonded multilayer films where one polymer is contains hydrophobic moieties on the chain ends[2] or along the backbone.[3] An approach to decrease the film

roughness would be to alter the fabrication method of the film. Using spin[4, 5] or spray[3, 6] Layer-by-Layer techniques for the poly(L-lysine) and the PGA-Diclof could lead to films with minimal roughness that are amenable to a passive release-blocking clay coating. It is hypothesized that the thermal properties of the films will not be altered by changing the mode of fabrication, as has been observed for an analogous hydrogen-bonded Layer-by-Layer system with hydrophobic moieties.[3]

Spray Layer-by-Layer also decreases fabrication time and increases scalability. The duration of assembly for eighty-bilayer films with dip Layer-by-Layer was 34.6 hr. If incorporating the polymers into the film by spin or spray, the duration of polyelectrolyte application would be reduced from 10 minutes to 3 seconds.[7] This would reduce the total film assembly time to 0.356 hr (21.3 minutes). On the other hand, micelle disruption during spray-assisted assembly may occur and may preclude the delayed release mechanism hypothesized in this work.

B.3 Materials and Methods

Assembly of clay barrier layers: After fabrication of bilayer or hexalayer films, the films underwent the following dip Layer-by-Layer protocol: 10 minute dip into 1 mg/mL solution of poly(L-lysine) (PLL) in 10 mM sodium phosphate buffer at pH 7.4; rinsing for 30s, 60s, and 90s-with-agitation in 18 MΩ•cm water; 10 minute dip into a suspension of 0.1 weight% Laponite (LAP) clay (Southern Clay Products) in 18 MΩ•cm water and pH-adjusted to 9;[1] and rinsing for 30s, 60s, and 90s-with-agitation in 18 MΩ•cm water. The final clay barrier layer was $(PLL/LAP)_{15}$.

Sample preparation for characterization by scanning electron microscopy (SEM): Twenty-hexalayer (20HL) and 20HL-LAP films were fabricated and stored under vacuum desiccation at room temperature until characterization by SEM.

B.4 References

1. Min, J.; Braatz, R. D.; Hammond, P. T., Tunable staged release of therapeutics from layer-by-layer coatings with clay interlayer barrier. *Biomaterials* **2014,** *35* (8), 2507-2517.
2. Seo, J.; Lutkenhaus, J. L.; Kim, J.; Hammond, P. T.; Char, K., Development of surface morphology in multilayered films prepared by layer-by-layer deposition using poly(acrylic acid) and hydrophobically modified poly(ethylene oxide). *Macromolecules* **2007,** *40* (11), 4028-4036.
3. Sung, C.; Hearn, K.; Reid, D. K.; Vidyasagar, A.; Lutkenhaus, J. L., A Comparison of Thermal Transitions in Dip- and Spray-Assisted Layer-by-Layer Assemblies. *Langmuir* **2013,** *29* (28), 8907-8913.
4. Seo, J.; Lutkenhaus, J. L.; Kim, J.; Hammond, P. T.; Char, K., Effect of the layer-by-layer (LbL) deposition method on the surface morphology and wetting behavior of hydrophobically modified PEO and PAA LbL films. *Langmuir* **2008,** *24* (15), 7995-8000.

5. Choi, I.; Suntivich, R.; Plamper, F. A.; Synatschke, C. V.; Muller, A. H. E.; Tsukruk, V. V., pH-Controlled Exponential and Linear Growing Modes of Layer-by-Layer Assemblies of Star Polyelectrolytes. *Journal of the American Chemical Society* **2011,** *133* (24), 9592-9606.
6. Krogman, K. C.; Lyon, K. F.; Hammond, P. T., Metal Ion Reactive Thin Films Using Spray Electrostatic LbL Assembly. *Journal of Physical Chemistry B* **2008,** *112* (46), 14453-14460.
7. Hsu, B. B.; Hagerman, S. R.; Hammond, P. T., Rapid and efficient sprayed multilayer films for controlled drug delivery. *Journal of Applied Polymer Science* **2016,** *133* (25), 8.